Efficient Detection of Coherent Structures in Non-Autonomous Dynamical Systems via Transfer Operator Methods

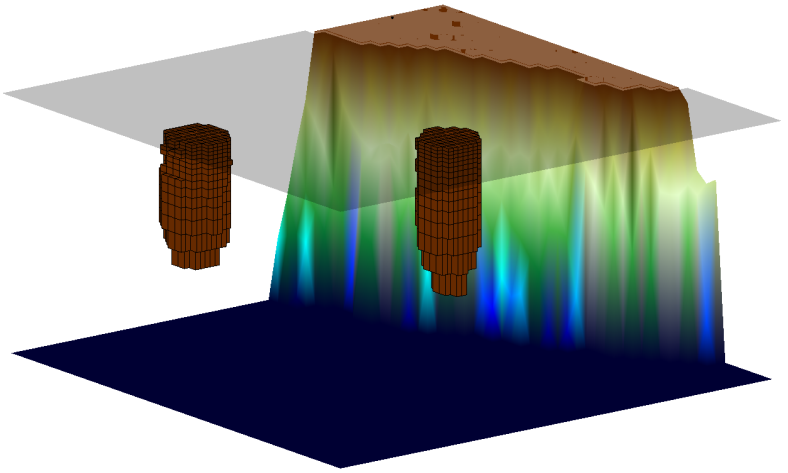

Christian Horenkamp

Paderborn 2014

Acknowledgements

First and foremost, I would like to thank my advisor Prof. Dr. Michael Dellnitz for his guidance, support, and motivation. He has always provided a very pleasant research environment to me and introduced me to a very interesting field of research. I also thank Professor Gary Froyland from the University of New South Wales for many fruitful discussions contributing to my thesis, mutual visits and exciting joint work.

I also want to thank Jun.-Prof. Dr. Kathrin Padberg-Gehle and Naratip Santitissadeekorn for many helpful discussions on my research topic and Vincent Rossi, Alex Sen Gupta and Erik van Sebille for effective joint work on ocean dynamics.

I acknowledge the financial support I have received from the Deutsche Forschungsgemeinschaft (DFG) within the *Research Training Group Scientific Computation* (GK 693) and from the German Academic Exchange Service (DAAD) within the *2011/12 Go8/DAAD Australia – Germany Joint Research Co-Operation Scheme*.

I would like to say thank you to Dr. Kathrin Flaßkamp, Dr. Sebastian Hage-Packhäuser and Robert Timmermann for many interesting and enlightening discussions and their constant support. Moreover, I would like to thank Dr. Mirko Hessel-von Molo, Marianne Kalle, Jun.-Prof. Dr. Sina Ober-Blöbaum, Sebastian Peitz, Bianca Thiere and all former members of the *Institute for Industrial Mathematics* and the *Chair of Applied Mathematics*.

Finally, I thank my family and friends for their constant support and encouragement.

Abstract

The analysis of transport phenomena – such as the detection and tracking of coherent structures – plays a crucial role in many applications, e. g. in the investigation of gyres and eddies in the ocean. In order to treat coherent structures of dynamical systems so-called transfer operator methods have been developed during the last years and extended in order to approximate transport phenomena in non-autonomous dynamical systems and related applications. These methods all have in common that they involve long-term simulations of trajectories on the whole state space which are computationally expensive. In this thesis, we develop efficient algorithms for the detection of coherent structures and present theoretical results in this context.

Transfer operators naturally fulfill the so-called *cocycle property* which does not generally hold for transition matrices which are the corresponding finite-dimensional representations of transfer operators. However, we use products of transition matrices to approximate single transfer operators. We successfully elaborate this approach and prove that the cocycle property holds under certain conditions.

In non-autonomous dynamical systems so-called coherent pairs are slowly mixing time-dependent structures in state space. In principle, for the detection of coherent pairs it is sufficient to focus on a region of the state space containing a coherent pair as opposed to the whole state space which in comparison considerably decreases the numerical effort. A priori it is not obvious in which part a coherent pair is contained. We formulate an algorithm that preselects a part of the state space as a candidate set containing a coherent pair and thereby significantly reduces the related numerical effort. In detail, we prove that if the transport process is slow enough transport phenomena over a fixed (long) time horizon imply the existence of almost invariant sets over shorter time intervals.

The novel results and algorithms obtained in this thesis allows one to analyze transport phenomena in oceanic fluid flow. As an application, we present the first three-dimensional study of a single Agulhas ring over a sufficiently long time interval. From a superior point of view, these results give rise to a new perspective on the analysis of oceanic structures.

Zusammenfassung

Die Analyse von Transportphänomenen – wie etwa die Identifikation kohärenter Strukturen – spielt eine wichtige Rolle in vielen Anwendungen, zum Beispiel bei der Untersuchung von Ozeanwirbeln. Um kohärente Strukturen im Kontext dynamischer Systeme zu behandeln, wurden in den letzten Jahren sogenannte Transferoperator-Methoden entwickelt. Diese sind unter anderem für die Approximation von Transportphänomenen in nicht-autonomen dynamischen Systemen erweitert worden. All diesen Methoden liegen rechenintensive Simulationen von Trajektorien im gesamten Phasenraum zugrunde. In dieser Arbeit werden sowohl effiziente Algorithmen zur Identifikation kohärenter Strukturen entwickelt als auch theoretische Ergebnisse in diesem Zusammenhang präsentiert.

Transferoperatoren erfüllen auf natürliche Weise die sogenannte Kozykel-Eigenschaft. In dieser Arbeit werden deshalb Produkte von Übergangsmatrizen verwendet um Transferoperatoren zu approximieren. Dieser Ansatz wird ausgearbeitet und erfolgreich angewendet. Zudem wird bewiesen, dass die Kozykel-Eigenschaft unter bestimmten Umständen auch für Übergangsmatrizen gilt.

Kohärente Paare im Kontext nicht-autonomer dynamischer Systeme sind Strukturen, die sich nur langsam mit dem übrigen Phasenraum durchmischen. Grundsätzlich ist es sinnvoll, sich für die Approximation kohärenter Paare auf einen Teil des Phasenraumes zu beschränken, um den numerischen Aufwand zu verringern. A priori ist es jedoch nicht offensichtlich, in welchen Bereichen des Phasenraumes sich ein kohärentes Paar befindet. In dieser Arbeit wird ein Algorithmus formuliert, welcher Bereiche identifiziert, die ein kohärentes Paar enthalten und damit signifikant den numerischen Aufwand reduziert. Es wird gezeigt, dass hinreichend langsame Transportprozesse über einen festen Zeitraum die Existenz fast-invarianter Mengen über kurze Zeitintervalle implizieren.

Diese neuartigen Ergebnisse und Algorithmen erlauben die Analyse von Transportphänomenen im Ozean. Als Anwendung wird die erste drei-dimensionale

Untersuchung eines Agulhas-Ringes dargestellt. Aus diesem Blickwinkel heraus zeigen diese Ergebnisse eine neue Perspektive für die Analyse von Transportphänomenen im Ozean auf.

Contents

CHAPTER 1

Introduction

In nature, we are faced with countlessly many complex processes that change their behavior over time: the wind blowing on the earth – for instance – or the currents flowing in the ocean. In many situations, the related transport of mass is significant. The climate, for example, is directly affected by the transport of heat by the wind and the currents in the ocean. Both the atmosphere and the ocean consist of different thermal zones, which are subject to temporal variation as the seasons change. In fact, the transport of heat between these thermal zones is little. The study of such zones or – more generally – structures interacting weakly with their environment is relevant in many applications. Similar phenomena also arise in the ocean in form of eddies – for instance – capturing pollutant over long periods of time.

In this thesis, we focus on such types of structures induced by various kinds of processes and develop numerical tools for their efficient approximation. In nature and sciences the underlying processes are generally driven by deterministic principles: Scientific experiments are subject to physical laws, particles in the ocean move according to the oceanic fluid flow.

In the following, we outline the thesis by introducing the main concepts our subsequent considerations are based on.

Dynamical Systems

The notion of *dynamical systems* provides a formal framework for the mathematical modeling of various kinds of processes. They formally consist of a set $\mathbb{T}$ representing *time*, a set X of *states* and an *evolution law*

$$\phi : X \times \mathbb{T} \times \mathbb{T} \to X$$

describing the behavior of the system in time. Mathematically, ϕ is required to fulfill certain fundamental conditions. The evolution law maps a state $x \in X$ at time $t \in \mathbb{T}$ to the state $\phi(x, t, \tau) \in X$ after $\tau \in \mathbb{T}$ time-units. Time can be modeled in a general way by an arbitrary *driving system* on $\mathbb{T}$. However, in this thesis we restrict to the time shift $\sigma_\tau(t) = t + \tau$ which is a natural choice when dealing with real-world applications, i. e. $t + \tau$ is the point in time we arrive at when starting at time $t \in \mathbb{T}$ and passing τ time-units.

In mathematics, dynamical systems are treated in divers settings. We distinguish between autonomous and non-autonomous dynamical systems. *Autonomous* dynamical systems only depend on a state x and the duration τ, but *not* on the time instant t the process starts at: this translates to the fact that the evolution law ϕ does not explicitly depend on time. However, real world processes are often subject to time-dependence, thus in many cases autonomous dynamical systems are not suitable to describe the dynamical phenomena adequately. Such systems can be modeled as so-called *non-autonomous* dynamical systems which explicitly depend on time in contrast to autonomous dynamical systems. For an overview on dynamical system theory we refer to the textbooks [ASY00, BS02, Den05, KH97].

Coherent Structures in Dynamical Systems

Transport in dynamical systems is characterized by *coherent structures* which are minimally mixing structures in state space. There mainly exist two distinct approaches to the numerical approximation of coherent structures, the *proba-*

bilistic approach and the *geometric approach*. A first comparison of both can be found in [FP09].

In the geometric approach, barriers of transport are identified. In autonomous systems, invariant objects such as *invariant manifolds* directly form transport barriers which cannot be crossed by trajectories, whereas in the non-autonomous case, hyperbolic structures, so-called *Lagrangian coherent structures*, which can be thought of as time-dependent invariant material curves or surfaces, act as time-dependent barriers of transport. For a detailed introduction, we refer to [Hal00] and [HY00]. To analyze transport in the special but important situation of periodically driven non-autonomous dynamical systems, the concept of *lobe dynamics* of invariant manifolds can be used [MW98]. Recently, a more general concept has been developed characterizing transport barriers as time-dependent curves experiencing minimal stretching in state space [HB12]. The geometric approach has been followed for a variety of applications, e. g. the investigation of blood-flow [ST08] or the analysis of the particle dynamics in a hurricane [dM10].

In this thesis, we focus on the *probabilistic approach*, which is developed to directly detect slowly mixing structures. These structures are characterized by the probability that trajectories leave the structure within a certain time horizon. Instead of studying the evolution of single states we study the evolution of distributions of particles in state space and the corresponding evolution of the whole distribution with respect to the underlying dynamics. This approach is successfully applied in a variety of situations, e. g. for the identification of slowly mixing structures in the stratospheric polar vortex [FSM10, SFM10] or in the oceanic fluid flow [DFH$^+$09, FHR$^+$12, FPET07, FSPD08]. An overview of the probabilistic approach for the autonomous case can be found in [DFHP09] and for the non-autonomous case in [Fro13].

Coherence Ratio

In particular, our interest focuses on the statistical long-term behavior of dynamical systems. We are especially interested in regions in the ocean in which plankton remains over a sufficiently long time. From the dynamical systems point of view, we aim to uncover subsets A_1, A_2 of the set X of states for which the probability is high that a state of the set A_1 will be in A_2 after a fixed time. To identify such sets we analyze the probability of ending up in A_2 after starting in A_1 at time t and flowing τ time-units. More precisely, we define the *coherence ratio*

$$\rho_t^\tau(A_1, A_2) = \frac{m(A_1 \cap \phi(A_2, t+\tau, -\tau))}{m(A_1)}$$

of two subsets A_1 and A_2 of the state space, where m denotes the Lebesgue measure on X. This notion of coherence is used to define *coherent pairs* in non-autonomous systems [FSM10] and goes back to the definition of *almost invariant sets* in autonomous systems [DJ99].

Since the flow of particles within the oceanic domain can be described by a dynamical system, the search for subsets A_1 and A_2 with coherence ratio close to one can be interpreted as follows: Water particles released in A_1 at a specific time end up in the set A_2 with a high probability after flowing over a fixed time. Consequently, this concept can be used to describe *oceanic structures* like eddies and gyres (cf. e. g. [DFH$^+$09, FHR$^+$12, FPET07, FSPD08]). Other examples for applications are hurricanes which also transport particles over a specific period of time through the atmosphere (cf. for instance [dM10]).

Transfer Operators

The distribution of particles in the state space X at time $t \in \mathbb{T}$ can be mathematically described by a measure $\mu_t : \mathcal{B}(X) \to \mathbb{R}$ on the Borel-σ algebra $\mathcal{B}(X)$ of X or, if it exists, by its corresponding density. Figure 1.1a shows the density of a measure on a state space X. The coloring describes the

concentration of mass where the red region indicates a high concentration of mass, while the blue region represents a comparatively low concentration.

The main tool we make use of in this thesis is the so-called *transfer operator* $\mathcal{P}_t^\tau : \mathcal{M}(X) \to \mathcal{M}(X)$ of a dynamical system for $t, \tau \in \mathbb{T}$, where $\mathcal{M}(X)$ denotes the space of signed measures on the state space X. This operator describes the evolution of measures or densities on X with respect to the evolution law ϕ. Let μ_t be a measure describing the distribution of mass at time $t \in \mathbb{T}$, then the measure

$$\mathcal{P}_t^\tau \mu_t = \mu_{t+\tau},$$

describes the distribution of mass at time $t + \tau$. This operator is used in the autonomous as well as in the non-autonomous case for the study of transport phenomena and it naturally induces a dynamical system on the set of measures.

A measure μ that satisfies $\mathcal{P}_t^\tau \mu = \mu$ for all $t, \tau \in \mathbb{T}$ is called an *invariant measure* of the underlying dynamical system. Such measures, if they exist, give rise to physically meaningful distributions of states in state space. These are studied in [BP02, LY73], for instance. However, we are interested in measures which are not strictly fixed but very persistent under the application of the transfer operator. Let us consider the density shown in Figure 1.1a: if we apply the transfer operator $\mathcal{P}_t^\tau$ to the corresponding measure for fixed $t, \tau \in \mathbb{T}$, we obtain a distribution of mass at time $t + \tau$ described by a density which is shown in Figure 1.1b. It is easily seen that the initial concentration of mass on the left side of the state space at time t is transported to a final concentration of mass on the right side of the state space at time $t + \tau$. In this thesis, we aim at the numerical identification of measures exhibiting a slow decay and, therefore, as will be seen later, indicate by their level-sets the presence of persistent structures.

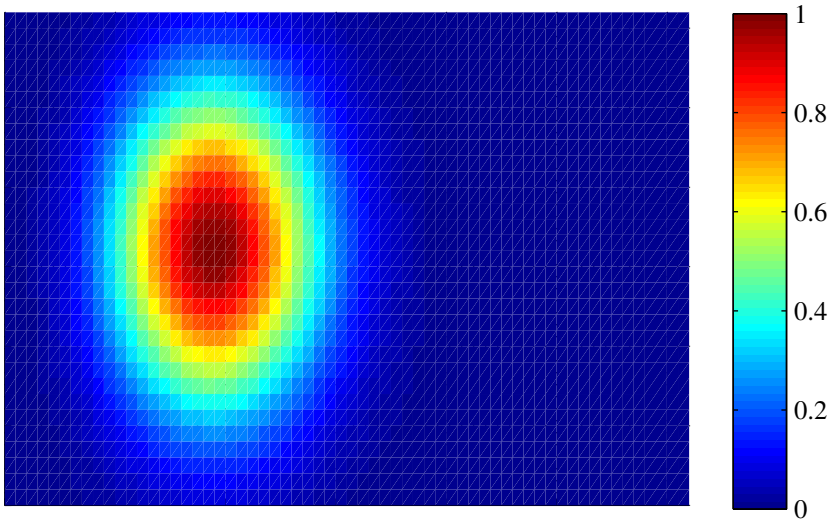

(a)

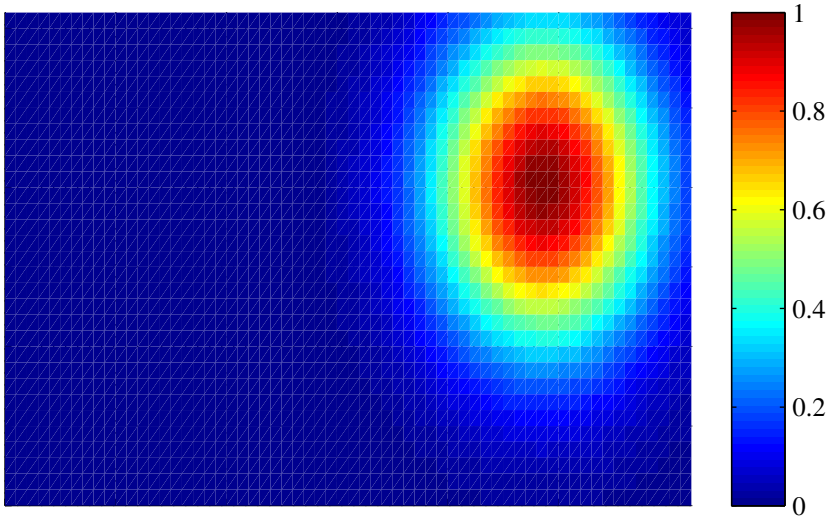

(b)

FIGURE 1.1: Densities of measures on the state space X describing the distribution of mass on X at time t (a) and time $t + \tau$ (b). The coloring relates to the concentration of mass where red indicates a high concentration and dark blue a vanishing concentration of mass.

Transition Matrix

For the numerical treatment of the transfer operator $\mathcal{P}_t^\tau$, the computation of a finite-dimensional representation is necessary. This is realized by projecting the infinite-dimensional space of measures to a suitable finite-dimensional space and we then numerically obtain the matrix representation of $\mathcal{P}_t^\tau$ on the according projected space which also works in the non-autonomous case. This ansatz goes back to Ulam [Ula60]. For instance, in [JK09], a certain Haar basis is considered. However, the most common way is to project the space of measures to the space of piecewise constant functions on a partition of X and to calculate the matrix representation which we refer to as the *transition matrix* $P^{t,\tau}$ (cf. e. g. [DJ99]). The entries of the matrix $P^{t,\tau}$ represent the probability for ending up in one partition element when starting in another partition element. In the autonomous case, it is also possible to approximate the corresponding finite-dimensional generator [FJK13].

Numerical Analysis of Transport

The interpretation of the evolution of a dynamical system in the context of measures and their corresponding transfer operators with respect to the dynamics has led to the development of a variety of methods to analyze transport phenomena. In the autonomous case *almost invariant sets* can be identified which are subsets of the state space with a coherence ratio close to one. It is shown by Dellnitz et al. [DJ99] that a closed level-set of an eigenmeasure corresponding to an eigenvalue close to one of the transfer operator $\mathcal{P}^\tau$ defines an almost invariant set. This approach has been successfully used to identify almost invariant sets in engineering applications like Chua's circuit (cf. [DJ97]) as well as in real world applications like the solar system (cf. [DJL$^+$05]).

The transition matrix corresponding to a transfer operator induces a finite Markov chain in a natural way and therefore we can apply methods developed for the analysis of Markov chains to analyze transport phenomena in the underlying dynamical system. With this notion, it is also possible to obtain

results on the eigenvectors of eigenvalues close to one of the transition matrix (cf. [FD03]). Based on the transition matrix one can also calculate rates of transport between two different regions in the state space. This has been used for example in [DJL+05] to analyze transport rates of asteroids in the solar system. In that contribution, also graph partitioning algorithms are utilized to analyze the graph induced by the transition matrix to identify regions in state space which are characterized by relatively little mixing with their surrounding.

The results obtained in the autonomous case have been extended to the approximation of transport phenomena in non-autonomous dynamical systems in the last years. As an example, spatially fixed structures can be identified as almost invariant sets in non-autonomous dynamical systems. A fully three-dimensional study of the subpolar gyres can be found in [DFH+09] which is based on the methods presented in this thesis. Furthermore, *coherent pairs* have been introduced by Froyland et al. [FSM10] which have to be viewed as a generalization of almost invariant sets in a non-autonomous framework. Such pairs of sets are characterized by a large coherence ratio. It is shown that the corresponding structures can be uncovered by singular vectors of singular values close to one of the normalized transition matrix. However, these structures often appear over large time horizons and therefore the transition matrix over a long time horizon has to be calculated which is numerically very expensive.

Outline and Contribution

The purpose of this thesis is to obtain theoretical results as well as to design efficient methods for the approximation of transport phenomena in non-autonomous dynamical systems based on transfer operators. There is a definitive need for such methods, since state-of-the-art methods rely on long-term simulations of the dynamical system which are numerically extremely costly. We exploit certain properties of the transfer operator and deal with products of transition matrices for the accurate approximation of transport phenomena. In this context, we obtain an error bound. Additionally, this approach can be used to visualize the pathways of transport. Also, we combine the concept of almost

invariant sets and coherent pairs to efficiently calculate coherent structures in non-autonomous dynamical systems. A theoretical result is presented describing this relation as well as a successful application of the developed techniques to the oceanic fluid flow to identify slowly mixing structures like eddies and gyres. This application is the first three-dimensional study of oceanic structures and gives a new perspective for the analysis of oceanic processes. Thereby, this thesis yields a relevant contribution to the efficient numerical approximation of coherent structures in non-autonomous dynamical systems as well as their application to the oceanic fluid flow.

The outline of this thesis is as follows: In **Chapter 2** we begin by formally introducing autonomous and non-autonomous dynamical systems and present some basic ergodic theoretic concepts. In particular, we introduce the concept of transfer operators for dynamical systems and describe a relevant approximation method.

The concepts we apply in this thesis in order to analyze transport in dynamical systems are formally described in **Chapter 3**. After we have introduced the coherence ratio of two subsets in the state space of a dynamical system, we embed almost invariant sets in the non-autonomous setting and discuss the definition of coherent pairs and corresponding state-of-the-art methods for their detection.

It is the purpose of **Chapter 4** to introduce a novel method for the approximation of transport phenomena over a sufficiently long time interval. We make use of the cocycle property of transfer operators in order to approximate a transfer operator by a product of transition matrices over even shorter time intervals. The single transition matrices can be calculated very efficiently and we avoid the explicit calculation of the product for the calculation of eigenvalues and singular values. It is shown that under certain assumptions a single transition matrix can be considered as a product of transition matrices. We conclude the chapter by introducing a novel algorithm to achieve this splitting automatically and show the effectiveness of the method by an example.

We prove in **Chapter 5** that coherent pairs in non-autonomous dynamical systems imply the existence of almost invariant sets over short time intervals under some weak assumptions. Based on this theoretic result a novel algorithm is proposed that firstly approximates almost invariant sets and secondly identifies coherent pairs within these almost invariant sets. The efficiency of this method is demonstrated by an example where we can reduce the computational effort significantly. The results of this chapter have already been published in [DH12].

The theoretical results of the previous chapters and the developed algorithms enable us to analyze transport phenomena within the oceanic fluid flow. This is presented in **Chapter 6**. Here, we document two successful applications of our results: The first one is the first fully three-dimensional investigation of the subpolar gyres and the second one is the first three-dimensional study of a single Agulhas ring over a sufficiently long time interval.

We conclude the thesis with **Chapter 7** by summarizing the results and discussing further directions of research.

CHAPTER 2

Dynamical System Theory - Basic Concepts

In this chapter, we set up the notation and terminology of *dynamical system theory* used in this thesis. For a comprehensive overview of dynamical system theory, we refer to [ASY00, BS02, Den05, KH97]. In Sections 2.1 and 2.2 we begin with a brief exposition of *autonomous* and *non-autonomous dynamical systems*, following [Arn98, Den05, KKS99, KS97]. For the treatment of non-autonomous dynamical systems, we introduce the general concept of *cocycles* which allows us to study both continuous and discrete systems. Beside mathematical notation, we discuss how cocycles can be generated using ordinary differential equations and difference equations. Section 2.3 provides a short exposition of *ergodic theory*. Here, we define basic measure-theoretic concepts and present their relation to the long-term behavior of dynamical systems. In the last section, we introduce *transfer operators* on a measure space and discuss some properties which will be important in Chapter 3 for the analysis of transport. Moreover, we provide a finite-dimensional approximation for the numerical treatment.

2.1 Autonomous Dynamical Systems

In this section, we introduce the terminology of time-independent (autonomous) dynamical systems following [Den05] even though it is not the purpose of this thesis to study autonomous systems. However, as we will see later, results from the autonomous case can be used for the efficient treatment of transport phenomena in non-autonomous dynamical systems. We start with a basic definition:

2.1 Definition (Autonomous Dynamical System)**:** *A family of mappings* $\sigma = \{\sigma_t : X \to X\}_{t\in\mathbb{T}}$ *on a non-empty set* X*, where* $(\mathbb{T}, +)$ *is a (semi)group, is called an* autonomous dynamical system *if*

1. $\sigma_0 = id_X$ *and*
2. $\sigma_{t_1+t_2} = \sigma_{t_1} \circ \sigma_{t_2} \quad \forall t_1, t_2 \in \mathbb{T}$

are satisfied.

In the following, we will represent an autonomous dynamical system by the tuple $(\sigma, X, \mathbb{T})$, where X denotes the *state space*, $\mathbb{T}$ the *time* and σ is called the *evolution* of the autonomous dynamical system. Throughout this thesis, the time $\mathbb{T}$ will be additive and either continuous, $(\mathbb{R}, +)$, or discrete, $(\mathbb{Z}, +)$. Furthermore, by $\mathbb{T}^+$ we denote the positive elements of $\mathbb{R}$ or $\mathbb{Z}$, respectively.

2.2 Remark (Continuous Autonomous Dynamical Systems)**:** *Consider an ordinary differential equation*

$$\dot{x} = f(x), \tag{2.1}$$

where $f : X \to \mathbb{R}^m$ *is a vector field on an* m*-dimensional vector space* X*. Assume that for every initial condition* $x(0) = x_0$*,* $x_0 \in X$*, there exists a unique solution* $x : \mathbb{R} \to X$ *of Equation* (2.1)*. Then* $(\{\sigma_t : X \to X\}_{t\in\mathbb{R}}, X, \mathbb{R})$*,*

with $\sigma_t x_0 = x(t)$ represents a continuous autonomous dynamical system. By $\sigma_t x_0$ we denote the endpoint of a trajectory starting in x_0 after flowing for t time-units. The autonomous dynamical system $(\{\sigma_t \colon X \to X\}_{t\in\mathbb{R}}, X, \mathbb{R})$ reflects the dynamics induced by the ordinary differential equation (2.1).

2.3 Remark (Discrete Autonomous Dynamical Systems)**:** *Let $T : X \to X$ be a mapping on a non-empty set X. Then $(\{\sigma_t : X \to X\}_{t\in\mathbb{Z}^+}, X, \mathbb{Z}^+)$ with*

$$\sigma_t : X \to X, \quad \sigma_t x = T^t(x)$$

represents a discrete autonomous dynamical system.

The following simple example of a continuous dynamical system will be repeatedly revisited throughout this thesis – in particular in Chapter 5 to illustrate an efficient algorithm for the approximation of transport.

2.4 Example: *Let us consider the following ordinary differential equation on the state space $X = [0, 2\pi] \times [0, \pi]$:*

$$\begin{aligned} \dot{x} &= A\sin(x - \nu t)\cos(y) + \epsilon\sin(2t)G(g(x, y, t)), \\ \dot{y} &= \cos(x - \nu t)\sin(y) \end{aligned} \tag{2.2}$$

where $G(z) = \frac{1}{(z^2+1)^2}$ and $g(x, y, t) = -2\sin(x - \nu t)\sin(y) - \frac{\pi}{4} + \frac{y}{2}$.

Let us fix the parameters $\nu = 0$, $A = -2$ and $\epsilon = 0$. Then, the system (2.2) *becomes autonomous and generates a simple double-gyre flow. Figure 2.1 shows the vector field of the ordinary differential equation* (2.2)*. As described in Remark 2.2, the ordinary differential equation defines a continuous autonomous dynamical system.*

This system is a slight modification of a differential equation which has been studied in [FLS10] with a nonzero parameter $\nu \in \mathbb{R}$. A similar system has also been considered in [SLM05], for instance, as a simplification of a double-gyre

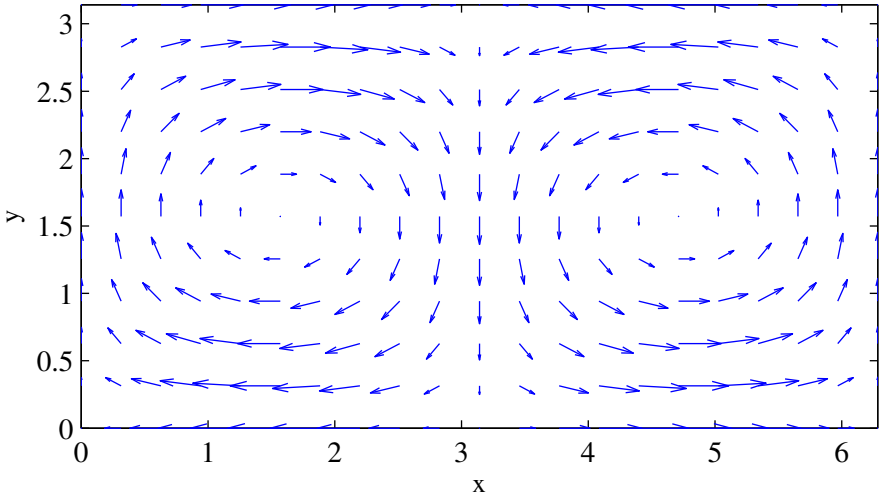

FIGURE 2.1: Vector field of the autonomous dynamical system defined by the ordinary differential equation (2.2) in Example 2.4.

pattern that often occurs in geophysical flows.

There are a variety of techniques for the analysis of autonomous dynamical systems. However, their detailed discussion will exceed the scope of this thesis, where our interest – in fact – mainly focusses on non-autonomous dynamical systems.

2.2 Non-Autonomous Dynamical Systems

In many applications, the evolution of the underlying dynamical system itself is subject to temporal changes. For example, the oceanic fluid flow explicitly depends on time. Such systems can be modeled as so-called *non-autonomous dynamical systems* which depend – in contrast to autonomous systems – on

an additional temporal parameter. In a more general setting, this dependence can also be interpreted as a random behavior of the underlying dynamics and thus, from that point of view, non-autonomous dynamical systems are closely related to random dynamical systems (cf. [Arn98]). In the following, we provide a formal definition of a non-autonomous dynamical system which follows the ones in [KS97, KKS99].

2.5 Definition (Non-Autonomous Dynamical System)**:** *A non-autonomous dynamical system on a non-empty state space X is given by an autonomous dynamical system $(\sigma, \Omega, \mathbb{T})$ and a map $\phi : \mathbb{T}^+ \times \Omega \times X \to X$ which satisfies the* cocycle property*, i. e.*

1. $\phi(0, \omega, \cdot) = id_X, \quad$ *and*
2. $\phi(t + t', \omega, \cdot) = \phi(t, \sigma_{t'}\omega, \phi(t', \omega, \cdot))$,

for all $t, t' \in \mathbb{T}^+$, $\omega \in \Omega$, and $x \in X$.

For the simplicity of notation, we write $\phi^t_\omega(x)$ instead of $\phi(t, \omega, x)$. Note that the cocycle is only defined on $\mathbb{T}^+$. If the cocycle is invertible, i. e. the map $\phi(-t, \omega, \cdot)$ exists for all $t \in \mathbb{T}^+$ and $\omega \in \Omega$, then ϕ can be defined for all $t \in \mathbb{T}$.

According to the preceding definition, a non-autonomous dynamical system is given by the tuple $(\phi, X, (\sigma, \Omega, \mathbb{T}))$, where time is controlled in terms of an autonomous dynamical system $(\sigma, \Omega, \mathbb{T})$ which is often referred to as the so-called *driving system*. This construction has technical reasons and is of principal importance in the context of the *Multiplicative Ergodic Theorem* (cf. [Arn98] and [FLQ09]). However, in many real world examples, e. g. the oceanic fluid flow (cf. Chapter 6), the autonomous dynamical system which keeps track of the time is given by $(\sigma, \mathbb{T}, \mathbb{T})$, with $\mathbb{T} = \mathbb{R}$ for the continuous case or $\mathbb{T} = \mathbb{Z}$ for the discrete case and with $\sigma_t s = t + s$ for all $t, s \in \mathbb{T}$. All applications studied in the following fall into this category and thus, for the remainder of this thesis, we will always assume that the underlying driving system is of such a

simple form. Therefore, unless stated otherwise, we identify a non-autonomous dynamical system with the triple $(\phi, X, \mathbb{T})$, where ϕ denotes the cocycle, X the state space and $\mathbb{T} = \mathbb{R}$ or $\mathbb{T} = \mathbb{Z}$ the time set.

In an analogous manner as in Remarks 2.2 and 2.3, non-autonomous dynamical systems are generated for example by ordinary differential equations or difference equations.

2.6 Remark (Continuous Non-Autonomous Dynamical Systems)**:** *Consider a non-autonomous ordinary differential equation*

$$\dot{x} = f(x, t), \tag{2.3}$$

where

$$f \colon X \times \mathbb{R} \to \mathbb{R}^m$$

is a time-dependent vector field on a m-dimensional vector space X. Let f be sufficiently smooth such that for every initial condition $x(t_0) = x_0$, $x_0 \in X$, $t_0 \in \mathbb{R}$, there exists a unique solution $x \colon \mathbb{R} \to X$. Then, the triple $(\phi, X, \mathbb{R})$ with $\phi \colon \mathbb{R} \times \mathbb{R} \times X \to X$ defined by $\phi_{t_0}^{\tau}(x_0) = x(\tau)$ represents a (continuous) non-autonomous dynamical system which satisfies the cocycle property (cf. [Arn98]).

2.7 Remark (Discrete Non-Autonomous Dynamical Systems)**:** *Let*

$$x_{n+1} = f_n(x_n),$$

where $f_n : \mathbb{R}^m \to \mathbb{R}^m$ $(n \in \mathbb{Z})$ are invertible continuous mappings. Then

$(\phi, \mathbb{R}^m, \mathbb{Z})$ *with*

$$\phi\colon \mathbb{Z}\times\mathbb{Z}\times\mathbb{R}^m \to \mathbb{R}^m, \quad \phi_l^r(x) = \begin{cases} (f_{l+r-1}\circ\ldots\circ f_{l+1}\circ f_l)(x) & \text{for } r \geq 1, \\ x & \text{for } r = 0 \\ (f_{l-(r+1)}^{-1}\circ\ldots\circ f_{l-1}^{-1}\circ f_l^{-1})(x) & \text{for } r \leq -1 \end{cases}$$

represents a (discrete) non-autonomous dynamical system which again satisfies the cocycle property.

2.3 Ergodic Theory

The tools we make use of in this thesis for the treatment of transport phenomena have in common that they consider distributions of trajectories on the state space rather than single trajectories. Therefore, these techniques are suitable for the study of mass transport in state space. In this section, we introduce the relevant ergodic theoretical background which allows us to study the long-term behavior of dynamical systems. For an overview of classical ergodic theory, we refer to [BS02], [KH97] and [Nad98]. Additionally we refer to [Doo94] for an overview of measure theory. The relevance of these concepts for the treatment of transport phenomena is emphazised – for instance – by a series of publications [DJ99, DJK$^+$05, FD03, FLQ09, FPET07, FSM10, HS05, SHD01]. We discuss the corresponding techniques in Chapter 3.

For a quantitative study of the evolution of mass in a dynamical system, it is sufficient to provide a framework for the statistical distribution of trajectories in the state space. The remainder of this section relies on a given non-autonomous dynamical system $(\phi, X, (\sigma, \Omega, \mathbb{T}))$, where $(\sigma, \Omega, \mathbb{T})$ is an autonomous dynamical system. Furthermore, we assume that X and Ω are metric spaces and we denote by $\mathcal{B}(X)$ or $\mathcal{B}(\Omega)$ the Borel-σ algebra of X and Ω, respectively. We call a function $\mu\colon \mathcal{B}(X), \mathcal{B}(\Omega) \to \mathbb{R}$ a measure on $\mathcal{B}(X)$ and $\mathcal{B}(\Omega)$, respectively, if it is countably additive, i. e. $\mu(\cup_{i\in I} E_i) = \sum_{i\in I}\mu(E_i)$ holds for all countable

collections $\{E_i\}_{i\in I}$ of pairwise disjoint sets in $\mathcal{B}(X)$ and $\mathcal{B}(\Omega)$. We denote by $\mathcal{M}_{\mathcal{B}(X)}$ and $\mathcal{M}_{\mathcal{B}(\Omega)}$ the set of measures on $\mathcal{B}(X)$ and $\mathcal{B}(\Omega)$, respectively.

Moreover, by

$$\mathcal{M}(X) = \{\mu | \mu \in \mathcal{M}_{\mathcal{B}(X)}, \mu(X) < \infty\},$$

we denote the set of bounded signed measures on X. The set $\mathcal{M}(X)$ is a linear space and can be equipped with the variational norm which is given by

$$\|\mu\|_V = \sup \sum_{k=1}^{n} |\mu(E_i)|, \tag{2.4}$$

for a measure $\mu \in \mathcal{M}(X)$, where the supremum is taken over all finite decompositions $\{E_1, \ldots, E_n\}$ into pairwise disjoint measurable subsets of the state space X. The norm properties are proven in [Rud87], for example. Later, we define an operator on $\mathcal{M}(X)$ which describes the temporal development of measures on the state space of a dynamical system.

Descriptively speaking, a measure describes the statistical distribution of trajectories in the state space of the according dynamical system. For an understanding of the long-term behavior of the system, it is important to identify the distribution of trajectories as time goes to infinity. Let us first consider the autonomous case. The measure μ given by

$$\mu(A) = \lim_{\tau\to\infty} \frac{\#\{\sigma_t(x) \in A : 0 \leq t < \tau\}}{\tau}$$

for Lebesgue almost all $x \in X$, is called *physical invariant measure* and appears in the Ergodic Theorem of Birkhoff (cf. [Nad98]). If it exists, it is left invariant under the evolution of the dynamical system.

2.8 Definition (Invariant Measure for Autonomous Dynamical Systems)**:** *We call $\mu \in \mathcal{M}_{\mathcal{B}(\Omega)}$ an invariant measure of an autonomous dynamical system $(\sigma, \Omega, \mathbb{T})$ if $\mu \circ \sigma_{-\tau} = \mu$ for all $\tau \in \mathbb{T}$.*

The existences of invariant measures for continuous σ_τ is summarized in the Krylov-Bogolubov theorem (cf. [BS02]) and a proof for the existence of piecewise continuous σ_τ can be found in [LY73]. The numerical approximation of invariant measures has been the subject of several publications (cf. e. g. [Hun94, DJ99]). These measures can be identified, for instance, as fixed points of the so-called transfer operator which will be introduced in the next section.

For the more general non-autonomous case (cf. [Arn98]), the definition of an invariant measure can be extended as follows:

2.9 Definition (Invariant Measure for Non-Autonomous Dynamical Systems)**:** *We call a measure μ on $X \times \Omega$ an invariant measure of a non-autonomous dynamical system $(\phi, X, (\sigma, \Omega, \mathbb{T}))$, if the map*

$$\Theta(\tau) : X \times \Omega \to X \times \Omega, \;\; (x, t) \mapsto (\phi_t^\tau(x), \sigma_\tau t)$$

preserves the measure μ, i. e. $\mu \circ \Theta(-\tau) = \mu$ for all $\tau \in \mathbb{T}$.

In general, the measure μ explicitly depends on time. However, in many examples, especially the oceanic fluid flow (cf. Chapter 6), the three-dimensional volume measure is preserved all the time. Thus, in the following we restrict to measures in $\mathcal{M}(X)$ which are independent of time. The map $\Theta(\tau)$ for a $\tau \in \mathbb{T}$ is also called the skew-product of the non-autonomous dynamical system $(\phi, X, (\sigma, \Omega, \mathbb{T}))$. A discussion of the existence of invariant measures of a non-autonomous dynamical system as well as a discussion of skew-products can be found in [Arn98].

2.4 Transfer Operators

In this section we introduce the concept of *transfer operators* which provide a powerful tool for the approximation of transport phenomena in dynamical

systems (cf. for instance [DJ99, Fro05] and the references therein). The transfer operator can be defined on the space of bounded signed measures $\mathcal{M}(X)$ and it can be used to describe the temporal development of a distribution of trajectories in the state space of a dynamical system. In the remainder of this section, we consider the case that the underlying non-autonomous dynamical system is given by $(\phi, X, \mathbb{T})$ and that the map $x \mapsto \phi_t^\tau(x)$ is continuous.

2.10 Definition (Transfer Operator)**:** *The transfer operator* $\mathcal{P}_t^\tau : \mathcal{M}(X) \to \mathcal{M}(X)$ *of a non-autonomous dynamical system* $(\phi, X, \mathbb{T})$ *is given by*

$$\mathcal{P}_t^\tau \mu(A) = \mu(\phi_{t+\tau}^{-\tau}(A)) \quad \forall A \in \mathcal{B}(X), t \in \mathbb{T}, \tau > 0.$$

For an arbitrary non-autonomous dynamical system, the cocycle is not necessarily invertible and thus, we denote by $\phi_{t+\tau}^{-\tau}(A)$ the pre-image of a set $A \subset X$. We also note that, therefore, the transfer operator itself is not necessarily invertible in general. It is also possible to define the transfer operator $\mathcal{P}_t^\tau$ on the space of Lebesgue-integrable functions $L^1(X)$ on the state space X by

$$\int_A \mathcal{P}_t^\tau f dm = \int_{\phi_{t+\tau}^{-\tau}(A)} f dm \quad \forall A \in \mathcal{B}(X).$$

If $f \in L^1(X)$ is the density of a measure μ, then the two definitions are equivalent. Furthermore, if f describes the distribution of mass at time t in the state space X, then the image $\mathcal{P}_t^\tau f$ describes the distribution of the initial mass after applying the cocycle of the dynamical system over time τ.

Some basic properties of the transfer operator are summarized in the following lemma:

2.11 Lemma (Properties of Transfer Operators)**:** *Let* $(\phi, X, \mathbb{T})$ *be a non-autonomous dynamical system and* $\mathcal{P}_t^\tau$ *for* $t, \tau \in \mathbb{T}$ *the corresponding transfer operator. Then the following holds:*

1. *$\mathcal{P}_t^\tau$ is linear.*
2. *A measure $\nu \in \mathcal{M}(X)$ is a fixed point of $\mathcal{P}_t^\tau$, i. e. $\mathcal{P}_t^\tau \nu = \nu$, if and only if ν is an invariant measure.*
3. *For an eigenmeasure[1] $\nu \in \mathcal{M}(X)$ with corresponding eigenvalue $\lambda \neq 1$ of $\mathcal{P}_t^\tau$, one has $\nu(X) = 0$ because*

$$\lambda\nu(X) = (\mathcal{P}_t^\tau \nu)(X) = \nu(\phi_{t+\tau}^{-\tau}(X)) = \nu(X), \ \forall t, \tau \in \mathbb{T}. \tag{2.5}$$

Moreover, the transfer operator naturally inherits the properties of the one-sided cocycle of the dynamical system (cf. [FLQ09]).

2.12 Proposition (Transfer Operator Cocycle)**:** *For a given non-autonomous dynamical system $(\phi, X, \mathbb{T})$, the transfer operator satisfies the one-sided cocycle property.*

Proof.

$$\mathcal{P}_t^0 \mu(A) = \mu(\phi_t^0(A)) = \mu(A), \quad \forall \mu \in \mathcal{M}(X), A \in \mathcal{B}(X), t \in \mathbb{T},$$

and

$$\begin{aligned}
\mathcal{P}_t^{\tau_1+\tau_2}\mu(A) &= \mu(\phi_{t+\tau_1+\tau_2}^{-(\tau_1+\tau_2)}(A)) \\
&= \mu(\phi_{t+\tau_1}^{-\tau_1}(\phi_{t+\tau_1+\tau_2}^{-\tau_2}(A))) \\
&= \mathcal{P}_t^{\tau_1}\mu(\phi_{t+\tau_1+\tau_2}^{-\tau_2}(A)) \\
&= \mathcal{P}_{t+\tau_1}^{\tau_2}(\mathcal{P}_t^{\tau_1}\mu(A)) \quad \forall \mu \in \mathcal{M}(X), A \in \mathcal{B}(X), \forall t \in \mathbb{T}, \tau_1, \tau_2 \in \mathbb{T}^+
\end{aligned}$$

□

[1] For an eigenvalue λ of a transfer operator $\mathcal{P}_t^\tau$, we call μ the corresponding eigenmeasure if $\mathcal{P}_t^\tau \mu = \lambda\mu$ holds.

Therefore, the tuple $(\widetilde{\phi}, \mathcal{M}(X), \mathbb{T})$ with $\widetilde{\phi}_t^\tau(\nu) = \mathcal{P}_t^\tau \nu$ for all $t, \tau \in \mathbb{T}$ defines a non-autonomous dynamical system which can be analyzed using dynamical system theory.

Finite-Dimensional Approximation

In this thesis, we focus on the approximation of transport phenomena. However, we will see later that the information on spectral properties is crucial for the understanding of transport processes. In order to extract such spectral properties of the transfer operator $\mathcal{P}_t^\tau$ of a non-autonomous dynamical system, we have to approximate $\mathcal{P}_t^\tau$ by a finite-dimensional representation.

There are several approaches to obtain a finite-dimensional representation. They all rely on the same ansatz which goes back to Ulam [Ula60]. The most common one is to calculate the finite-dimensional representation of a transfer operator on a space of piecewise constant functions (cf. e. g. [DJ99]). Here, one has to numerically compute transition probabilities between disjoint subsets of the state space which can be carried out either by a Monte-Carlo approach [Hun94] or by an exhaustion technique if the map $x \mapsto \phi_t^\tau(x)$ is locally Lipschitz [DFJ01]. Instead of piecewise constant functions, one can consider a certain Haar basis for the finite-dimensional representation of the transfer operator (cf. [JK09]). Alternatively, for autonomous dynamical systems, instead of approximating the transfer operators $\mathcal{P}^\tau$ for each fixed τ individually, one can approximate the so-called generator of the semi-group induced by the transfer operators $\{\mathcal{P}^\tau\}_{\tau \in \mathbb{T}}$ (cf. [FJK13]).

In the following we give a brief overview of the most natural approximation method, which we use for the algorithms in this thesis following [DJ99]. The starting point is a partition of the state space X into $N \in \mathbb{N}$ disjoint subsets $\mathcal{B} = \{B_1, \ldots, B_N\}$. For simplicity, we assume that the subsets in $\mathcal{B}$ are n-dimensional boxes with $n = \dim(X)$. The partition into boxes can be efficiently carried out with the software package GAIO [DFJ01] which successively bisects

the state space into boxes using a binary tree for the storage. The partition is the discrete structure in which we look for coherent structures, e. g. unions of subsets $A = \cup_{i \in I} B_i$ which have little mixing with their surrounding. To obtain a good approximation, the sets in the partition have to be chosen sufficiently small. Then, we define for each $i \in \{1, \ldots, N\}$ indicator functions $\chi_{B_i} : X \to \mathbb{R}$, with $\chi_{B_i}(x) = 1$ if $x \in B_i$ and $\chi_{B_i}(x) = 0$ otherwise. The space $\mathcal{N} = \text{span}\{\frac{1}{m(B_1)}\chi_{B_1}, \ldots, \frac{1}{m(B_N)}\chi_{B_N}\}$ spanned by the indicator functions of a partition can be interpreted as a finite-dimensional space of densities on the state space. Furthermore, we calculate the finite-dimensional representation of $\mathcal{P}_t^\tau$ on $\mathcal{N}$ using the projection $\pi : L^1(X) \to \mathcal{N}$ with

$$\pi f = \sum_{i=1}^{N} \frac{1}{m(B_i)} \chi_{B_i} \int_{B_i} f dm,$$

where m denotes the Lebesgue measure on X. The entries of the representation matrix $P^{t,\tau} \in \mathbb{R}^{N,N}$ of $\mathcal{P}_t^\tau$ are given by

$$P_{ij}^{t,\tau} = \frac{m(\phi_{t+\tau}^{-\tau}(B_i) \cap B_j)}{m(B_j)}. \tag{2.6}$$

These can be interpreted as the probability that a trajectory which starts in box B_j at time t ends in box B_i after flowing τ time-units. Therefore, we call the matrix $P^{t,\tau}$ a *transition matrix*. This matrix is the finite-dimensional representation of the transfer operator $\mathcal{P}_t^\tau$.

2.13 Remark (Markov Chain Interpretation)**:** *Consider an autonomous dynamical system with discrete time $\mathbb{T} = \mathbb{Z}$. If we denote the partition $\mathcal{B}$ as the set of states, then P^1 defines a transition matrix of a discrete time Markov chain (cf. [Bré99]). Additionally, such a transition matrix defines a transition graph where the nodes are the states in $\mathcal{B}$. Hence, many of the concepts described in this thesis are inspired by results in Markov chain theory and graph theory.*

Numerical Realization

For a numerical realization of Equation (2.6), the calculation of the Lebesgue measure of $\phi_{t+\tau}^{-\tau}(B_i) \cap B_j$ for each combination of two boxes in the present partition has to be performed. To this end, we apply a Monte Carlo approach as suggested in [DHJR97] and approximate $m(\phi_{t+\tau}^{-\tau}(B_i) \cap B_j)$ by $\sum_{k=1}^{K} \chi_{B_i}(\phi_t^{\tau}(p_{j,k}))$, where $p_{j,k} \in B_j$ are the so-called $K \in \mathbb{N}$ test points which are chosen on the basis of a uniform distribution in B_j. In more detail, we form the numerical realization

$$\widetilde{P}_{ij}^{t,\tau} = \frac{\sum_{k=1}^{K} \chi_{B_i}(\phi_t^{\tau}(p_{j,k}))}{K} \tag{2.7}$$

of P_t^{τ}. A crucial point in the computation of $\widetilde{P}_{ij}^{t,\tau}$ is the number of test points representing the box B_j and, therefore, the image $\phi(t, \tau, B_i)$ after flowing τ time-units. The appropriate amount of test points directly depends on the flow time τ and therefore influences the computational effort significantly. In Chapter 4, we develop an approach aiming at the reduction of the number of test points without loosing accuracy in the approximation. The binary tree representing the box partition within the software package GAIO [DFJ01] allows a very efficient search for the box which contains a fixed state $x \in X$.

2.14 Remark: *In some applications, the relevant information for the identification of transport phenomena is captured by a subset S of the state space X and its image $\phi_t^{\tau}(S)$. Therefore, it is not necessary to discretize the entire state space X. In such situations, the subset S is covered by an initial partition $\mathcal{B} = \{B_1, \ldots, B_{M_1}\}$ and its image under ϕ is covered by a second partition $\mathcal{C} = \{C_1, \ldots, C_{M_2}\}$. Consequently, the entries of the transition matrix restrict to the probabilities that a trajectory starts within a set of the partition $\mathcal{B}$ and ends within a set of the partition $\mathcal{C}$. Later, we present an algorithm that preselects a subset S which contains all relevant dynamical information. The benefit is that the approximation of the transfer operator can be performed with less computational effort on a smaller subset S than on the whole state space.*

CHAPTER 3

Transport in Dynamical Systems

The main contribution of this thesis is the development of an efficient approximation method for transport phenomena in dynamical systems and the application of the presented algorithms. To this aim, we provide concepts for the treatment of transport phenomena in dynamical systems in this chapter. There mainly exist two branches, the *probabilistic approach*, which we are going to make use of in this thesis and the *geometric approach*. An overview and a first comparison of both can be found in [FP09].

In the geometric approach, barriers of transport are identified, e. g. by approximating *finite-time hyperbolic structures* which separate certain regions in state space. In the autonomous setting, *invariant manifolds* directly form transport barriers which cannot be crossed by trajectories, whereas in the non-autonomous case, hyperbolic structures, so-called *Lagrangian coherent structures*, have been identified as transport barriers. For more details, we refer to [Hal00] for the two-dimensional and to [HY00] for the three-dimensional case. Numerically, such structures can be approximated, in the autonomous as well as in the non-autonomous case, by the *expansion rate approach* [Pad05], for example. To analyze transport in periodically driven non-autonomous dynamical systems, for instance, *lobe dynamics* of invariant manifolds can be used [MW98]. A

more general concept consists in the identification of time dependent curves experiencing minimal stretching in state space acting as transport barriers [HB12].

The geometric approach has been used for a variety of applications, e. g. the investigation of blood-flow [ST08] or the analysis of the particle dynamics in a hurricane [dM10].

The probabilistic approach – on the contrary – focuses on the approximation of *coherent structures* which are structures in state space mixing slowly with their neighborhood. In the autonomous setting, so-called *almost invariant sets* can be identified by the analysis of the transfer operator of the dynamical system. This approach goes back to Dellnitz and Junge [DJ99] and has been successfully applied to a variety of problems e. g. to analyze transport in dynamical astronomy [DJK$^+$05, DJL$^+$05]. In the time-dependent setting, the so-called *coherent pairs* serve as a time-dependent analog to almost invariant sets. Similarly, the analysis of a time-dependent transfer operator and its corresponding finite-dimensional representation leads to the approximation of coherent pairs, which are characterized by the property that most of the mass is transported from one set into the other over a fixed finite time. This approach was developed by Froyland et al. [FSM10, SFM10]. Another concept is the approximation of the so-called Oseledets subspaces occurring in the *Multiplicative Ergodic Theorem* (cf. [Arn98]). In more detail, Lyapunov exponents of the corresponding time-dependent transfer operator cocycle are related to coherent structures in the state space of the underlying dynamical system, cf. [FLQ09, FLS10]. Transfer operator methods in the non-autonomous case have been successfully applied to the stratospheric polar vortex [FSM10, SFM10] or to identify slowly mixing oceanic structures in the oceanic fluid flow [DFH$^+$09, FHR$^+$12, FPET07, FSPD08].

For the analysis of transport, we make the following assumption throughout this chapter:

3.1 Assumption: *We consider a non-autonomous dynamical system* $(\phi, X, \mathbb{T})$ *and fix the initial time* $t \in \mathbb{T}$ *as well as the length of the duration* $\tau \in \mathbb{T}$ *over which we analyze transport phenomena.*

Within this setting, we begin in Section 3.1 by introducing the coherence ratio of two sets and use it to define and analyze *autonomous coherent structures* in Section 3.2. These are minimally mixing structures which are spatially fixed in the state space of the underlying non-autonomous dynamical system. We proceed in Section 3.3 with the definition and identification of minimally mixing structures which are mobile in state space. Later, in Chapters 4 and 5, we provide an efficient approximation method for these *non-autonomous coherent structures* and apply these techniques to the oceanic fluid flow in Chapter 6.

3.1 Coherence Ratio

In the autonomous as well as in the non-autonomous case, it is essential to quantify the amount of mass transported from one structure into another. This can be specified with respect to the physical reference measure $\mu \in \mathcal{M}(X)$ on the state space X by the so-called *coherence ratio*.

3.2 Definition (Coherence Ratio)**:** *Let* $\mu \in \mathcal{M}(X)$ *be a probability measure on* X*. For two sets* $A_1, A_2 \subset X$ *with* $\mu(A_1) > 0$*, the* coherence ratio *over the time interval* $[t, t+\tau]$ *is defined as*

$$\rho_t^\tau(A_1, A_2) := \frac{\mu(A_1 \cap \phi_{t+\tau}^{-\tau}(A_2))}{\mu(A_1)}.$$

The coherence ratio $\rho_t^\tau(A_1, A_2)$ for sets $A_1, A_2 \subset X$ is bounded from above by one. If $\rho_t^\tau(A_1, A_2) = 1$ holds, all of the mass of A_1 flows into the set A_2 over time τ. If $\rho_t^\tau(A_1, A_2) = 0$ no mass flows from A_1 to A_2. The reference measure μ is often chosen such that it is preserved by the cocycle, i. e. $\mu \circ \phi_t^\tau(A) = \mu(A)$

holds for every $t, \tau \in \mathbb{T}$ and $A \in \mathcal{B}(X)$. However, the choice of the reference measure μ depends on the underlying application: In several applications, the *Lebesgue measure* is selected or the physical invariant measure (cf. Section 2.3) of the underlying dynamical system (cf. [DJ99]) – in case it exists.

In the situations where μ is the physical invariant measure, we can numerically approximate the coherence ratio.

3.3 Remark (Numerical Calculation of the Coherence Ratio)**:** *Let X be partitioned into $N \in \mathbb{N}$ disjoint subsets $\mathcal{B}_N = \{B_1, ..., B_N\}$. To numerically evaluate the coherence ratio with respect to the physical reference measure $\mu \in \mathcal{M}(X)$, we follow [FD03] and define an approximation of μ by*

$$\mu_N(A) = \sum_{i=1}^{N} \frac{m(A \cap B_i)}{m(B_i)} p_i, \tag{3.1}$$

where $p \in \mathbb{R}^N$ is the eigenvector of the eigenvalue 1 of the transition matrix $P^{t,\tau}$ on $\mathcal{B}_N = \{B_1, ..., B_N\}$ and m the Lebesgue measure. The entries of $P^{t,\tau}$ are given by Equation (2.6). For instance, it is shown that, if the dynamical system is subject to small random perturbations, μ_N converges to the physical invariant measure μ if N tends to infinity and the diameter of the boxes approaches zero (cf. [DJ99, Fro95]). In this setting, it is straightforward to show that for two sets $A_1 = \bigcup_{i \in I} B_i$ and $A_2 = \cup_{j \in J} B_j$, with $I, J \subset \{1, ..., N\}$, the coherence ratio $\rho_t^\tau(A_1, A_2)$ with $t, \tau \in \mathbb{T}$ can be calculated by

$$\rho_t^\tau(A_1, A_2) = \frac{\sum_{i \in I, j \in J} P_{ji}^{t,\tau} p_i}{\sum_{i \in I} p_i},$$

with respect to μ_N (cf. [FD03] in case of $A_1 = A_2$).

3.2 Autonomous Coherent Structures

In this section, we are going to approximate subsets A of X for which

$$\phi_t^\tau(A) \approx A,$$

holds. These so-called *almost invariant sets* can be identified in a completely autonomous setting by the analysis of the transfer operator (cf. [DJ99]). Here, we embed the corresponding theory of (autonomous) almost invariant sets in the context of a non-autonomous dynamical system. In the time-dependent case, almost invariant sets appear as slowly mixing structures that are fixed in state space.

3.2.1 Invariant Sets

The simplest case of an autonomous coherent structure in a non-autonomous dynamical system $(\phi, X, \mathbb{T})$ is a subset S of the state space X with closed dynamical behavior on it, i. e. $(\phi|_S, S, \mathbb{T})$, where $\phi|_S$ is the restriction of ϕ on S, defines a dynamical system itself because $\phi(t, \tau, S) = S$ for all $t, \tau \in \mathbb{T}$. In terms of the coherence ratio, we can define:

3.4 Definition (Invariant Set)**:** *Let $A \subset X$ be a non-empty set. We call the set A a (t, τ)-invariant set if*

$$\rho_t^\tau(A, A) = 1,$$

where ρ_t^τ is the coherence ratio.

Let $\mu_A \in \mathcal{M}(X)$ be the measure with density χ_A for a measurable subset A of X, i. e. $\mu_A(B) = \int_B \chi_A d\mu$ for all $B \in \mathcal{B}(X)$. It is easy to check that A is a (t, τ)-invariant set if the measure μ_A is invariant under the action of the transfer

operator $\mathcal{P}_t^\tau$. In that case, the state space X can be subdivided into the sets A and $X \setminus A$ with independent dynamics in each part.

3.2.2 Almost Invariant Sets

In many dynamical systems, the only existing (t, τ)-invariant set is the whole state space X itself. However, we can still observe parts of the state space which are *almost invariant* (cf. [DJ99]).

3.5 Definition ((ρ, t, τ)-Almost Invariant Set)**:** *Let $A \subset X$ be a non-empty set, $\rho \in [0, 1]$ and $\mu \in \mathcal{M}(X)$ a probability measure such that the cocycle ϕ preserves μ. We call the set A a (ρ, t, τ)-almost invariant set if*

$$\rho_t^\tau(A, A) = \rho.$$

In real world applications (ρ, t, τ)-almost invariant sets in the state space with ρ close to 1 appear for example as metastable configurations of molecules (cf. [DHFS00, SHD01]) or, as we will see in Section 6, as so-called gyres and eddies within the oceanic fluid flow [FPET07, FSPD08, DFH$^+$09].

The main approach for the detection of almost invariant sets was introduced by Dellnitz and Junge in [DJ99], where a connection between spectral properties of the transfer operator $\mathcal{P}_t^\tau$ and the existence of (ρ, t, τ)-almost invariant sets with ρ close to 1 is uncovered. More precisely, in the situation where the underlying dynamical system is subject to small random perturbations, the following result has been proved:

3.6 Theorem ([DJ99])**:** *Suppose that the eigenmeasure μ of $\mathcal{P}_t^\tau$ corresponding to a real eigenvalue $\lambda \neq 1$ is scaled such that $|\mu|$ is a probability measure, and*

let $A \subset X$ be a set with $\mu(A) = \frac{1}{2}$. Then

$$\rho_{t,\tau}(A, A) + \rho_{t,\tau}(X \setminus A, X \setminus A) = \lambda + 1, \tag{3.2}$$

where $\rho_{t,\tau}$ is measured with respect to $|\mu|$.

The measure $|\mu|$ is the total variation of the measure μ and given for real-valued measures by $|\mu| = \mu^+ + \mu^-$ with

$$\mu^+(B) = \sup_{A \subset B} \mu(A) \qquad \text{and} \qquad \mu^-(B) = -\inf_{A \subset B} \mu(A).$$

For such measures, there exists the so-called *Hahn decomposition* of X into two measurable sets $A^+, A^- \subset X$ with $A^+ \cup A^- = X$, $\mu(A^+) \geq 0$ and $\mu(A^-) \leq 0$ (cf. [Doo94]). By Lemma 2.11, for the eigenmeasure μ, the identity $\mu(X) = 0$ holds true. Combining this with the fact that $|\mu|(X) = 1$, we conclude that there exists a set A with $\mu(A) = \frac{1}{2}$. In more detail, if λ is close to 1, using Equation (3.2), we can deduce that there exist two almost invariant sets A^+ and its complement $A^- = X \setminus A^+$ given by the Hahn decomposition with a coherence ratio close to 1 and $\mu(B) \geq 0$ for all $B \subset A^+$ and $\mu(B) < 0$ for all $B \subset A^-$. Thus, the sign-structure of the eigenmeasure μ splits the state space X into two almost invariant sets A^+ and A^- if the corresponding eigenvalue is close to 1.

Consider a partition $\mathcal{B} = \{B_1, ..., B_N\}$ of the state space X by $N \in \mathbb{N}$ boxes and the corresponding finite-dimensional matrix representation P_t^τ of the transfer operator $\mathcal{P}_t^\tau$ for fixed $t, \tau \in \mathbb{T}$ (cf. Equation (2.6)). Within this setting, we can formulate the following approach for the approximation of almost invariant sets (see e. g. [DJ99, FD03]). Let v be the eigenvector corresponding to a real eigenvalue of $P^{t,\tau}$ near 1. Then, the corresponding almost invariant sets A^+ and A^- can be approximated by

$$A_c^+ = \bigcup_{v_i \geq c} B_i \qquad \text{and} \qquad A_c^- = \bigcup_{v_i < c} B_i, \tag{3.3}$$

Algorithm 1 AlmostInvariantSet(t, τ, N, μ)

1: Cover the state space X by N boxes $\{B_1, ..., B_N\}$.
2: Approximate $\mathcal{P}_t^\tau$ by $P^{t,\tau}$.
3: Calculate the eigenvector v of $P^{t,\tau}$ corresponding to the second largest real eigenvalue.
4: Choose $c \in \mathbb{R}$ such that $\mu(A_c^+) \leq \frac{1}{2}$, $\mu(A_c^-) \leq \frac{1}{2}$ and $\min\{\rho_t^\tau(A_c^+, A_c^+), \rho_t^\tau(A_c^-, A_c^-)\}$ is maximized, where $A_c^+ = \bigcup_{v_i \geq c} B_i$ and $A_c^- = \bigcup_{v_i < c} B_i$.
5: Return $A = \operatorname{argmin}_{A_c^+, A_c^-}\{\rho_t^\tau(A_c^+, A_c^+), \rho_t^\tau(A_c^-, A_c^-)\}$.

where c is equal to 0. To allow almost invariant sets with measure not equal to $\frac{1}{2}$, we can choose the value c in Equation (3.3) freely. Heuristically we can select a $c \in \mathbb{R}^+$ in such a way that

$$\min\left\{\rho_t^\tau(A_c^+, A_c^+), \rho_t^\tau(A_c^-, A_c^-)\right\} \tag{3.4}$$

is maximized in order to obtain a maximized coherence ratio of the almost invariant set.

Indeed, Equation (3.4) is an optimization problem which cannot be solved easily. In the above setting, we can only define finitely many sets $A_c^+ = \bigcup_{v_i \geq c} B_i$ since the vector v has finitely many entries. Therefore, we can easily solve the optimization problem in Equation (3.4) by checking finitely many $c \in \{v_i\}_{i=1,...,N}$. This procedure can be summarized in Algorithm 1 for the approximation of a (ρ, t, τ)-almost invariant sets.

3.7 Remark: *Algorithm 1 makes use of the eigenvector of the second largest eigenvalue of the transition matrix $P^{t,\tau}$. It has been shown that also subsequent eigenvalues close to* 1 *and their corresponding eigenvectors can be used instead of v to reveal other almost invariant sets. For a more detailed discussion on this we refer to [DJ99] and [FD03].*

3.8 Remark: *The transition matrix $P^{t,\tau} \in \mathbb{R}^{N,N}$ induces a finite Markov chain (cf. Remark 2.13) which is not necessarily reversible, i. e. $p_i P_{ji}^{t,\tau} \neq p_j P_{ij}^{t,\tau}$ for $i, j \in \{1, ..., N\}$, where p is the fixed eigenvector of $P^{t,\tau}$. Hence, for further analysis, we transform the transition matrix $P^{t,\tau}$ into a "time symmetric" transition matrix $R^{t,\tau}$ by*

$$R_{ij}^{t,\tau} = \frac{1}{2}\left(P_{ij}^{t,\tau} + \frac{p_i P_{ji}^{t,\tau}}{p_j}\right), \tag{3.5}$$

which induces a reversible Markov chain. The matrix $R^{t,\tau}$ is stochastic and possesses real eigenvalues throughout [Bré99]. Consider again the measure μ_N given by Equation (3.1) and let $\mathcal{A} = \{A \subset X : \mu_N(A) \leq \frac{1}{2}, A = \bigcup_{i \in I} B_i\}$ be the set of all possible combinations of boxes in $\mathcal{B}$ with measure smaller than $\frac{1}{2}$. By denoting λ_2 as the second largest eigenvalue of $R^{t,\tau}$, it is shown in [Fro05] that

$$1 - \sqrt{2(1-\lambda_2)} \leq \max_{A \in \mathcal{A}} \rho_t^\tau(A, A) \leq \frac{1+\lambda_2}{2},$$

holds. In principle, instead of calculating the eigenvalues and eigenvectors of $P^{t,\tau}$ in Algorithm 1, we can make use of the eigenvalues and eigenvectors of the matrix $R^{t,\tau}$. This would lead to structures that are almost invariant under the forward and backward dynamics.

In the following example, we apply Algorithm 1 to the non-autonomous dynamical system generated by the ordinary differential equation (2.2) with a non-zero parameter value ϵ. The identification of autonomous structures in non-autonomous dynamical system plays an important role in various applications, for example in the identification of large spatially fixed structures in the oceanic fluid flow [DFH$^+$09, FPET07, FSPD08].

3.9 Example: *Reconsider the ordinary differential equation (2.2) from Example 2.4 and let $\epsilon = 1$, $A = -2$ and $\nu = 0$ such that (2.2) generates a non-autonomous dynamical system $(\phi, X, \mathbb{R})$. The application of Algorithm 1*

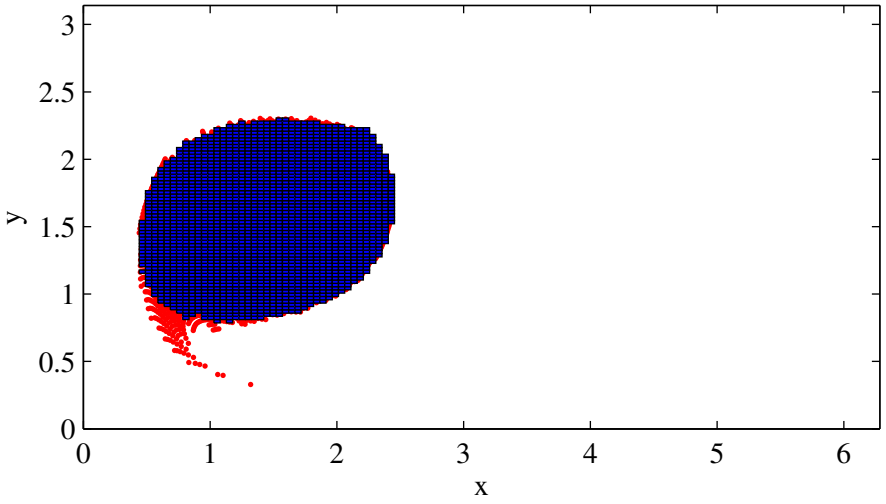

FIGURE 3.1: Covering of a $(0.98, 0, \pi)$-almost invariant set within the state space X of the non-autonomous dynamical system discussed in Example 3.9. The red dots indicate the endpoints of sample trajectories leaving the covering of the almost invariant set.

with $N = 16\,384$, $t = 0$ *and* $\tau = \pi$ *uncovers a* $(0.98, 0, \pi)$*-almost invariant set* A*. The box collection covering this almost invariant set is shown in Figure 3.1. Additionally, the end points of test point trajectories which start in* A *and end up in* $X \setminus A$ *are indicated by red dots.*

In the following, we illustrate the strength and variability of the transfer operator method concerning the analysis of almost invariant sets in a non-autonomous dynamical system $(\phi, X, \mathbb{T})$, as we introduced in the previous section. Consider a transfer operator $\mathcal{P}_t^\tau$ and its corresponding transition matrix $P^{t,\tau}$ with respect to the partition $\mathcal{B} = \{B_1, ..., B_N\}$ for fixed $t, \tau \in \mathbb{T}$. Furthermore, we assume that A_1 and A_2 are two sets each of written as a union of sets of $\mathcal{B}$ i. e. $A_1 = \bigcup_{i \in I} B_i$ and $A_2 = \bigcup_{j \in J} B_j$, $I, J \subset \{1, ..., N\}$. The sets A_1 and A_2 themselves can be assumed to be almost invariant sets; however, this is not necessary for the subsequent calculations. In this section we are

interested in two quantities. The first one is the *mean residence time* which is the average time a particle originating from different parts in A_1 remains within the set A_1 (cf. [Fro01]). The second one is the *transport rate* between two sets A_1 and A_2 (cf. [DJK$^+$05]).

Mean Residence Time

The coherence ratio $\rho_t^\tau(A_1, A_1)$ of the almost invariant set $A_1 = \bigcup_{i\in I} B_i$ reflects the probability that a trajectory which starts at time t in A_1 ends up in A_1 after flowing τ time-units. For a further analysis, we calculate how long the trajectory starting in A_1 remains in A_1. For this end, we assume that $I = \{1, \ldots, k\}$, for a fixed $k \in \{1, \ldots, N\}$. This is not a restriction and can be easily obtained by reordering the elements of the box-covering. In case the underlying dynamical system is autonomous and discrete, i. e. $\mathbb{T} = \mathbb{N}$ or $\mathbb{Z}$, we can assume that $P^{t,1}$ is the same transition matrix for each $t \in \mathbb{T}$ and we can drop the t-dependence. To calculate the mean residence time we only consider the restriction $P^1|_{A_1} \in \mathbb{R}^{k,k}$ of the transition matrix to the set A_1 and assume that it satisfies $\lim_{\tau\to\infty} P^\tau|_{A_1} = 0$. It is shown in [FA01] and [Fro01] that the average time a_i required for a particle originating in B_i, for an $i \in I$, to leave the set A_1 is given by the solution of the linear system of equations

$$(\mathrm{Id} - P^1|_{A_1})a = (1, 1, ..., 1)^T,$$

where Id denotes the $(k \times k)$-identity matrix. An exemplary calculation of the mean residence time can be found in Section 6.2.2.

Transport Rates

The transport rate between two sets indicates the magnitude of transport with respect to a certain reference measure. For autonomous dynamical systems, transport rates have been introduced in [DJK$^+$05] and extended to the non-

autonomous case in [Pad05]. We fix a point $t \in \mathbb{T}$ in time and define the transport rate between A_1 and A_2 over the time interval $[t, t+\tau]$ with respect to the Lebesgue measure by

$$T_{A_1,A_2,t}(\tau) = m(A_1 \cap \phi_{t+\tau}^{-\tau}(A_2)),$$

for $\tau \in \mathbb{T}$. The following calculations are true for arbitrary probability measures; we choose the Lebesgue measure for simplicity. The transport rate can be written in terms of the transfer operator as $T_{A_1,A_2,t}(\tau) = (\mathcal{P}_t^\tau m_{A_1})(A_2)$ with $m_{A_1}(A_2) = m(A_1 \cap A_2)$ and approximated by

$$T_{A_1,A_2,t}(\tau) \approx e_{A_2}^T P^{t,\tau} u_{A_1}, \tag{3.6}$$

where $(e_{A_2})_j = 1$ if $B_j \subset A_2$ and 0 otherwise and $(u_{A_1})_j = m(B_j)$ if $B_j \subset A_1$ and 0 otherwise. If we have a sequence of partitions $(\mathcal{B}_N)_{N\in\mathbb{N}}$ such that the diameters of the boxes in $\mathcal{B}_N$ approach 0 for increasing N, we obtain equality in Equation (3.6) in the limit (cf. [DJK+05] and [Pad05]).

3.3 Non-Autonomous Coherent Structures

In this section, we introduce mathematical concepts for the description of *non-autonomous coherent structures*, which are based on the notion of almost invariant sets in autonomous systems as introduced in Section 3.2.2. Non-autonomous coherent structures are time-dependent and particles starting in such a structure at a certain time stay within this structure over time with a high probability.

The geometric theory for analyzing transport in dynamical systems can be naturally extended for the treatment of non-autonomous transport phenomena [HY00]. Nevertheless, in this thesis, we focus on the probabilistic approach developed in a series of publications by Froyland et al. [FLS10, FSM10, SFM10]. Two concepts are suggested for a transfer operator based analysis. The first

one relies on ergodic theory and uses so-called *Oseledets subspaces* occurring in the *Multiplicative Ergodic Theorem*. The main result of [FLS10] relates Lyapunov exponents of the corresponding transfer operator cocycle to coherent structures in the underlying dynamical system. The theory of Lyapunov exponents deals with an *infinite* time horizon and a basic assumption of the Multiplicative Ergodic Theorem is an ergodic measure-preserving driving system in a probability space. However, such technical construction cannot be fulfilled in many applications. Also, transport phenomena only appear over finite time. Therefore, we will focus on another approach that is designed to identify pairs of sets which are characterized by the fact that most of the mass is transported from one set into the other over a fixed *finite* time [FSM10, SFM10].

3.3.1 Coherent Pairs

Coherent pairs can be defined analogously to almost invariant sets by taking into account a second set (cf. [FSM10]).

3.10 Definition ((ρ, t, τ)-Coherent Pair)**:** *Let μ and ν be probability measures on X and $A_1, A_2 \subset X$ with $\mu(A_1) > 0$. For fixed $t, \tau \in \mathbb{T}$ the pair (A_1, A_2) is called a* (ρ, t, τ)-coherent pair *if*

$$\rho_t^\tau(A_1, A_2) = \rho \tag{3.7}$$

and $\mu(A_1) = \nu(A_2)$.

The measures μ and ν are reference measures for measuring the coherence at initial time t and final time $t + \tau$, respectively. This differs slightly from the definition given in [FSM10], where $\mu(A_1) = \mu(A_2)$ is required. In many applications, the measure μ is chosen according to a certain physical meaning in which case ν is given by $\mathcal{P}_t^\tau \mu$ and can be interpreted as the so-called *push forward* of the measure μ under the dynamics. In the following, we will only

choose the initial reference measure depending on the underlying application and assume that the measure at final time is given by its push forward.

3.11 Remark: *In case μ is an invariant measure for ϕ, we observe that the construction of trivial $(1,t,\tau)$-coherent pairs (A_1, A_2) is possible. More precisely, we can select an arbitrary $A \subset X$ with positive μ-measure, set $\nu = \mu$ and simply define $A_1 = A$ and $A_2 = \phi_t^\tau(A)$. These trivially constructed $(1,t,\tau)$-coherent pairs are of no dynamical interest. In turbulent dynamical systems, such sets are subject to high stretching and folding and, therefore, geometrically irregular. Hence, by adding a small amount of diffusion to the underlying dynamics, these trivially constructed pairs will disappear. In fact, numerical methods based on the transfer operator approximation described in Section 2.4 naturally add diffusion to the dynamics. This natural diffusion allows the identification of nontrivial (ρ,t,τ)-coherent pairs with a large value of ρ. A detailed discussion of this topic and a theoretical interpretation of diffusion in the transfer operator setting can be found in [Fro13].*

The numerical method for the identification of (ρ,t,τ)-coherent pairs with large ρ was proposed by Froyland et al. [FSM10] and is characterized by the fact that it has the ability to work only on subparts of the state space. In fact, one only needs a subset S of the state space X which – together with $\phi_t^\tau(S)$ – already captures all the relevant information for the identification of a coherent pair.

Let $(\phi, X, \mathbb{T})$ be a non-autonomous dynamical system. Furthermore, let S be a subset of the state space and $\phi_t^\tau(S)$ its image. We calculate the transition matrix $P^{t,\tau}$ between a partition $\mathcal{B} = \{B_1, ..., B_N\}$ of S and a partition $\mathcal{C} = \{C_1, ..., C_M\}$ of $\phi_t^\tau(S)$ (cf. Remark 2.14). Moreover, we consider two reference probability measures μ and $\nu = \mathcal{P}_t^\tau \mu$ on S and $\phi_t^\tau(S)$. In the following, we work exclusively with the finite-dimensional approximation of the transition matrix. However, a more formal transfer operator setting can be found in [Fro13].

The main idea of this approach is the formulation of an optimization problem

which partitions the set S and its image into two sets of equal volume. It is solved by thresholding the left and right singular vectors corresponding to the second largest singular value of the normalized (with respect to a certain inner product) transition matrix $P^{t,\tau}$. We first define vectors $p \in \mathbb{R}^N$ and $q \in \mathbb{R}^M$, with $p_i = \mu(B_i)$, $i = 1, ..., N$ and $q = P^{t,\tau}p$, which are the discretized versions of the reference measures μ and $\nu = \mathcal{P}_t^\tau \mu$. The coherence ratio between two sets $A_1 = \bigcup_{i \in I} B_i$ and $A_2 = \bigcup_{j \in J} C_j$, where $I \subset \{1, ..., N\}$ and $J \subset \{1, ..., M\}$, is given by

$$\rho_t^\tau(A_1, A_2) = \frac{\sum_{i \in I, j \in J} P_{ji}^{t,\tau} p_i}{\sum_{i \in I} p_i}, \tag{3.8}$$

cf. Remark 3.3. Therefore, coherent pairs with large ρ can be obtained by finding index sets I, J such that Equation (3.8) is maximized. We encode the index sets I and J by vectors $x \in \{-1, 1\}^N$, $y \in \{-1, 1\}^M$ such that $x_i = 1$ if and only if $i \in I$ and $y_j = 1$ if and only if $j \in J$, therefore $A_1 = \bigcup_{i:x_i=1} B_i$ and $A_2 = \bigcup_{j:y_j=1} C_j$. Additionally, we introduce the inner products $\langle x_1, x_2 \rangle_p = \sum_{i=1}^N x_{1,i} x_{2,i} p_i$ and $\langle y_1, y_2 \rangle_q = \sum_{j=1}^M y_{1,j} y_{2,j} q_j$ and formulate the constraint that $|\langle x, \mathbf{1} \rangle_p|$ and $|\langle y, \mathbf{1} \rangle_q|$ are minimized. This guarantees that $\mu(A_1)$ and $\nu(A_2)$ are approximately $\frac{1}{2}$ each. For technical reasons, we normalize the transition matrix and form $L_{ij} = p_j P_{ij}^{t,\tau} / q_i$. Considering the setting in Remark 3.3, we can calculate:

$$\begin{aligned}
\langle Lx, y \rangle_q &= \left(\sum_{j \in I, i \in J} L_{ij} q_i + \sum_{j \notin I, i \notin J} L_{ij} q_i \right) - \left(\sum_{j \in I, i \notin J} L_{ij} q_i + \sum_{j \notin I, i \in J} L_{ij} q_i \right) \\
&= \left(\sum_{j \in I, i \in J} P_{ij}^{t,\tau} p_j + \sum_{j \notin I, i \notin J} P_{ij}^{t,\tau} p_j \right) - \left(\sum_{j \in I, i \notin J} P_{ij}^{t,\tau} p_j + \sum_{j \notin I, i \in J} P_{ij}^{t,\tau} p_j \right) \\
&= \rho_t^\tau(A_1, A_2) \mu_N(A_1) + \rho_t^\tau(S \setminus A_1, \phi_t^\tau(S) \setminus A_2) \mu_N(S \setminus A_1) \\
&\quad - \rho_t^\tau(A_1, \phi_t^\tau(S) \setminus A_2) \mu_N(A_1) - \rho_t^\tau(S \setminus A_1, A_2) \mu_N(S \setminus A_1),
\end{aligned}$$

where the coherence ratio is measured with respect to μ_N. This calculation shows

that maximizing $\langle Lx, y\rangle_q$ will lead to coherent pairs with large ρ (cf. [FSM10]). Therefore, to obtain a (ρ, t, τ)-coherent pair with ρ close to 1, we can formulate the following maximization problem:

$$\max_{x\in\{-1,1\}^N, y\in\{-1,1\}^M} \left\{\langle Lx, y\rangle_q : |\langle x, \mathbf{1}\rangle_p|, |\langle y, \mathbf{1}\rangle_q| \leq \epsilon\right\}, \tag{3.9}$$

for a small $\epsilon \in \mathbb{R}$. For $\epsilon = 0$ it cannot be expected that a solution of the problem exists since it is not possible to form a finite set of boxes with a measure of exactly $\frac{1}{2}$, in general.

However, the optimization problem in Equation (3.9) is a large-scale combinatorial problem and therefore, finding a solution is a difficult task. Froyland et al. proposed to relax this problem and instead of finding binary vectors $x \in \{-1, 1\}^N, y \in \{-1, 1\}^M$, they may taken on continuous values. Thereby, the optimization problem given in Equation (3.9) is relaxed. This also allows to set $\epsilon = 0$ such that the constraints become $|\langle x, \mathbf{1}\rangle_p| = |\langle x, \mathbf{1}\rangle_q| = 0$. Finally, we can formulate the relaxed problem as:

$$\max_{x\in\mathbb{R}^N, y\in\mathbb{R}^M} \left\{ \frac{\langle Lx, y\rangle_q}{\|x\|_p \|y\|_q} : \langle x, \mathbf{1}\rangle_p = \langle y, \mathbf{1}\rangle_q = 0 \right\}, \tag{3.10}$$

where $\|x\|_p = \langle x, x\rangle_p^{\frac{1}{2}}$ and $\|y\|_q = \langle y, y\rangle_q^{\frac{1}{2}}$. The normalization terms are due to the fact that in Equation (3.9) we implicitly stipulate that $\|x\|_p = \sum_{i=1}^N p_i = 1$ and $\|y\|_q = \sum_{j=1}^M q_i = 1$ since μ and ν are probability measures.

The solution of the corresponding relaxed optimization problem in Equation (3.10) is given by $x = \Pi_p^{-1/2}\hat{x}$ and $y = \Pi_q^{-1/2}\hat{y}$, where $\hat{x}$ and $\hat{y}$ are the right and left singular vectors corresponding to the second largest singular value of $\Pi_q^{-1/2} P^{t,\tau} \Pi_p^{1/2}$. Here $\Pi_p = \mathrm{diag}(p)$ and $\Pi_q = \mathrm{diag}(q)$ are diagonal matrices. Finally, we summarize this approach in Algorithm 2. Furthermore, the algorithm relaxes the condition that the set S has to be subdivided into two sets with equal measure in the same manner as Algorithm 1. Therefore, it allows to approximate coherent pairs with a flexible size.

Algorithm 2 *CoherentPair*(t, τ, N, M, S, μ)

1: Cover $S \subset X$ by N boxes $\{B_1, ..., B_N\}$ and $\phi_t^\tau(S)$ by M boxes $\{C_1, ..., C_M\}$.

2: Discretize $\mathcal{P}_t^\tau$ by $P^{t,\tau}$ on S and $\phi_t^\tau(S)$.
3: Calculate $p_i = \mu(B_i)$, $i = 1, ..., N$ and $q = P^{t,\tau}p$.
4: Calculate the left and right singular vectors v^l and v^r of $\Pi_q^{-1/2} P^{t,\tau} \Pi_p^{1/2}$ corresponding to the second largest singular value.
5: Choose $c \in \mathbb{R}$ such that $\rho_t^\tau(A_c, A_{b(c)})$ is maximized, where

$$A_c = \bigcup_{v_i^l \geq c} B_i \quad \text{and} \quad A_{b(c)} = \bigcup_{v_i^r \geq b(c)} C_i$$

with $b(c) = \text{argmin}_{b(c)} \left| \sum_{v_i^l \geq c} p_i - \sum_{v_i^r \geq b(c)} q_i \right|$.
6: Return $A_1 = A_c$ and $A_2 = A_{b(c)}$.

3.12 Remark: *Algorithm 2 makes use of the left and right singular vectors corresponding to the second largest singular values. In the same manner as discussed in Remark 3.7 for the identification of almost invariant sets, we can use subsequent singular values close to* 1 *and their corresponding left and right singular vectors.*

3.13 Example: *We reconsider the ordinary differential equation*

$$\begin{aligned} \dot{x} &= A \sin(x - \nu t) \cos(y) + \epsilon \sin(2t) G(g(x, y, t)), \\ \dot{y} &= \cos(x - \nu t) \sin(y), \end{aligned}$$

where $G(z) = \frac{1}{(z^2+1)^2}$ *and* $g(x, y, t) = -2 \sin(x - \nu t) \sin(y) - \frac{\pi}{4} + \frac{y}{2}$. *In Example 3.9, we fixed the parameters* $\nu = 0$, $A = -2$ *and* $\epsilon = 1$ *and identified an almost invariant set using Algorithm 1. Now, we set* $\nu = \frac{1}{4}$ *which implies that the coherent structure identified in Example 2.4 starts to move through the state space. We apply Algorithm 2 to the whole state space of the non-autonomous*

dynamical system by using the same partition at initial and final time. Therefore, with $N = M = 16\,384$*,* $S = X$*,* $t = 0$ *and* $\tau = 4\pi$*, the computation leads to a* $(0.9874, 0, 4\pi)$*-coherent pair* (A_1, A_2) *which is shown in Figure 3.2. In Figure 3.3 we illustrate the vectors* $x = \Pi_p^{-1/2}\hat{x}$ *and* $y = \Pi_q^{-1/2}\hat{y}$*, where* $\hat{x}$ *and* $\hat{y}$ *are the left and right singular vectors corresponding to the second largest singular value of* $\Pi_q^{-1/2} P^{0,4\pi} \Pi_p^{1/2}$*. Observe that by construction the changing from red to yellow in these vectors coincide with the sets* A_1 *and* A_2 *of the related coherent pair.*

From the numerical point of view, the most expensive part in Algorithm 2 is the numerical approximation of the transfer operator $\mathcal{P}_t^\tau$ in the second step. A sufficiently high amount of $K \in \mathbb{N}$ test points has to be integrated to form the transition matrix $P_{ij}^{t,\tau} \approx \frac{\sum_{k=1}^{K} \chi_{B_i}(\phi_t^\tau(p_{j,k}))}{K}$ (cf. Equation (2.7)). The total number of sample trajectory integrations directly depends on the number of boxes covering the initial domain S. Thus, the identification of an appropriate (i. e. as small as possible) subset $S \subset X$ is crucial for the efficiency of this approach. In Chapter 5, we present an appropriate numerical approach which preselects a set S and allows us to reduce the related numerical effort significantly.

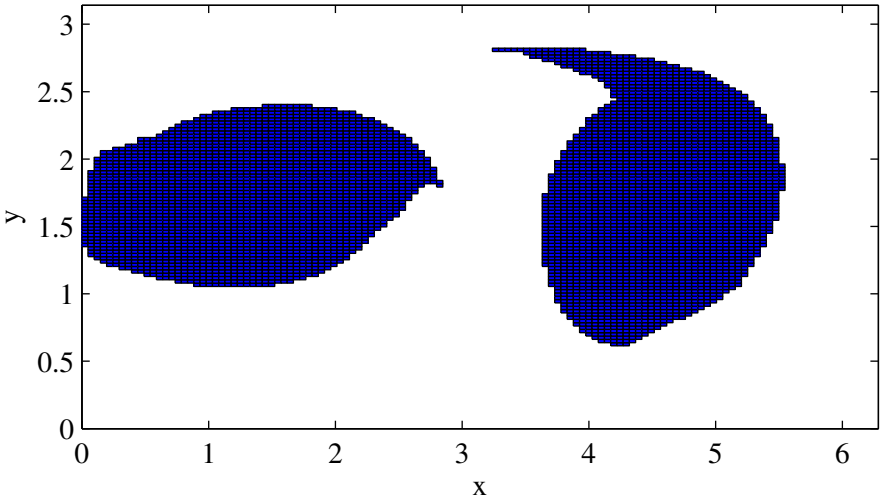

FIGURE 3.2: A $(0.9874, 0, 4\pi)$-coherent pair (A_1, A_2) calculated by Algorithm 2.

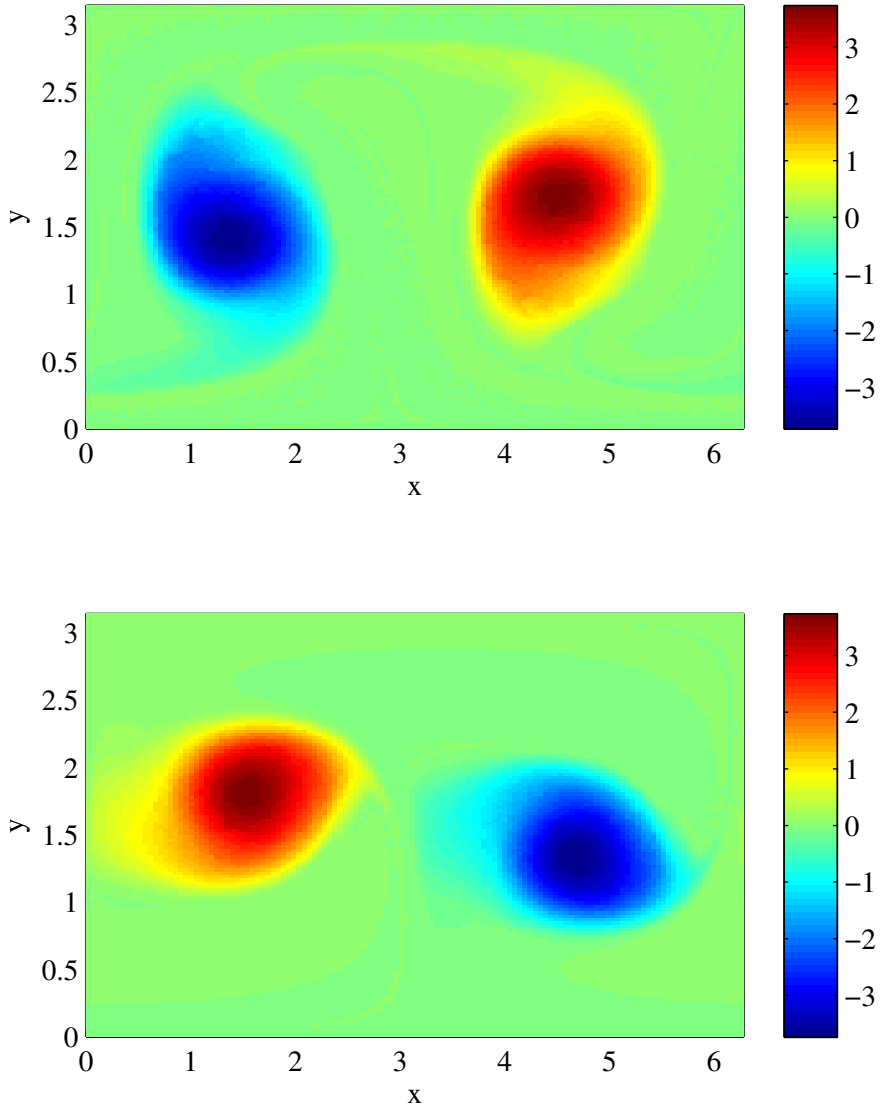

FIGURE 3.3: Normalized left (top) and right (bottom) singular vectors corresponding to the second largest singular value of the matrix $\Pi_q^{-1/2} P^{0,4\pi} \Pi_p^{1/2}$. (Color scale represents the magnitude of the entries of the singular vectors.)

CHAPTER 4

Analysis of Transport over Long Time Intervals

For analyzing transport phenomena by the concepts introduced in Chapter 3, spectral properties of transfer operators play a central role. The transfer operator captures the relevant dynamics of a dynamical system $(\phi, X, \mathbb{T})$ over a fixed given time horizon (e. g. from time $t \in \mathbb{T}$ to time $t + \tau \in \mathbb{T}$). The numerical analysis of spectral properties requires the calculation of the transition matrix $P^{t,\tau}$ (cf. Equation (2.6) in Section 2.4), which is a finite-dimensional representation of the transfer operator $\mathcal{P}_t^\tau$.

In many applications, the numerical realization of the finite-dimensional representation $P^{t,\tau}$ of the transfer operator $\mathcal{P}_t^\tau$ is based on a Monte Carlo approach (cf. Equation (2.7) in Section 2.4). More precisely, the state space X is partitioned into boxes $\mathcal{B} = \{B_1, \ldots, B_N\}$ with $B_i \subset X$ and $B_i \cap B_j = \emptyset$ for all $i, j = 1, \ldots, N$ with $i \neq j$. Furthermore, each box B_j is represented by $K \in \mathbb{N}$ test points $p_{j,k} \in B_j$, $k = 1, \ldots, K$. Then the finite sum

$$\sum_{k=1}^{K} \chi_{B_i}(\phi_t^\tau(p_{j,k})) \tag{4.1}$$

approximates the mass $m(\phi_{t+\tau}^{-\tau}(B_i) \cap B_j)$ which occurs in the definition of the transition matrix. However, we cannot compute expression (4.1) exactly, because, in general, there is no analytic formulation for the cocycle ϕ and thus we have to approximate it numerically by means of a map $\widetilde{\phi}$. In case the underlying dynamical system is chaotic and exhibits very turbulent dynamics, the numerical approximation of ϕ is costly. Additionaly, if the time τ is large, due to numerical errors, the image of the box B_j under the cocycle will not be represented very well by the points $\{\widetilde{\phi}_t^\tau(p_{j,k}) : k = 1, \ldots, K\}$. In these situations, physical properties of the underlying dynamical system cannot be represented by the numerical realization of $P^{t,\tau}$. For example, in case ϕ_t^τ preserves the Lebesgue measure m for each $t, \tau \in \mathbb{T}$, m is a fixed point of $\mathcal{P}_t^\tau$ and therefore, the vector $p \in \mathbb{R}^N$ with $p_i = m(B_i)$, $i = 1, \ldots, N$, is a fixed point of the corresponding transition matrix $P^{t,\tau}$. This may be violated in the presence of numerical errors.

In order to reduce the error in the numerical approximation of ϕ, in this section we propose a heuristic for the approximation of $\mathcal{P}_t^\tau$ based on the numerical realization of transition matrices on *intermediate* time intervals. We utilize the fact that the underlying transfer operator satisfies the cocycle property (cf. Proposition 2.12). In more detail, we partition the time interval $[t, t+\tau]$ into subintervals and approximate the transition matrices on each subinterval, respectively. The product of these matrices serves as an approximation of the transfer operator on the whole time interval we focus on. This is beneficial since the calculation of transition matrices on shorter subintervals is numerically more applicable than on the whole time interval. This idea has already been used for the calculation of transport rates in [Pad05]. However, we extend this ansatz in Section 4.1 to calculate eigenvalues by avoiding the explicit calculation of the matrix product, follow an eigenvalue product approach to efficiently compute eigenvalues, and eigenvectors and discuss an error bound in Section 4.2. Finally, we formulate an algorithm for the determination of the intermediate subintervals in Section 4.3.

4.1 Product Approach

Let $(\phi, X, \mathbb{T})$ be a non-autonomous dynamical system with $\mathbb{T} = \mathbb{R}$ or $\mathbb{R}^+$ and $t, \tau \in \mathbb{T}$ with $\tau > 0$. We define a finite series $(\tau_i)_{i=1,\dots,L} \subset \mathbb{T}$ of length $L \in \mathbb{N}$ denoting the length of the intermediate intervals with $\sum_{i=1}^{L} \tau_i = \tau$ and $\tau_i > 0$ for each $i \in \{1, \dots, L\}$. By Proposition 2.12 the cocycle property

$$\mathcal{P}_t^\tau = \mathcal{P}_{t+\tau_1+\dots+\tau_{L-1}}^{\tau_L} \circ \dots \circ \mathcal{P}_{t+\tau_1}^{\tau_2} \circ \mathcal{P}_t^{\tau_1} \tag{4.2}$$

holds.

Up to now, to calculate e. g. eigenvalues and eigenvectors of $\mathcal{P}_t^\tau$ numerically we have partitioned the state space into a collection of boxes $\mathcal{B} = \{B_1, \dots, B_N\}$ and computed the finite-dimensional approximation $P^{t,\tau}$. Then, the eigenvalues and eigenvectors of $P^{t,\tau}$ approximate those of $\mathcal{P}_t^\tau$. For simplicity, in the following we consider the case that all boxes B_i have equal Lebesgue measure. Since the transfer operator satisfies Equation (4.2) one could expect that the corresponding transition matrices also satisfy the cocycle property. However, this is not true in general, which is discussed in detail in Section 4.2.

Nevertheless, to avoid problems given by the numerical approximation of the matrix entries $P_{ij}^{t,\tau}$ for large τ as described in the beginning of this chapter and to reduce the number of test points involved we approximate the transfer operator $\mathcal{P}_t^\tau$ by

$$\prod_{i=1}^{L} P^{t+\sum_{j=1}^{i-1}\tau_j, \tau_i}, \tag{4.3}$$

for $L \in \mathbb{N}$. A discussion on the error can be found in Section 4.2. The approximation of the transfer operator $\mathcal{P}_t^\tau$ by the product (4.3) has already been successfully used for the calculation of transport probabilities between two different regions in the state space (cf. [Pad05]).

To obtain the spectral properties of the term (4.3) we avoid to explicitly calculate the product, but apply a product eigenvalue approach instead which goes back to [Var62] and has been used in a variety of settings, e. g. for the computation of singular values and singular vectors of matrices (cf. [Wat07]). To be more precise, we use the following result:

4.1 Theorem ([Wat07])**:** *The nonzero complex number λ is an eigenvalue of*

$$\widehat{Q}_L \cdot \widehat{Q}_{L-1} \cdot \ldots \cdot \widehat{Q}_1 \in \mathbb{C}^{N,N}, N \in \mathbb{N}$$

if and only if all of the values $\lambda^{1/L}, \lambda^{1/L}\psi, \lambda^{1/L}\psi^2, \ldots, \lambda^{1/L}\psi^{L-1}$ are eigenvalues of the cyclic matrix

$$C = \begin{pmatrix} & & & & \widehat{Q}_L \\ \widehat{Q}_1 & & & & \\ & \widehat{Q}_2 & & & \\ & & \ddots & & \\ & & & \widehat{Q}_{L-1} & \end{pmatrix} \in \mathbb{C}^{NL,NL}. \tag{4.4}$$

Here, $\psi = e^{\frac{2\pi i}{L}}$ and $\lambda^{1/L}$ denotes one of the Lth roots of λ.

Moreover, if $\lambda^{1/L}$ is an eigenvalue of C with the corresponding eigenvector $x = (x_1, x_2, \ldots, x_L)^T$, $x_i \in \mathbb{R}^N$, then $y = x_1$ is an eigenvector with eigenvalue λ of $\widehat{Q}_L \cdot \widehat{Q}_{L-1} \cdot \ldots \cdot \widehat{Q}_1$.

When approximating almost invariant sets, we can directly form the cyclic matrix C with $\widehat{Q}_i = P^{t+\sum_{j=1}^{i-1}\tau_j,\tau_i}$, $i = 1, \ldots, L$ and calculate the corresponding eigenvectors and eigenvalues. Here, the product $\widehat{Q}_L \cdot \ldots \cdot \widehat{Q}_1$ is the approximation of the transition matrix over the time interval $[t, t+\tau]$ as in Equation (4.3). For the approximation of coherent pairs we have to calculate the singular values and singular vectors of $\widetilde{A} = \Pi_q^{-1/2} \left(\prod_{i=1}^{L} P^{t+\sum_{j=1}^{i-1}\tau_j,\tau_i} \right) \Pi_p^{1/2}$ (cf. Section 3.3) which is equivalent to the calculation of the eigenvalues

and eigenvectors of the products $\widetilde{A} \cdot \widetilde{A}^T$ and $\widetilde{A}^T \cdot \widetilde{A}$ (cf. [Wat07]). Along the lines of Theorem 4.1, we can form the cyclic matrix C for the product $\widetilde{A}^T \cdot \widetilde{A} = \Pi_p^{1/2} \left(\prod_{i=L}^{1} \left(P^{t+\sum_{j=1}^{i-1}\tau_j,\tau_i} \right)^T \right) \Pi_q^{-1} \left(\prod_{i=1}^{L} P^{t+\sum_{j=1}^{i-1}\tau_j,\tau_i} \right) \Pi_p^{1/2}$ and for $\widetilde{A} \cdot \widetilde{A}^T$, respectively.

Another advantage of the product approach is that one obtains knowledge of the dynamics on the intermediate time intervals without any further effort. This can be used for example to visualize the evolution of mass. Consider an almost invariant set A within the state space X. To analyze the leakage of mass of A, we define a vector $v \in \mathbb{R}^N$, which has uniform non-zero entries v_i if $B_i \subset A$ and $v_i = 0$ otherwise. The vectors v^l given by $v^l = \left(\prod_{i=1}^{l} P^{t+\sum_{j=1}^{i-1}\tau_j,\tau_i} \right) v$, for $1 \leq l \leq L$, represent the distribution of mass at time $t + \sum_{j=1}^{l} \tau_j$ starting at time t in A. This is used, for example, for the detection of pathways of water in Section 6.2.3.

4.2 Error Estimate

In the following, using an appropriate norm $\| \cdot \|$, we discuss the error

$$\left\| \prod_{i=1}^{L} P^{t+\sum_{j=1}^{i-1}\tau_j,\tau_i} - P^{t,\tau} \right\| \tag{4.5}$$

in more detail and make the following assumption throughout this section:

4.2 Assumption: *Let $t, \tau \in \mathbb{T}$ be two points in time and $(\tau_i)_{i=1,\dots,L}$ a finite series of length $L \in \mathbb{N}$ denoting the length of the intermediate intervals with $\sum_{i=1}^{L} \tau_i = \tau$ and $\tau_i > 0$ for each $i \in \{1, \dots, L\}$. Furthermore, let $\mathcal{B} = \{B_1, \dots, B_N\}$ be a partition of the state space X with $m(B_i) = m(B_j)$ for every $i, j \in \{1, \dots, N\}$. We assume that ϕ preserves the Lebesgue measure m and $\phi_t^\tau(X) = X$ holds for all $t, \tau \in \mathbb{T}$.*

To begin with, we consider the case $L = 2$ and study Equation (4.5) using two intermediate intervals in time and we estimate the matrix entries of the product of two transition matrices.

4.3 Lemma: *For $t \in \mathbb{T}$ and $\tau_1, \tau_2 \in \mathbb{T}^+$ fixed, we have*

$$m_j^{\tau_1} \left(P_{ij}^{t,\tau_1+\tau_2} + F_{ij}^{\tau_1,\tau_2} \right) \leq (P^{t+\tau_1,\tau_2} P^{t,\tau_1})_{ij} \leq M_j^{\tau_1} \left(P_{ij}^{t,\tau_1+\tau_2} + F_{ij}^{\tau_1,\tau_2} \right) \tag{4.6}$$

for each $i, j \in \{1, \ldots, N\}$ with

$$M_j^{\tau_1} = \max_{s \in I_j^{\tau_1}} \frac{m(\phi_{t+\tau_1}^{-\tau_1}(B_s) \cap B_j)}{m(B_j)}, \; m_j^{\tau_1} = \min_{s \in I_j^{\tau_1}} \frac{m(\phi_{t+\tau_1}^{-\tau_1}(B_s) \cap B_j)}{m(B_j)}$$

and

$$F_{ij}^{\tau_1,\tau_2} = \frac{m(\phi_{t+\tau_1+\tau_2}^{-\tau_2-\tau_1}(B_i) \cap \widetilde{B}_j^{\tau_1})}{m(B_j)},$$

with $\widetilde{B}_j^{\tau_1} = \bigcup_{s \in I_j^{\tau_1}} \phi_{t+\tau_1}^{-\tau_1}(B_s) \setminus B_j$ and $I_j^{\tau_1} = \{s \in \{1, \ldots, N\} : \phi_{t+\tau_1}^{-\tau_1}(B_s) \cap B_j \neq \emptyset\}$.

Proof. Fix $i, j \in \{1, \ldots, N\}$. Since the preimage of an intersection is equal to the intersection of the preimages and the sets in $\mathcal{B}$ all have the same Lebesgue measure, we obtain for each $s \in \{1, \ldots, N\}$

$$\left(P^{t+\tau_1,\tau_2}\right)_{is} = \frac{m(\phi_{t+\tau_1+\tau_2}^{-\tau_2}(B_i) \cap B_s)}{m(B_s)} = \frac{m(\phi_{t+\tau_1+\tau_2}^{-\tau_2-\tau_1}(B_i) \cap \phi_{t+\tau_1}^{-\tau_1}(B_s))}{m(B_j)}.$$

Therefore,

$$\begin{aligned} \left(P^{t+\tau_1,\tau_2} P^{t,\tau_1}\right)_{ij} &= \sum_{s=1}^{N} \left(P^{t+\tau_1,\tau_2}\right)_{is} \left(P^{t,\tau_1}\right)_{sj} \\ &= \sum_{s=1}^{N} \frac{m(\phi_{t+\tau_1+\tau_2}^{-\tau_2-\tau_1}(B_i) \cap \phi_{t+\tau_1}^{-\tau_1}(B_s))}{m(B_j)} \frac{m(\phi_{t+\tau_1}^{-\tau_1}(B_s) \cap B_j)}{m(B_j)}. \end{aligned}$$

Considering the set $I_j^{\tau_1} = \{s \in \{1,\dots,N\} : \phi_{t+\tau_1}^{-\tau_1}(B_s) \cap B_j \neq \emptyset\}$ we perform the following estimation

$$\begin{aligned}\left(P^{t+\tau_1,\tau_2}P^{t,\tau_1}\right)_{ij} &\leq \max_{s\in I_j^{\tau_1}} \frac{m(\phi_{t+\tau_1}^{-\tau_1}(B_s)\cap B_j)}{m(B_j)} \sum_{s\in I_j^{\tau_1}} \frac{m(\phi_{t+\tau_1+\tau_2}^{-\tau_2-\tau_1}(B_i)\cap \phi_{t+\tau_1}^{-\tau_1}(B_s))}{m(B_j)} \\ &= M_j^{\tau_1} \frac{m(\phi_{t+\tau_1+\tau_2}^{-\tau_2-\tau_1}(B_i)\cap \bigcup_{s\in I_j^{\tau_1}} \phi_{t+\tau_1}^{-\tau_1}(B_s))}{m(B_j)} \\ &= M_j^{\tau_1} \frac{m(\phi_{t+\tau_1+\tau_2}^{-\tau_2-\tau_1}(B_i)\cap B_j) + m(\phi_{t+\tau_1+\tau_2}^{-\tau_2-\tau_1}(B_i)\cap \widetilde{B}_j^{\tau_1})}{m(B_j)},\end{aligned}$$

with $M_j^{\tau_1} = \max_{s\in I_j^{\tau_1}} \frac{m(\phi_{t+\tau_1}^{-\tau_1}(B_s)\cap B_j)}{m(B_j)}$ and $\widetilde{B}_j^{\tau_1} = \bigcup_{s\in I_j^{\tau_1}} \phi_{t+\tau_1}^{-\tau_1}(B_s) \setminus B_j$, since $\bigcup_{s\in I_j^{\tau_1}} \phi_{t+\tau_1}^{-\tau_1}(B_s) = B_j \cup \widetilde{B}_j^{\tau_1}$. Replacing $\frac{m(\phi_{t+\tau_1+\tau_2}^{-\tau_2-\tau_1}(B_i)\cap \widetilde{B}_j^{\tau_1})}{m(B_j)}$ by $F_{ij}^{\tau_1,\tau_2}$ we conclude that

$$(P^{t+\tau_1,\tau_2}P^{t,\tau_1})_{ij} \leq M_j^{\tau_1}\left(P_{ij}^{t,\tau_1+\tau_2} + F_{ij}^{\tau_1,\tau_2}\right).$$

Similarly we obtain

$$m_j^{\tau_1}\left(P_{ij}^{t,\tau_1+\tau_2} + F_{ij}^{\tau_1,\tau_2}\right) \leq (P^{t+\tau_1,\tau_2}P^{t,\tau_1})_{ij}$$

with $m_j^{\tau_1} = \min_{s\in I_j^{\tau_1}} \frac{m(\phi_{t+\tau_1}^{-\tau_1}(B_s)\cap B_j)}{m(B_j)}$ which completes the proof. □

Now, we can estimate the error between the matrix entries $(P^{t,\tau_1+\tau_2})_{ij}$ and $(P^{t+\tau_1,\tau_2}P^{t,\tau_1})_{ij}$.

4.4 Theorem: *For $t \in \mathbb{T}$ and $\tau_1, \tau_2 \in \mathbb{T}^+$ fixed, we have*

$$|(P^{t+\tau_1,\tau_2}P^{t,\tau_1})_{ij} - P_{ij}^{t,\tau_1+\tau_2}| \leq P_{ij}^{t,\tau_1+\tau_2}\left(M_j^{\tau_1} - 2m_j^{\tau_1} + 1\right) + M_j^{\tau_1}F_{ij}^{\tau_1,\tau_2} \quad (4.7)$$

for each $i,j \in \{1,\dots,N\}$ with $M_j^{\tau_1}$, $m_j^{\tau_1}$ and $F_{ij}^{\tau_1,\tau_2}$ as in Lemma 4.3.

Proof. We have

$$\begin{aligned}|(P^{t+\tau_1,\tau_2}P^{t,\tau_1})_{ij} - P_{ij}^{t,\tau_1+\tau_2}| &\leq |(P^{t+\tau_1,\tau_2}P^{t,\tau_1})_{ij} - m_j^{\tau_1}(P_{ij}^{t,\tau_1+\tau_2} + F_{ij}^{\tau_1,\tau_2})| \\ &\quad + |m_j^{\tau_1}(P_{ij}^{t,\tau_1+\tau_2} + F_{ij}^{\tau_1,\tau_2}) - P_{ij}^{t,\tau_1+\tau_2}| \\ &= (P^{t+\tau_1,\tau_2}P^{t,\tau_1})_{ij} - m_j^{\tau_1}(P_{ij}^{t,\tau_1+\tau_2} + F_{ij}^{\tau_1,\tau_2}) \\ &\quad + |(m_j^{\tau_1} - 1)P_{ij}^{t,\tau_1+\tau_2} + m_j^{\tau_1}F_{ij}^{\tau_1,\tau_2}|,\end{aligned}$$

because $m_j^{\tau_1}\left(P_{ij}^{t,\tau_1+\tau_2} + F_{ij}^{\tau_1,\tau_2}\right) \leq (P^{t+\tau_1,\tau_2}P^{t,\tau_1})_{ij}$. Since $0 < m_j^{\tau_1} \leq 1$ we obtain $(m_j^{\tau_1} - 1)P_{ij}^{t,\tau_1+\tau_2} \leq 0$ and $m_j^{\tau_1}F_{ij}^{\tau_1,\tau_2} \geq 0$. Thus, it can be estimated

$$\begin{aligned}|(P^{t+\tau_1,\tau_2}P^{t,\tau_1})_{ij} - P_{ij}^{t,\tau_1+\tau_2}| &\leq (P^{t+\tau_1,\tau_2}P^{t,\tau_1})_{ij} - m_j^{\tau_1}(P_{ij}^{t,\tau_1+\tau_2} + F_{ij}^{\tau_1,\tau_2}) \\ &\quad - (m_j^{\tau_1} - 1)P_{ij}^{t,\tau_1+\tau_2} + m_j^{\tau_1}F_{ij}^{\tau_1,\tau_2}.\end{aligned}$$

Furthermore, using $(P^{t+\tau_1,\tau_2}P^{t,\tau_1})_{ij} \leq M_j^{\tau_1}\left(P_{ij}^{t,\tau_1+\tau_2} + F_{ij}^{\tau_1,\tau_2}\right)$ we estimate

$$\begin{aligned}|(P^{t+\tau_1,\tau_2}P^{t,\tau_1})_{ij} - P_{ij}^{t,\tau_1+\tau_2}| &\leq M_j^{\tau_1}(P_{ij}^{t,\tau_1+\tau_2} + F_{ij}^{\tau_1,\tau_2}) - 2m_j^{\tau_1}P_{ij}^{t,\tau_1+\tau_2} + P_{ij}^{t,\tau_1+\tau_2} \\ &\leq P_{ij}^{t,\tau_1+\tau_2}(M_j^{\tau_1} - 2m_j^{\tau_1} + 1) + M_j^{\tau_1}F_{ij}^{\tau_1,\tau_2}.\end{aligned}$$

□

In the next step, we use this result to show that $P^{t+\tau_1,\tau_2}P^{t,\tau_1}$ is equal to $P^{t,\tau_1+\tau_2}$ under certain assumptions.

4.5 Corollary: *Consider that B_j is exactly the preimage $\phi_{t+\tau_1}^{-\tau_1}(B_i)$ of B_i for fixed $i, j \in \{1, \ldots, N\}$. Then, the identity*

$$(P^{t+\tau_1,\tau_2}P^{t,\tau_1})_{ij} = P_{ij}^{t,\tau_1+\tau_2} \tag{4.8}$$

holds.

Proof. Let $i, j \in \{1, \ldots, N\}$. In case B_j is exactly the preimage $\phi_{t+\tau_1}^{-\tau_1}(B_i)$ of B_i we obtain $I_j^{\tau_1} = \{i\}$, $M_j^{\tau_1} = m_j^{\tau_1} = 1$ and $F_{ij}^{\tau_1,\tau_2} = 0$, since $\widetilde{B}_j^{\tau_1} = \emptyset$. Therefore,

we obtain equality in Equation (4.6). □

We proceed by considering the more general case $L > 2$. For simplicity, we write

$$\widehat{Q}_k = P^{t+\sum_{j=1}^{k-1}\tau_j,\tau_k}, \text{ for } k = 1,\dots,L,$$

in the following. These matrices can be interpreted as the one-step transition matrices over each intermediate time interval $[t + \sum_{j=1}^{k-1}\tau_j, t + \sum_{j=1}^{k}\tau_j]$. Furthermore, we define

$$Q_k = P^{t,\sum_{i=1}^{k}\tau_i}, \text{ for } k = 1,\dots,L$$

which are the transition matrices on the interval $[t, t + \sum_{i=1}^{k}\tau_i]$. Using this notation we estimate the error

$$\left\| \prod_{i=1}^{L} \widehat{Q}_i - Q_L \right\| = \left\| \prod_{i=1}^{L} P^{t+\sum_{j=1}^{i-1}\tau_j,\tau_i} - P^{t,\tau} \right\|, \tag{4.9}$$

for an appropriate matrix norm $\|\cdot\|$. We begin by proving a formula for Q_L based on the matrices $\widehat{Q}_j$, for $j = 1,\dots,L$ and on the error

$$\Delta_k = \widehat{Q}_{k+1}Q_k - Q_{k+1}, \text{ for } k \in \{0,\dots,L-1\}$$

which we obtain at each intermediate time interval.

4.6 Lemma: *For $L \in \mathbb{N}$, the identity*

$$Q_L = \prod_{i=1}^{L} \widehat{Q}_i - \sum_{i=3}^{L} \left(\prod_{j=i}^{L} \widehat{Q}_j \right) \Delta_{i-2} - \Delta_{L-1}, \tag{4.10}$$

holds with $\Delta_k = \widehat{Q}_{k+1}Q_k - Q_{k+1}$ for $k \in \{0,\dots,L-1\}$.

Proof. We prove Equation (4.10) by induction and therefore begin to verify the

statement for $L = 1$:

$$\begin{aligned} Q_1 &= \widehat{Q}_1 - \Delta_0 \\ &= \widehat{Q}_1 - \widehat{Q}_1 Q_0 + Q_1. \end{aligned}$$

This identity holds since $Q_0 = \mathrm{id}$. We proceed by showing that Equation (4.10) holds for $L+1$ under the assumption that the statement is true for L: With $Q_{L+1} = \widehat{Q}_{L+1} Q_L - \Delta_L$ we obtain

$$Q_{L+1} = \widehat{Q}_{L+1} \left(\prod_{i=1}^{L} \widehat{Q}_i - \sum_{i=3}^{L} \left(\prod_{j=i}^{L} \widehat{Q}_j \right) \Delta_{i-2} - \Delta_{L-1} \right) - \Delta_L,$$

since the statement holds for L. Furthermore,

$$\begin{aligned} Q_{L+1} &= \prod_{i=1}^{L+1} \widehat{Q}_i - \sum_{i=3}^{L} \left(\prod_{j=i}^{L+1} \widehat{Q}_j \right) \Delta_{i-2} - \widehat{Q}_{L+1} \Delta_{L-1} - \Delta_L \\ &= \prod_{i=1}^{L+1} \widehat{Q}_i - \sum_{i=3}^{L+1} \left(\prod_{j=i}^{L+1} \widehat{Q}_j \right) \Delta_{i-2} - \Delta_L, \end{aligned}$$

which is the formula for $L+1$. □

Using this formula for Q_L we estimate Equation (4.9) in terms of the matrices $(\Delta_k)_{k=1,\dots,L-1}$.

4.7 Theorem: *Let $L \in \mathbb{N}$. Furthermore, let $\|\cdot\|$ be a matrix norm with $\|\widehat{Q}_i\| \leq 1$, $\forall i \in \{1, \dots, L\}$, then*

$$\left\| \prod_{i=1}^{L} \widehat{Q}_i - Q_L \right\| \leq \sum_{i=1}^{L-1} \|\Delta_i\|, \tag{4.11}$$

with $\Delta_k = \widehat{Q}_{k+1} Q_k - Q_{k+1}$ for $k \in \{0, \dots, L-1\}$.

Proof. Using Lemma 4.6 for $L \in \mathbb{N}$, the following estimation holds

$$\begin{aligned}\left\|\prod_{i=1}^{L}\widehat{Q}_i - Q_L\right\| &= \left\|\sum_{i=3}^{L}\left(\prod_{j=i}^{L}\widehat{Q}_j\right)\Delta_{i-2} + \Delta_{L-1}\right\| \\ &\leq \sum_{i=3}^{L}\left\|\left(\prod_{j=i}^{L}\widehat{Q}_j\right)\Delta_{i-2}\right\| + \|\Delta_{L-1}\|\,.\end{aligned}$$

Since $\|\cdot\|$ is a matrix norm with $\|\widehat{Q}_i\| \leq 1$ for each $i = 1, \ldots, L$ we further estimate

$$\begin{aligned}\left\|\prod_{i=1}^{L}\widehat{Q}_i - Q_L\right\| &\leq \sum_{i=3}^{L}\|\Delta_{i-2}\| + \|\Delta_{L-1}\| \\ &= \sum_{i=3}^{L+1}\|\Delta_{i-2}\| = \sum_{i=1}^{L-1}\|\Delta_i\|\,,\end{aligned}$$

which completes the proof. □

This result is used to obtain a more rigorous error bound in the matrix norm $\|\cdot\|_1$ given by the maximum absolute column sum. We begin by estimating the norm of each Δ_i for $i = 1, \ldots, L-1$.

4.8 Lemma: *Let $L \in \mathbb{N}$. Then, the inequality*

$$\|\Delta_k\|_1 \leq \max_{j=1,\ldots,N}\left(\left(M_j^{s_1(k)} - 2m_j^{s_1(k)} + 1\right) + M_j^{s_1(k)}\frac{m\left(\widetilde{B}_j^{s_1(k)}\right)}{m(B_j)}\right) \tag{4.12}$$

holds for each $k \in \{1, \ldots, L-1\}$ with $s_1(k) = \sum_{r=1}^{k}\tau_r$. Here, $m_j^{s_1(k)}$, $M_j^{s_1(k)}$, and $\widetilde{B}_j^{s_1(k)}$ are defined as in Lemma 4.3.

Proof. We begin with an inspection of the entries

$$\begin{aligned}(\Delta_k)_{ij} &= \left(\widehat{Q}_{k+1}Q_k - Q_{k+1}\right)_{ij} \\ &= \left(P^{t+\sum_{r=1}^{k}\tau_r,\tau_{k+1}}P^{t,\sum_{r=1}^{k}\tau_r} - P^{t,\sum_{r=1}^{k+1}\tau_r}\right)_{ij}\end{aligned}$$

of the matrix Δ_k for a fixed $k \in \{1,\dots,L\}$. By defining $s_1(k) = \sum_{r=1}^{k}\tau_r$ and $s_2(k) = \tau_{k+1}$ we can apply Theorem 4.4 and estimate

$$\begin{aligned}\left|(\Delta_k)_{ij}\right| &= \left|\left(P^{t+s_1(k),s_2(k)}P^{t,s_1(k)} - P^{t,s_1(k)+s_2(k)}\right)_{ij}\right| \\ &\leq P_{ij}^{t,s_1(k)+s_2(k)}\left(M_j^{s_1(k)} - 2m_j^{s_1(k)} + 1\right) + M_j^{s_1(k)}F_{ij}^{s_1(k),s_2(k)}.\end{aligned}$$

The obtained inequality can be used for all k, thus, we can proceed by estimating

$$\begin{aligned}\|\Delta_k\|_1 &= \max_{j=1,\dots,N}\sum_{i=1}^{N}\left|(\Delta_k)_{ij}\right| \\ &\leq \max_{j=1,\dots,N}\sum_{i=1}^{N}\left(P_{ij}^{t,s_1(k)+s_2(k)}\left(M_j^{s_1(k)} - 2m_j^{s_1(k)} + 1\right) + M_j^{s_1(k)}F_{ij}^{s_1(k),s_2(k)}\right) \\ &\leq \max_{j=1,\dots,N}\left(\left(M_j^{s_1(k)} - 2m_j^{s_1(k)} + 1\right)\sum_{i=1}^{N}P_{ij}^{t,s_1(k)+s_2(k)} + M_j^{s_1(k)}\sum_{i=1}^{N}F_{ij}^{s_1(k),s_2(k)}\right).\end{aligned}$$

It holds $\sum_{i=1}^{N}P_{ij}^{t,s_1(k)+s_2(k)} = 1$ and $\sum_{i=1}^{N}F_{ij}^{s_1(k),s_2(k)} = \frac{m(\widetilde{B}_j^{s_1(k)})}{m(B_j)}$, since ϕ preserves the Lebesgue measure and $\phi(X) = X$. Therefore, we have

$$\|\Delta_k\|_1 \leq \max_{j=1,\dots,N}\left(\left(M_j^{s_1(k)} - 2m_j^{s_1(k)} + 1\right) + M_j^{s_1(k)}\frac{m\left(\widetilde{B}_j^{s_1(k)}\right)}{m(B_j)}\right),$$

which completes the proof. □

Similar to Corollary 4.5, we can show that the error vanishes under certain assumptions.

4.9 Corollary: *Let $L \in \mathbb{N}$. If B_j is exactly the preimage $\phi_{t+\tau_k}^{-\tau_k}(B_i)$ of B_i for all $i, j \in \{1, \ldots, N\}$ and all $k \in \{1, \ldots, L\}$ it follows that*

$$\prod_{i=1}^{L} P^{t+\sum_{j=1}^{i-1}\tau_j, \tau_i} = P^{t,\tau}.$$

Proof. Let $i, j \in \{1, \ldots, N\}$ and $k \in \{1, \ldots, L-1\}$. In case B_j is exactly the preimage $\phi_{t+\tau_k}^{-\tau_k}(B_i)$ of B_i we obtain $I_j^{s_1(k)} = \{i\}$, $M_j^{s_1(k)} = m_j^{s_1(k)} = 1$, and $F_{ij}^{s_1(k), s_2(k)} = 0$, since $\widetilde{B}_j^{s_1(k)} = \emptyset$, with $s_1(k) = \sum_{r=1}^{k} \tau_r$ and $s_2(k) = \tau_{k+1}$. Therefore, we obtain $\|\Delta_k\|_1 = 0$ by Lemma 4.8 for each $k \in \{1, \ldots, L-1\}$ and thus

$$\left\| \prod_{i=1}^{L} P^{t+\sum_{j=1}^{i-1}\tau_j, \tau_i} - P^{t,\tau} \right\|_1 = \left\| \prod_{i=1}^{L} \widehat{Q}_i - Q_L \right\|_1 \leq \sum_{i=3}^{L+1} \|\Delta_{i-2}\|_1 = 0.$$

Then, $\prod_{i=1}^{L} P^{t+\sum_{j=1}^{i-1}\tau_j, \tau_i}$ is equal to $P^{t,\tau}$. □

The situation considered in Corollary 4.9 corresponds to the case that the box covering of the state space X exactly matches the preimages of the single boxes and demonstrates the sharpness of the estimate given in Equation (4.12). However, this special situation cannot generally be expected in real world applications. In the considerably different case, when the jth column of the matrix $P^{t,s_1(k)}$ contains $g \in \{1, ..., N\}$ non-zero entries, the value of $m_j^{s_1(k)}$ is bounded from above by $\frac{1}{g}$. For $m_j^{s_1(k)} = \frac{1}{g}$ fixed, it follows that $M_j^{s_1(k)} = \frac{1}{g}$ since $\sum_{i=1}^{N} P_{ij}^{t,s_1(k)} = 1$ holds. Consequently, for increasing g the value $\left(M_j^{s_1(k)} - 2m_j^{s_1(k)} + 1\right) + M_j^{s_1(k)} \frac{m\left(\widetilde{B}_j^{s_1(k)}\right)}{m(B_j)}$, which is a lower bound of the right hand side of Equation (4.12), tends to one. Also the value $m_j^{s_1(k)}$ is obviously not depending continuously on $s_1(k)$. Nevertheless, we use the fact, that the error (4.9) is bounded from above by the sum of the errors which we obtain at each intermediate time step and formulate in the next section an algorithm which successively generates a series of intermediate points in time.

4.3 Algorithmic Realization

In the algorithmic realization, the question arises how to select the finite series $(\tau_i)_{i=1,\dots,L}$ of intermediate points in time with $\sum_{i=1}^{L} \tau_i = \tau$ to calculate the family of transition matrices $(P^{t+\sum_{j=1}^{i-1}\tau_j,\tau_i})_{i=1,\dots,L}$. The purpose of the product approach is to force the numerical approximation of $\mathcal{P}^{t,\tau}$ to conserve physical properties of the underlying dynamical system, e. g. volume preservation. In this section we formulate an algorithm which successively generates a series of transition matrices such that each of the matrices guarantees that a certain property of the underlying system is fulfilled up to a maximal error. Based on this series of transition matrices one can apply the product eigenvalue approach described in Section 4.1 to approximate the eigenvalues and eigenvectors of the transfer operator $\mathcal{P}_t^\tau$ for fixed $t, \tau \in \mathbb{T}$.

Let us assume that we can measure the deviation of the physical property over the time interval $[t, t+\tau]$ by a function $E : \mathbb{R}^{N,N} \to \mathbb{R}$. For example, if the system preserves the Lebesgue measure at all time instances we can chose $E(P^{t,\tau}) = \|P^{t,\tau}p - p\|_1$ for $p \in \mathbb{R}^N$ with $p_i = m(B_i)$, $i = 1, \dots, N$. Using this function we formulate Algorithm 3, which checks at fixed points in time if the error is larger than a value ϵ and restarts the approximation of the transition matrix if necessary.

The algorithm calculates for a given starting time t and duration τ a series of transition matrices between L intermediate points $(\tau_i)_{i=1,\dots,L}$ in time. The procedure depends on the error function E, the maximal error ϵ and a step size h which has to be chosen such that $\tau = k \cdot h$ for one $k \in \mathbb{Z}$. In case h is chosen too large, the error $E(P^{T,h})$ at time $T \in \mathbb{T}$ over one step h is larger than ϵ and the algorithm terminates with an error.

For the numerical realization of $P^{T,k\cdot h}$ with $k > 1$, a set G_T of test points has to be integrated to obtain a set $G_{T+k\cdot h}$ of terminal points after flowing $k \cdot h$ time-units. However, we can reuse the set of terminal points $G_{T+(k-1)\cdot h}$ computed

Algorithm 3 ProductApproach(E,t,τ,h,ϵ)

Set $T = t$
Set $L = 1$
Set $k = 1$
Set $\tau_1 = T$
while $T + k \cdot h \leq t + \tau$ **do**
  Approximate the transfer operator $\mathcal{P}_T^{k \cdot h}$ by $P^{T,k \cdot h}$.
  if $E(P^{T,k \cdot h}) < \epsilon$ **then**
    Set $\mathfrak{P}(L) = P^{T,k \cdot h}$
    Set $k = k + 1$
  else
    if $k = 1$ **then**
      return Computation not possible.
    end if
    Set $L = L + 1$
    Set $\tau_L = (k - 1) \cdot h$
    Set $T = T + \tau_L$
    Set $k = 1$
  end if
end while
return $\mathfrak{P}$ and $(\tau_i)_{i=1,\ldots,L}$

within the approximation of $P^{T,(k-1) \cdot h}$ and integrate them h time-units further to obtain $G_{T+k \cdot h}$. In total, Algorithm 3 has the same effort for the integration of test points as for the numerical realization of $P^{t,\tau}$ directly, plus the effort for the integration over one step h at each intermediate point in time. However, this effort is small for small h and few intermediate points in time.

4.10 Remark: *The product approach and the corresponding Algorithm 3 can be easily extended to consider non-square transition matrices which appear if we restrict to a subpart of the state space (cf. Remark 2.14). In such cases, we have*

to approximate a series of transition matrices between a series of box-collections covering the sets $S, \phi_t^{\tau_1}(S), \ldots, \phi_t^{\tau}(S)$ *in the state space.*

To show the effectiveness of Algorithm 3 we reconsider the ordinary differential equation (2.2) from Example 2.4.

4.11 Example: *In the ordinary differential equation* (2.2) *from Example 2.4 let* $\epsilon = 0$ *and* $\nu = 0.25$*. For* $A = -1$*, the ODE generates a non-autonomous dynamical system* $(\phi, X, \mathbb{R})$ *which preserves the Lebesgue measure* m *at all time instances. We define a partition* $\mathcal{B} = \{B_1, \ldots, B_N\}$ *of* $N = 16\,384$ *boxes of the state space* X *on which we calculate the transition matrices involved in Algorithm 3 and choose a step size of* 0.1 *for the integration of the ODE to deliberately induce numerical errors in the approximation of the cocycle* ϕ*.*

We apply Algorithm 3 with $t = 0$*,* $\tau = 12.5$*,* $h = 0.5$*,* $\epsilon = 0.01$ *and define*

$$E : \mathbb{R}^{N,N} \to \mathbb{R}, \quad E(P) = \|P \cdot p - p\|_1,$$

where $p \in \mathbb{R}^N$ *and* $p_i = \frac{m(B_i)}{m(X)}$ *is the discrete version of the normalized Lebesgue measure, to stipulate that the approximation on* $\mathcal{P}_t^{\tau}$ *preserves the Lebesgue measure up to a fixed error. We obtain a series of seven transition matrices* $(P^{t+\sum_{j=1}^{i-1}\tau_j,\tau_i})_{i=1,\ldots,7}$ *with* $\tau_1 = \tau_2 = \tau_4 = \tau_5 = 2$ *and* $\tau_3 = \tau_6 = \tau_7 = 1.5$*. Then, for the error we have*

$$E\left(\prod_{i=1}^{7} P^{t+\sum_{j=1}^{i-1}\tau_j,\tau_i}\right) = 0.0114$$

and, in comparison, we obtain

$$E(P^{t,\tau}) = 0.0167$$

using the transition matrix over the whole time span, which is significantly larger. The normalized right singular vector corresponding to the second largest

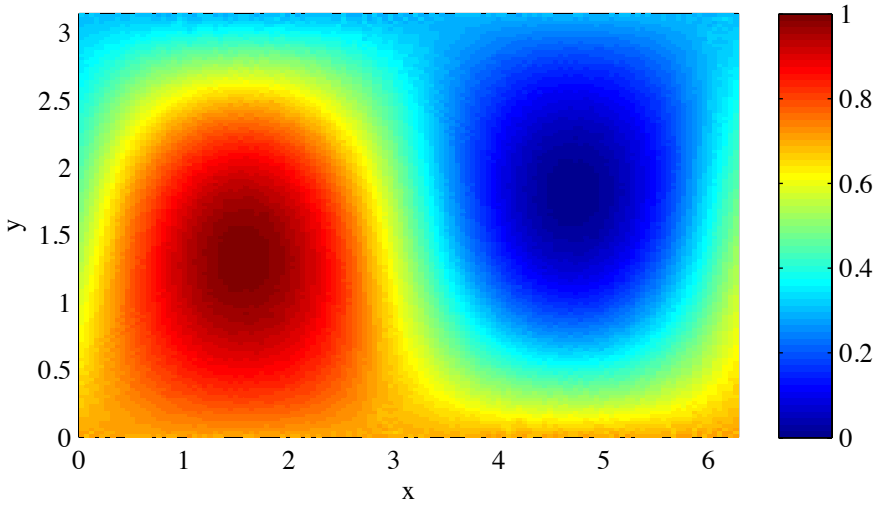

FIGURE 4.1: Normalized right singular vector of the product approach indicating coherent structures.

singular value of $\Pi_q^{-1/2}\left(\prod_{i=1}^{L} P^{t+\sum_{j=1}^{i-1}\tau_j,\tau_i}\right)\Pi_p^{1/2}$ *is shown in Figure 4.1, which is almost the same as the one of* $\Pi_q^{-1/2}P^{t,\tau}\Pi_p^{1/2}$ *shown in Figure 4.2.*

Another example illustrating the effectiveness of the product approach is given in Chapter 5 where a variant of Algorithm 3 is used to analyze coherent structures in the oceanic fluid flow in a turbulent region close to South Africa, the so-called Agulhas rings. Additionally, one can find in Section 6.3.2 a sensitivity analysis on the selection of the points in time where we split the approximation of the transfer operator.

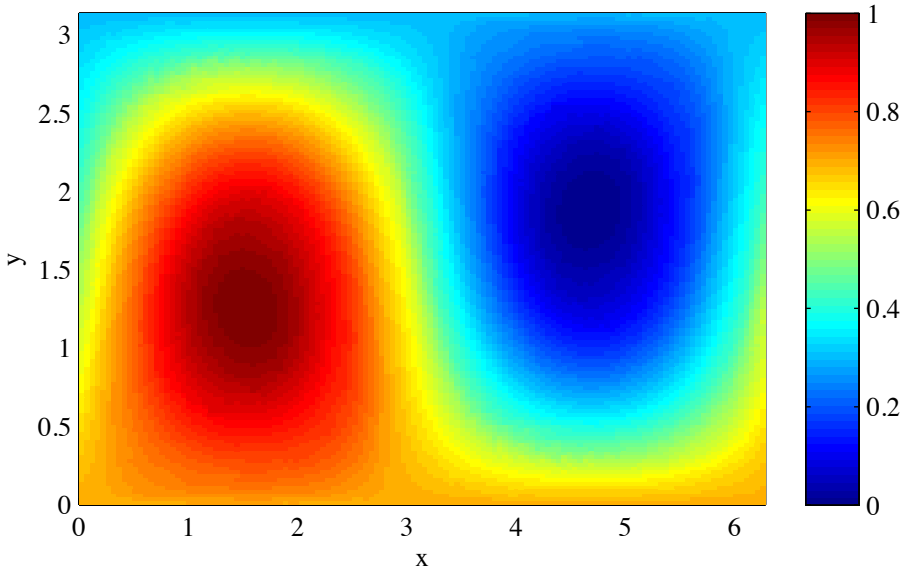

FIGURE 4.2: Normalized right singular vector of the direct approach indicating coherent structures.

CHAPTER 5

Efficient Numerical Approximation of Coherent Structures in Dynamical Systems

In this chapter, we review the results of [DH12] and reconsider the method for the approximation of coherent pairs over the time interval $[t, t+\tau] \subset \mathbb{T}$ for a non-autonomous dynamical system $(\phi, X, \mathbb{T})$, which has been introduced in Section 3.3 and first proposed by Froyland et al. [FSM10]. The method is summarized in Algorithm 2 which approximates coherent pairs of a non-autonomous dynamical system based on a partition $\mathcal{B} = \{B_1, ..., B_N\}$ of the state space X. The runtime of the algorithm directly depends on the number of test points in each element of the partition $\mathcal{B}$ which are involved in the approximation of the entries of the transition matrix $P^{t,\tau}$. In consequence, if each partition element is assigned the same number of test points, the smaller the domain $S \subset X$ in which we seek coherent pairs is, the fewer test points are needed to achieve sufficiently fine results and the faster the coherent structure can be approximated. The question directly arising is how the subpart S of the state space can be chosen as small as possible, but still large enough to find the coherent pair. For dynamical systems where we have no knowledge about the

location of a coherent pair in advance, we have to choose the whole state space X as the starting point of our investigation, which is the worst option from a computational point of view. As an answer of this question, we introduce a novel method which allows us to locate a subset in state space which is a candidate for containing a part of a coherent pair and is generally smaller than the whole state space. In the main result of this chapter (cf. Section 5.1), we show that transport phenomena over a fixed (long) time horizon imply the existence of almost invariant sets over shorter time intervals if the transport process is slow enough. The approximation of such a subset can be viewed as a preselection process for the computation of coherent pairs and is algorithmically formulated in Section 5.2.

5.1 Connecting Almost Invariant Sets and Coherent Pairs

The main idea for the preselection process is based on the fact that in many real world applications the coherent structures we are interested in are transported relatively slowly in comparison to the velocity of single particles in the system. On the ground of this observation, we identify an almost invariant set S over a short time interval which contains the first part of a coherent pair and can then be used as an input for Algorithm 2. Later, in Chapter 6, we analyze the movement of eddies in a very turbulent region of the ocean which naturally fulfills all assumptions made in this section. Concretely, it is shown in [Fli81] that water mass can only be advected by a rotating coherent structure if the rotational component of the velocity is larger than the translational component of the velocity (cf. [dvD04]). Therefore, in such systems we can distinguish between two time scales. On the one hand, there is the large time scale which exhibits non-autonomous coherent structures such as coherent pairs and on the other hand, the small time scale in which the coherent pairs leave their fingerprints as almost invariant sets. In this section, we consider a non-

autonomous dynamical system $(\phi, X, \mathbb{T})$ which is subject to these two different time scales and contains a (ρ, t, τ)-coherent pair (A_1, A_2). Furthermore, by $\tau \in \mathbb{T}$ and $s \in \mathbb{T}$ we denote the long and the small time scale, respectively.

We begin with an elementary observation with regard to the coherence ratio of two arbitrary subsets $A, B \subset X$:

5.1 Lemma ([DH12])**:** *Let μ be a probability measure on X and $t, \tau \in \mathbb{T}$. For two sets $A, B \subset X$, with $\mu(A) = \mu(\phi_{t+\tau}^{-\tau+s}(B)) > 0$, $s \in [0, \tau]$ fixed, we have*

$$\frac{\mu(\phi_{t+\tau}^{-\tau+s}(B) \cup A)}{\mu(A)} + \rho_{t+s}^{\tau-s}(A, B) = 2.$$

Proof. First we compute

$$\begin{aligned}\mu(\phi_{t+\tau}^{-\tau+s}(B) \cup A) + \mu(\phi_{t+\tau}^{-\tau+s}(B) \cap A) &= \mu(\phi_{t+\tau}^{-\tau+s}(B)) + \mu(A) \\ &= 2\mu(A).\end{aligned}$$

Dividing the equation by $\mu(A)$ and replacing $\frac{\mu(\phi_{t+\tau}^{-\tau+s}(B) \cap A)}{\mu(A)}$ by $\rho_{t+s}^{\tau-s}(A, B)$ completes the proof. □

In other words, the more coherent the sets A and B are over the interval $[t+s, t+\tau]$, the closer the fraction $\frac{\mu(\phi_{t+\tau}^{-\tau+s}(B) \cup A)}{\mu(A)}$ is to 1. In this case, most of the volume of $\phi_{t+\tau}^{-\tau+s}(B)$ is contained in A.

Based on this observation, we can directly state the following theorem which relates the coherence of a (ρ, t, τ)-coherent pair on the large time scale to the coherence of an almost invariant set on the small time scale.

5.2 Theorem ([DH12])**:** *Let μ be a probability measure, (A_1, A_2) a (ρ, t, τ)-coherent pair and $s \in [0, \tau]$ with $\mu(A_1) = \mu(\phi_{t+\tau}^{-\tau+s}(A_2)) > 0$. Then, for the set S defined by*

$$S = A_1 \cup \phi_{t+\tau}^{-\tau+s}(A_2),$$

we have the following estimate:

$$\rho_t^s(S,S) \geq \frac{1}{2 - c(t,\tau,s)} \rho_t^\tau(A_1, A_2) = \frac{1}{2 - c(t,\tau,s)} \rho, \tag{5.1}$$

where $c(t,\tau,s) = \rho_{t+s}^{\tau-s}(A_1, A_2)$.

Proof. By definition of ρ_t^s and S, we can write

$$\begin{aligned}
\rho_t^s(S,S) &= \frac{\mu(S \cap \phi_{t+s}^{-s}(S))}{\mu(S)} \\
&= \frac{\mu\left([A_1 \cup \phi_{t+\tau}^{-\tau+s}(A_2)] \cap \phi_{t+s}^{-s}(A_1 \cup \phi_{t+\tau}^{-\tau+s}(A_2))\right)}{\mu\left(A_1 \cup \phi_{t+\tau}^{-\tau+s}(A_2)\right)}.
\end{aligned}$$

Since $\phi_{t+s}^{-s}(\phi_{t+\tau}^{-\tau+s}(A_2)) = \phi_{t+\tau}^{-\tau}(A_2)$, we obtain by elementary facts from set calculus

$$\begin{aligned}
\rho_t^s(S,S) &= \frac{\mu\left([A_1 \cup \phi_{t+\tau}^{-\tau+s}(A_2)] \cap [\phi_{t+s}^{-s}(A_1) \cup \phi_{t+\tau}^{-\tau}(A_2)]\right)}{\mu\left(A_1 \cup \phi_{t+\tau}^{-\tau+s}(A_2)\right)} \\
&\geq \frac{\mu\left(A_1 \cap \phi_{t+\tau}^{-\tau}(A_2)\right)}{\mu\left(A_1 \cup \phi_{t+\tau}^{-\tau+s}(A_2)\right)} \qquad (*) \\
&= \frac{\mu(A_1)}{\mu\left(A_1 \cup \phi_{t+\tau}^{-\tau+s}(A_2)\right)} \frac{\mu\left(A_1 \cap \phi_{t+\tau}^{-\tau}(A_2)\right)}{\mu(A_1)} \\
&= \frac{\mu(A_1)}{\mu\left(A_1 \cup \phi_{t+\tau}^{-\tau+s}(A_2)\right)} \rho_t^\tau(A_1, A_2).
\end{aligned}$$

By Lemma 5.1, we have

$$\frac{\mu(A_1)}{\mu(\phi_{t+\tau}^{-\tau+s}(A_2) \cup A_1)} = \frac{1}{2 - \rho_{t+s}^{\tau-s}(A_1, A_2)}.$$

Therefore,

$$\begin{aligned}\rho_t^s(S,S) &\geq \frac{1}{2-\rho_{t+s}^{\tau-s}(A_1,A_2)}\rho_t^\tau(A_1,A_2),\\ &= \frac{1}{2-c(t,\tau,s)}\rho_t^\tau(A_1,A_2)\\ &= \frac{1}{2-c(t,\tau,s)}\rho,\end{aligned}$$

since (A_1, A_2) is a (ρ, t, τ)-coherent pair and $c(t, \tau, s) := \rho_{t+s}^{\tau-s}(A_1, A_2)$. □

We have $c(t, \tau, s) \in [0, 1]$ and suppose that the (ρ_1, t, τ)-coherent pair (A_1, A_2) has the property that both ρ_1 and $c(t, \tau, s)$ are near 1 for a fixed $s \in [0, \tau]$. Then the estimate in Equation (5.1) implies that there exists a (ρ_2, t, s)-almost invariant set S with $\rho_2 \approx 1$ and S contains the set A_1. We summarize this fact in the following corollary.

5.3 Corollary ([DH12])**:** *Let (A_1, A_2) be a (ρ_1, t, τ)-coherent pair and $s \in [0, \tau]$ with $\mu(A_1) = \mu(\phi_{t+\tau}^{-\tau+s}(A_2)) > 0$ and $c(t, \tau, s) = \rho_{t+s}^{\tau-s}(A_2, A_1) \approx 1$. Then there exists a (ρ_2, t, s)-almost invariant set S with $S = A_1 \cup \phi_{t+\tau}^{-\tau+s}(A_2)$ and ρ_2 close to one.*

Figure 5.1 illustrates the statement of Theorem 5.2. In detail, the interval X on the horizontal axis represents the state space of a non-autonomous dynamical system and the time is measured on the vertical axis. The two sets A_1 and A_2 of a coherent pair are shown at times t and $t + \tau$, respectively. We can see that the estimate provided by Theorem 5.2 is particularly useful in the case where the coherent structure is transported relatively slowly, i. e. A_1 is close to $\phi_{t+\tau}^{-\tau+s}(A_2)$ in comparison to the movement of other structures, e. g. the movement of B into $\phi_t^s(B)$. The choice of the small time scale s is not canonical and strongly depends on the specific application. Later in Section 5.2.3, we discuss how the small time scale can be chosen automatically.

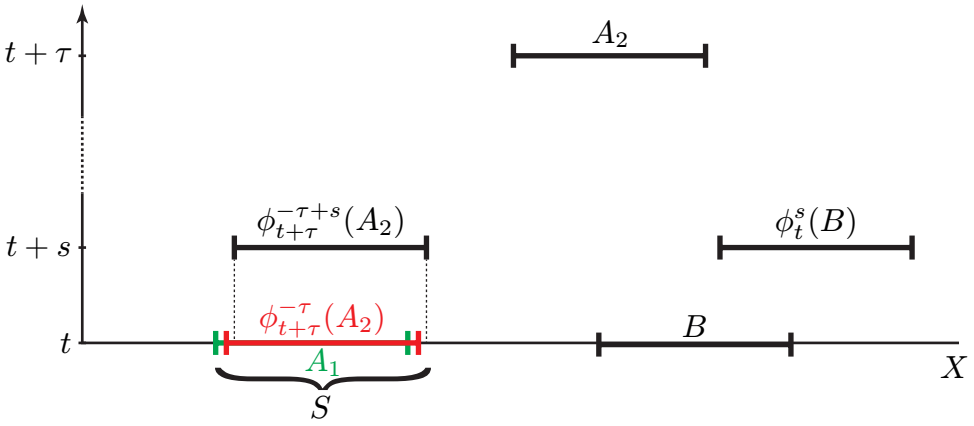

FIGURE 5.1: On the left, a (ρ, t, τ)-coherent pair (A_1, A_2) with ρ close to one is illustrated. The preimage $\phi_{t+\tau}^{-\tau+s}(A_2)$ of A_2 is almost identical to the set A_1. Therefore $S = \phi_{t+\tau}^{-\tau+s}(A_2) \cup A_2$ denotes a (ρ_2, t, s)-almost invariant set with $\rho_2 \approx 1$ as shown in Theorem 5.2. On the right, an arbitrary set B is chosen and the image $\phi_t^s(B)$ indicates that most of the mass of B leaves B after s time-units.

The choice of the set S has no direct dynamical interpretation but can be motivated by considering that $c(t, \tau, s) = \rho_{t+s}^{\tau-s}(A_1, A_2)$ is close to one. In that case, most of the mass of $\phi_{t+\tau}^{-\tau+s}(A_2)$ is contained in A_1 and thus S is approximately the set A_1 itself as in Figure 5.1.

In the proof of Theorem 5.2, the estimate $(*)$ appears to be very rough at first glance. However, equality can be obtained in Equation (5.1) by considering the specific situation where the set A_1 is invariant, i. e. A_1 is equal to $\phi_{t+s}^{-s}(A_1)$ and μ is an invariant measure of the underlying dynamical system. We can

compute

$$\begin{aligned} c(t,\tau,s) &= \frac{\mu(A_1 \cap \phi_{t+\tau}^{-\tau+s}(A_2))}{\mu(A_1)} \\ &= \frac{\mu(\phi_{t+s}^{-s}(A_1) \cap \phi_{t+s}^{-s}(\phi_{t+\tau}^{-\tau+s}(A_2)))}{\mu(A_1)} \\ &= \frac{\mu(A_1 \cap \phi_{t+\tau}^{-\tau}(A_2))}{\mu(A_1)} = \rho. \end{aligned}$$

Then the lower bound of $\rho_t^s(S,S)$ in Theorem 5.2 is given by $\frac{1}{2-\rho}\rho$ which tends to 1 for $\rho \to 1$. In that case, we obtain equality in Equation (5.1).

5.2 Algorithm for the Efficient Approximation of Coherent Pairs

The result of the previous section revealing that coherent pairs imply the existence of almost invariant sets allows us to directly design an algorithm for the efficient approximation of coherent pairs: Firstly, S is approximated and afterwards, Algorithm 2 is applied to S in order to approximate A_1.

If there is no separation of time scales as discussed in the previous section, then we cannot guarantee that the value $c(t,\tau,s)$ is large. Consequently, we will not be able to identify a (ρ,t,τ)-coherent pair in step 2 of Algorithm 4 with ρ close to one. In such situations, we can reuse the trajectory simulations of step 2 for the computation of the transfer matrix on S and combine them with trajectory simulations starting in $X \setminus S$ to compute the transition matrix on the whole state space X. As the trajectory calculations are the computationally most expensive task, the efficiency of the algorithm is mainly improved by seducing the number of trajectory calculations involved. In case, the value $c(t,\tau,s)$ is small, the number of trajectory calculations is the same as applying Algorithm 2 directly.

Algorithm 4 EfficientCoherentPairApproximation(t, τ, s, N, μ)

1: Apply Algorithm 1 to obtain $S = AlmostInvariantSet(t, s, N, \mu)$.
2: Apply Algorithm 2 to obtain $(A_1, A_2) = CoherentPair(t, \tau, N, M, S, \mu)$.
3: Return (A_1, A_2).

5.2.1 Numerical Effort

Now, we discuss the numerical effort of Algorithm 4 in more detail. It has been designed to avoid the calculation of the transition matrix over the whole interval $[t, t+\tau]$. Obviously, in step 2 of the algorithm the transition matrix $P^{t,\tau}$ needs to be approximated. However, for this computation, we can reuse test points already integrated over time s in step 1 which are located in S and integrate them further over the time interval $[t+s, t+\tau]$. In summary, the main computational effort of Algorithm 4 consists in the integration of test points distributed over the whole state space X over time s plus the integration of test points on the smaller set S over the rest of the time from $t+s$ to $t+\tau$. For a more detailed comparison of Algorithms 2 and 4, we assume that the boxes involved are filled with the same number of test points in each case. Then, we measure the runtime of an algorithm by the sum of the lengths of the integration intervals for each test point involved in the algorithms. In detail, the runtime of Algorithm 2 without the preselection step is dominated by $N \cdot \tau$ where $N \in \mathbb{N}$ is the number of boxes covering the whole state space X. On the other hand, the runtime of Algorithm 4 is dominated by $\mathrm{E}(N, N', \tau, s) = N \cdot s + N' \cdot (\tau - s)$, where $N' \in \mathbb{N}$ is the number of boxes covering the subset $S \subset X$. It is clear that $N \geq N'$ holds if we cover the state space X and the subset S by boxes of the same size. Then, we have $N \cdot \tau \geq N \cdot s + N' \cdot (\tau - s)$.

TABLE 5.1: Numerical effort of the integration process involved in the approximation of a coherent pair.

selection of S	numerical effort E	coherence ratio of the coherent pair
$S = X$	205 887	0.9874
S thresholded by -0.006	150 580	0.9874
S = maximal almost invariant set	105 003	0.9865
S thresholded by 0.006	60 454	0.9862

5.2.2 Example

Now, we discuss an example which applies this novel algorithm for the approximation of coherent pairs to the non-autonomous dynamical system given by the ordinary differential equation (2.2) considered in Example 3.9.

5.4 Example: *Again, we consider the non-autonomous ordinary differential equation of Example 2.4 with* $\nu = \frac{1}{4}$, $A = -2$ *and* $\epsilon = 1$. *Now, we apply Algorithm 4 with* $t = 0$, $\tau = 4\pi$, $s = \frac{\pi}{10}$ *and* $N = 16\,384$ *boxes. The result is a* $(0.9865, 0, 4\pi)$*-coherent pair* (B_1, B_2), *where the set* B_1 *is located in a preselected superset* $S \subset X$, *which is covered by* 8 150 *boxes. The superset* S *and the set* B_1 *are shown in Figure 5.2.*

The first obvious observation is that we have roughly halved the number of boxes used for the computation of the coherent pair in comparison to Example 3.13, whereas the coherence ratio is almost identical (see Table 5.1).

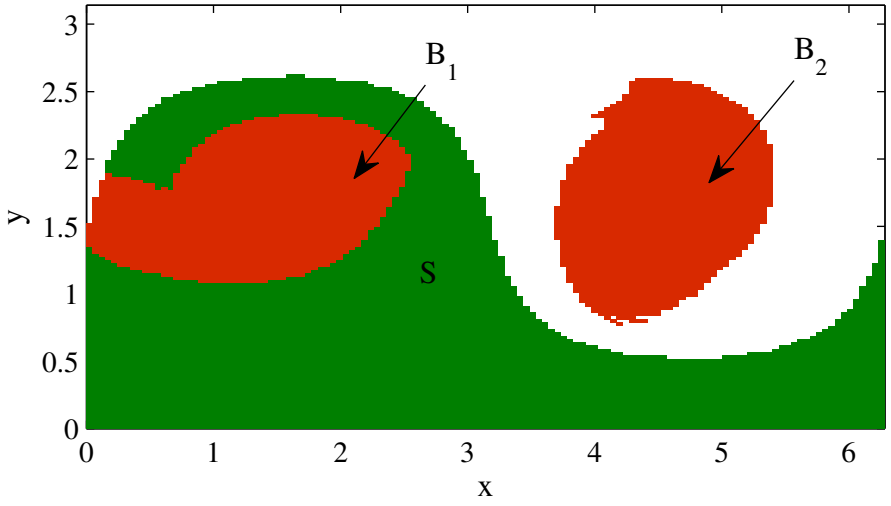

FIGURE 5.2: A $(0.9865, 0, 4\pi)$-coherent pair (B_1, B_2) and the set S covered by 8 150 boxes returned by the preselection process in Algorithm 4.

5.2.3 Parameter Adaption

Parameter s An adequate choice of the parameter s for the computation of the preselection S is not obvious in the example. Consider that we have chosen a fixed box-discretization of the state space on which we calculate the transition matrix. Therefore, the selection of s such that $\phi_t^s(B_i) \subset B_i$ for all $i = 1, ..., N$ will result in a transition matrix that is equal to the identity matrix. In consequence, we cannot identify any almost invariant set since all boxes themselves seem to be invariant. To avoid this, in Example 5.4, we have chosen a sufficiently large s such that most of the test points are mapped from one box into another. In contrast, the smaller the parameter s is the smaller is the numerical effort $\mathrm{E}(N, N', \tau, s)$. However, finding an a priori upper bound of s depends on the underlying application and, therefore, a theoretical statement cannot generally be expected to exist. Nevertheless, heuristically, we can start with a small value s and increase it successively while observing the eigenvalues of $P^{t,s}$. We stop if we obtain isolated eigenvalues close to one. They indicate the existence of the slowly decaying structure we seek for (cf. [DFS00]). In this procedure, we can reuse all the trajectory integrations used in the calculation of $P^{t,s}$ for the computation of $P^{t,s'}$ for an $s' > s$. Therefore, this is a suitable heuristic for choosing the parameter s.

Size of S Another parameter we can adjust is the size of the almost invariant set S. In step 1 of Algorithm 4, the almost invariant set S is computed based on the thresholding of the eigenvector v corresponding to the second largest eigenvalue of $P^{t,\tau}$. In this procedure, the threshold value is chosen in such a way that the coherence of the set S is maximized. Obviously, the requirement that the set S itself is maximally coherent is not necessary. Therefore, the choice of the set S can even be improved by selecting more appropriate level-sets of the eigenvector v.

In Figure 5.3, the eigenvector from Example 3.13 is shown together with the

resulting set A_1. For comparison, we have chosen the set S to be the level-set thresholded by the condition that the components of the eigenvector in Figure 5.3 are greater or equal to 0.006. This leads to a preselected set where the number of boxes covering it is again almost halved in comparison to the set S in Example 5.4. The result is a coherent pair (C_1, C_2) with a coherence ratio still acceptable (cf. Table 5.1). The preselected set S and the coherent pair (C_1, C_2) are illustrated in Figure 5.4. In contrast, we choose the set S to be the level-set determined by the components of the eigenvector in Figure 5.3 that are greater or equal to -0.006. In this case, the number of boxes covering the preselected set is equal to 11 870 in comparison to 16 384 boxes covering the whole state space X and the resulting (D_1, D_2) coherent pair has the same coherence ratio as the coherent pair (A_1, A_2) even though the according computational effort is reduced. The set D_1 and the corresponding preselection S are shown in Figure 5.5. The comparison of the numerical effort dominating the runtime of the algorithms for different choices of the size of the set S is given in Table 5.1.

For the automated (adapted) choice of the set S, it is possible to apply Algorithm 2 on every feasible level-set which are given by level-sets of an eigenvector of the transition matrix $P^{t,s}$. More precisely, we define an ascending series of level-sets starting with the smallest possible non-empty one and successively calculate – beginning with the smallest one – a coherent pair and stop if the coherence ratio is no longer rising. However, this procedure assumes monotony in the coherence ratio for the series of level-sets.

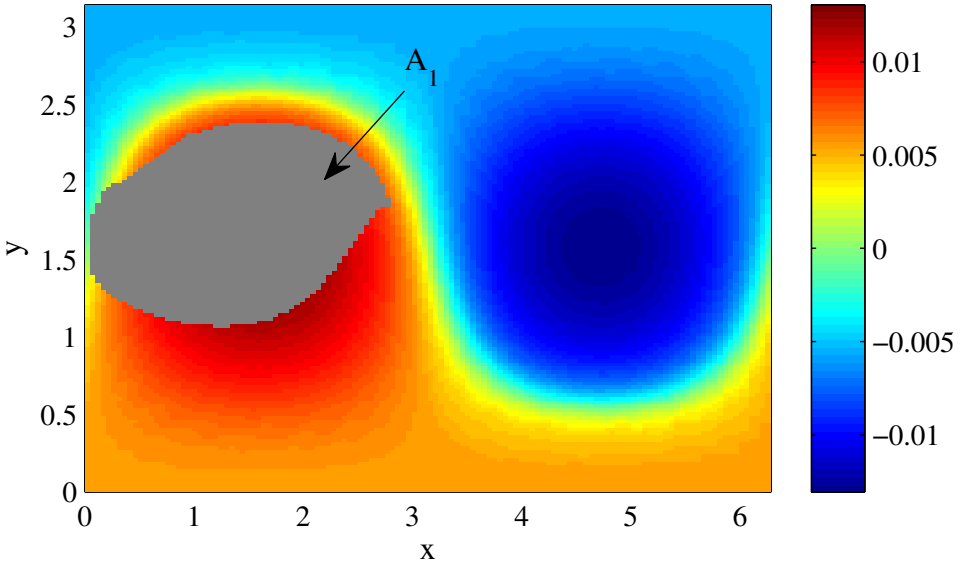

FIGURE 5.3: Eigenvector corresponding to the second largest eigenvalue of $P^{0,\frac{\pi}{10}}$ which is used by Algorithm 4 in Example 5.4 and the set A_1 calculated in Example 3.13. (Color scale represents the magnitude of the entries of the eigenvector.)

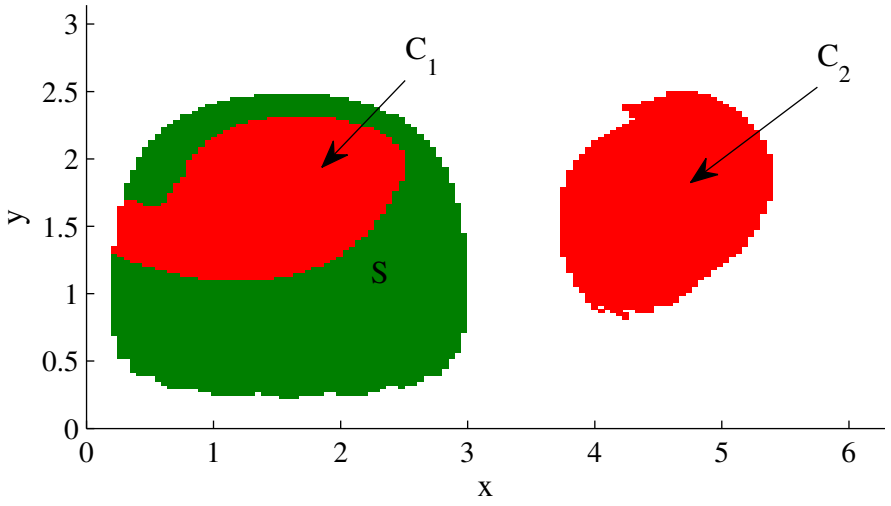

FIGURE 5.4: A $(0.9862, 0, 4\pi)$-coherent pair (C_1, C_2) returned by Algorithm 2 on a set S covered by 4 514 boxes which is given by a threshold on the entries of the eigenvector shown in Figure 5.3.

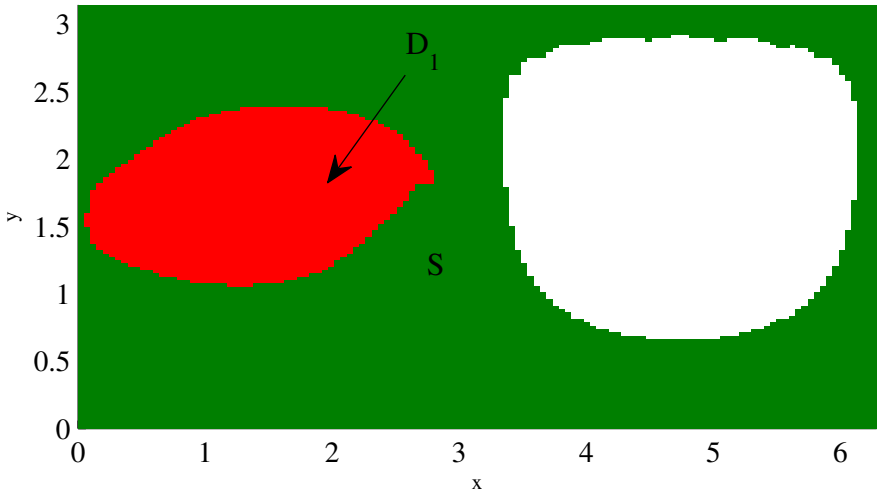

FIGURE 5.5: The set D_1 of a $(0.9874, 0, 4\pi)$-coherent pair (D_1, D_2) returned by Algorithm 2 on a set S covered by 11 870 boxes which is given by a threshold on the entries of the eigenvector shown in Figure 5.3.

CHAPTER 6

Detection of Coherent Structures in the Ocean

The purpose of this chapter is to demonstrate the successful application of the techniques developed in Chapters 4 and 5 for the treatment of transport phenomena in dynamical systems such as the oceanic fluid flow. Within the oceanic domain, many large and small scale transport processes have considerable impact on the movement of thermal energy around the planet. For example, the so-called *global oceanic overturning*, which is a complex network of currents at and underneath the sea surface, transports warm and cold water through the entire oceanic domain. This network can be interpreted as the heating system of our planet and, therefore, it directly effects the planet Earth's climate (cf. e. g. [MS12, WRSD02]). Induced by this network of currents in the oceanic fluid flow are large and small scale coherent structures, e. g. the *subpolar gyres* in the southern hemisphere or the so-called *Agulhas rings* in the North Atlantic. The subpolar gyres are also crucial for physical and biochemical processes in the Southern Ocean. The Weddell gyre, for example, exports a large quantity of carbon dioxide, which is formed by the remineralization of falling organic material into the deep ocean. The Agulhas rings are mobile ocean eddies which influence the transport of water mass from the Indian Ocean

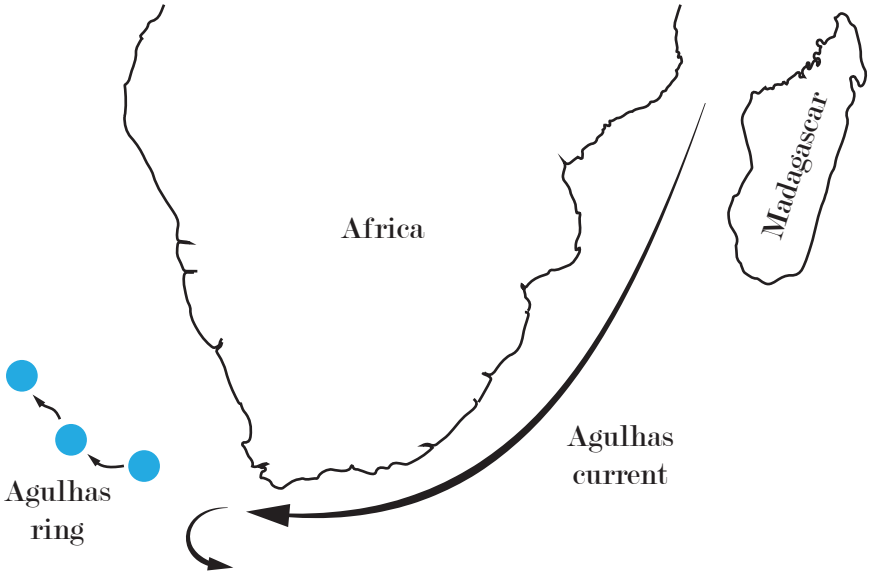

FIGURE 6.1: Surface view of the region around South Africa indicating the Agulhas current close to South Africa and an exemplary path of a single Agulhas ring (blue).

into the upper Atlantic Ocean. Agulhas rings originate periodically from the retroflection zone of the Agulhas current which sources in the Indian Ocean and flows along the east coast of Africa towards the southern tip. In Figure 6.1, the part of the Agulhas current close to South Africa is illustrated and the blue discs sketch the path of an exemplary Agulhas ring. For a review of the influence of the Agulhas current on the climate we refer to [BDBZ11].

Several approaches in ocean sciences have been developed for the observation of coherent oceanic structures. They often rely on two-dimensional satellite altimetry such as the sea surface height (SSH) or the surface velocity field and, in consequence, they only allow a study of gyres and eddies at the surface of the ocean. For an overview of recent two-dimensional approaches we refer to [CSS11]. However, for a comprehensive study of mass transported by these oceanic structures, a three-dimensional characterization method is required. In this chapter, we apply the mathematical methods developed in the previous chapters to the fully three-dimensional oceanic domain. The study is only

based on three-dimensional velocity fields which are an output of a global oceanic model but on no other information. For a comparison of the results, we discuss in Section 6.3 an extension of the two-dimensional velocity field based techniques to three-dimensions.

In dynamical systems theory, as already mentioned in Chapter 3, there mainly exist two approaches for the analysis of transport in dynamical systems. On the one hand, there is the geometric approach discussed in Chapter 3 which is designed to detect barriers of transport such as finite-time invariant manifolds via *finite-time Lyapunov exponents* (cf. [HY00, Hal01]). This approach has been successfully employed for the analysis of transport in many applications (cf. [SLM05]). However, Froyland et al. showed in [FPET07] that the approach performs poorly in the context of the investigation of the subpolar gyres. On the other hand, there is the probabilistic approach based on *transfer operator techniques* which has been successfully applied to identify oceanic structures at the surface and up to a depth of 500 m (cf. [FPET07, FSPD08]). In the following chapter, we apply the transfer operator techniques described in this thesis to the fully three-dimensional oceanic domain. This enables us to investigate the seasonal variability of the subpolar gyres and to study an Agulhas ring in three dimensions ([DFH$^+$09, FHR$^+$12]).

6.1 Transfer Operator Methods for the Oceanic Fluid Flow

In this section, we consider the oceanic fluid flow as a dynamical system as defined in Chapter 2. Then, we can apply the transfer operator machinery described in this thesis.

Let us denote the oceanic domain by $\mathcal{X} \subset [-180°, 180°] \times [-90°, 90°] \times [-11\,034\,\mathrm{m}, 0\,\mathrm{m}]$, where the landmass consisting of parts of the continents and islands is removed. The position of a particle $x_0 \in \mathcal{X}$ is given by its

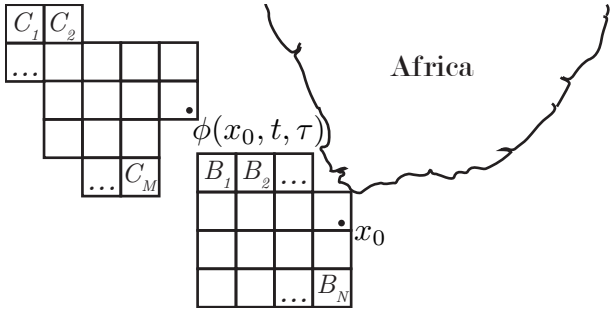

FIGURE 6.2: Part of the surface of the oceanic domain $\mathcal{X}$. The value $\phi(x_0, t, \tau)$ denotes the position of a particle starting at position x_0 at time t after flowing τ time-units. Furthermore, two coverings by boxes $B_1, \ldots, B_N$ and $C_1, \ldots, C_M$ of parts of the surface are illustrated.

longitude, latitude and depth coordinates and its flow through the oceanic domain is described by a time-dependent ordinary differential equation

$$\dot{x} = f(x, t), \tag{6.1}$$

with $f : \mathcal{X} \times \mathbb{T} \to \mathbb{R}^3$, where $\mathbb{T} = \mathbb{R}$ denotes the time in months. For this reason, as described in Remark 2.6, we can define the non-autonomous dynamical system $(\phi, \mathcal{X}, \mathbb{R})$ generated by the ordinary differential equation (6.1). Hence, we can interpret the oceanic fluid flow as follows: Let $x_0 \in \mathcal{X}$ be the position of a particle at time $t \in \mathbb{R}$. Then, the final position of the particle after flowing time $\tau \in \mathbb{R}$ is given by $\phi(x_0, t, \tau)$ (cf. Figure 6.2 for an example on the surface). Note that the generated non-autonomous dynamical system preserves the three-dimensional volume measure which we denote by V in the following.

The final position $\phi(x_0, t, \tau)$ of a particle x_0 can be obtained from the output of a global ocean model. However, we have to be careful with the approximation of the cocycle or the discretization of the oceanic state space to guarantee reliable results. In the remainder of this chapter, we use the output of the global ORCA025 model (cf. [BMP+06]). It provides five-day averaged velocities on a grid with 0.25° resolution in longitude and latitude direction and with

46 non-uniform levels of depth. In the model, the year is considered to have 360 days and a month 30 days. The velocity field $f(x,t)$ for non-grid points is approximated by linear interpolation independently in each direction (spatially and temporally). To obtain the terminal point $\phi(x_0,t,\tau)$, we use a standard Runge-Kutta approach with a step size of several hours.

Additionally, water particles close to the surface of the oceanic domain are subject to strong mixing affected by the wind, the waves, and surface cooling. This part underneath the surface is called the *mixed layer*. The information about the depth of the mixed layer is also provided by the ORCA025 model and the mixing between the surface and the mixed layer is simulated by a random uniform redistribution of the particles in depth direction after the integration over one month.

For an application of the techniques described in Chapter 3 and 5, we have to approximate a transfer operator $\mathcal{P}_t^\tau$ for a specific starting time t and duration τ. In the remainder of this chapter we choose as the starting time the first day of a specific month and we specify the flow duration τ in month, e. g. $\mathcal{P}^1_{May,2000}$ denotes the transfer operator beginning at May 1st, 2000 over 1 month. To approximate a transfer operator $\mathcal{P}_t^\tau$ we have to calculate a transition matrix $P^{t,\tau}$ on a box-covering of a subdomain X of $\mathcal{X}$ on which we seek coherent structures. Let $\mathcal{B} = \{B_1,\dots,B_N\}$ denote the initial covering of X by $N \in \mathbb{N}$ boxes and $\mathcal{C} = \{C_1,\dots,C_M\}$ the final covering of the image $\phi(X,t,\tau)$ of X. The numbers $N, M \in \mathbb{N}$ of boxes are chosen with respect to the according application. Figure 6.2 shows the box-covering of an oceanic domain X and its image on the surface. The numerical realization of $P^{t,\tau}$ is calculated as follows: Select for each box B_j in $\mathcal{B}$, $K \in \mathbb{N}$ water particles (test points) $p_{j,k} \in B_j$, integrate them over time τ beginning at time t and compute the transition matrix

$$P_{ij}^{t,\tau} = \frac{\sum_{k=1}^{K} \chi_{C_i}(\phi(p_{j,k},t,\tau))}{K}. \tag{6.2}$$

The entry $P_{ij}^{t,\tau}$ can be interpreted as the probability that a water particle

selected uniformly at random in B_j at time t will be in C_i at time $t + \tau$. For further technical details we refer to Section 2.4.

The dynamical system defined above and the corresponding transition matrix are the starting point for the transfer operator based analysis of the oceanic fluid flow. Two applications will be shown, the first one is an investigation of the subpolar gyres and the second one is a three-dimensional study of an Agulhas ring.

6.2 Seasonal Variability of the Subpolar Gyres in the Southern Ocean

The first one of the two applications we describe in this chapter is the investigation of the seasonal variability of the subpolar gyres in the Southern Ocean. As already mentioned, these gyres are crucial for physical and biochemical processes in this region. In particular, to identify the coherent structures in the Weddell and Ross Seas, we focus on a part $X = \mathcal{X} \cap ([-180°, 180°] \times [-76°, -48°] \times [-5\,570\,\mathrm{m}, 0\,\mathrm{m}])$ of the oceanic domain $\mathcal{X}$.

The subpolar gyres are spatially almost fixed structures and, thus, we are able to identify them as almost invariant sets in the non-autonomous dynamical system induced by the oceanic fluid flow. Nevertheless, these structures slowly change their shape between the seasons. Therefore, we identify almost invariant sets over each season in the southern hemisphere. To investigate the seasonal variability, Algorithm 1 is applied to the domain X with $\tau = 3$ months and t equal to the first day of November, 2003, February, 2004, May 2004 and August, 2004, for each season in the southern hemisphere. For our computations we concentrate on trajectories for which the initial and terminal points are in X. Therefore, the initial and final box-covering is the same for the computation of the transition matrix. However, some of these may pass into $\mathcal{X} \setminus X$ and reenter X. The four transition matrices for each season are $P^{November,2003;3}$,

$P^{February,2004;3}$, $P^{May,2004;3}$ and $P^{August,2004;3}$. The Algorithm is adapted in such a way that the eigenvalues and eigenvectors of the reversible version of the transition matrix are calculated (cf. Remark 3.8). Also, for the identification of the Weddell and Ross gyres we take into account more eigenvalues than those discussed in Remark 3.7.

The computations reveal almost invariant sets in the Weddell and Ross Sea for each season, respectively, which are shown in Figure 6.3. The coherence ratio and the volume of each structure is given in Table 6.1. Significant differences over the four seasons can be identified to lie in the volume of the gyres in each season. During spring and summer, the Weddell gyre extends from the surface to depths exceeding 4 000 m, while in autumn and winter the main structures of the gyres are subsurface and extend to much shallower depths. We remark that a robustness analysis of such results would require an investigation of the Weddell and Ross gyre over multiple years. However, the results show the successful application of transfer operator methods for the detection of oceanic coherent structures in principle.

In the following, we present further methods for the analysis of coherent structures based on the transition matrix. We study the flux of water through the boundary of the identified gyres as well as the mean residence time of water within the Weddell gyre for each season.

6.2.1 Water Flux of the Subpolar Gyres

The flux of water through a boundary box of a coherent structure $A = \cup_{i \in I} B_i \subset X$ can be calculated as follows: We call a box B a boundary box if it has at least one neighbor box outside the structure. Let $J \subset I$ be the index set of the boundary boxes of A and P the transition matrix of the season for which we calculate the flux of water and V the three-dimensional volume measure. We

TABLE 6.1: Coherence ratios of the coherent structures in the Weddell and Ross Sea for each season.

Weddell Gyre

Season	Coherence Ratio	Volume
Summer	0.9265	$1\,484\,272\,\mathrm{km}^3$
Autumn	0.9112	$856\,851\,\mathrm{km}^3$
Winter	0.9106	$986\,105\,\mathrm{km}^3$
Spring	0.9190	$1\,049\,534\,\mathrm{km}^3$

Ross Gyre

Season	Coherence Ratio	Volume
Summer	0.9235	$1\,279\,044\,\mathrm{km}^3$
Autumn	0.9179	$1\,645\,748\,\mathrm{km}^3$
Winter	0.8865	$1\,286\,165\,\mathrm{km}^3$
Spring	0.9042	$1\,800\,793\,\mathrm{km}^3$

define the flux through a boundary box $B_j, j \in J$, out of A by

$$\text{flux}_{\text{out}}(B_j) = V(B_j) \sum_{k \in \{1,\dots,N\} \setminus I} P_{kj},$$

where the indices $\{1, \dots, N\} \setminus I$ denote all the outside of the structure A. Recall that P_{kj} denotes the probability that a trajectory starts at random in B_j ends up in B_k and that the domain X is covered by $N \in \mathbb{N}$ boxes. Furthermore, we denote the flux through the boundary box B_j from outside A by

$$\text{flux}_{\text{in}}(B_j) = \sum_{k \in \{1,\dots,N\} \setminus I} V(B_k) P_{jk}.$$

Then the total flux(B_j) trough a boundary box B_j, $j \in J$, is the difference between the flux through a boundary box out of A and the flux into B_j from outside A:

$$\text{flux}(B_j) = \text{flux}_{\text{out}}(B_j) - \text{flux}_{\text{in}}(B_j).$$

The boundaries of the structures in Figure 6.3 are colored according to the flux of water through a boundary box and indicates in which region water enters or escapes from the gyre.

6.2.2 Mean Residence Time

For a further analysis of transport phenomena the transfer operators can also be used to calculate the mean residence time of water within gyres as described in Section 3.2.2. For the moment, in order to describe the computation of the mean residence time, we focus on the coherent structure $A^W = \bigcup_{i \in I} B_i$ identified in the Weddell Sea in the summer season, for example. Beginning

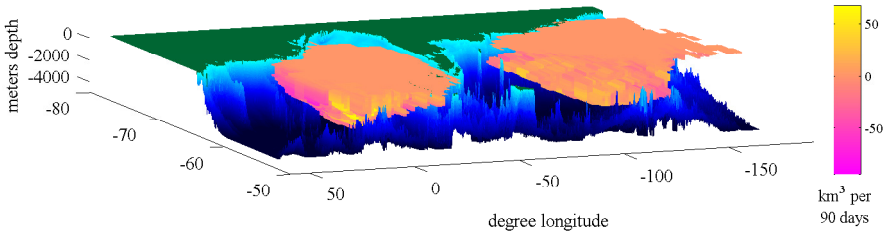

(a)

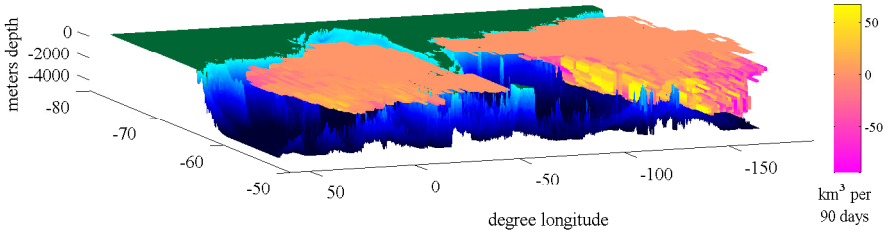

(b)

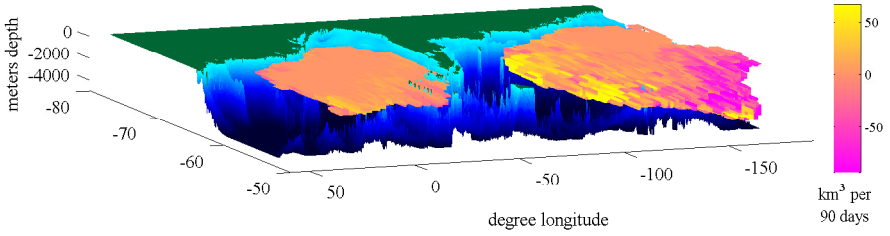

(c)

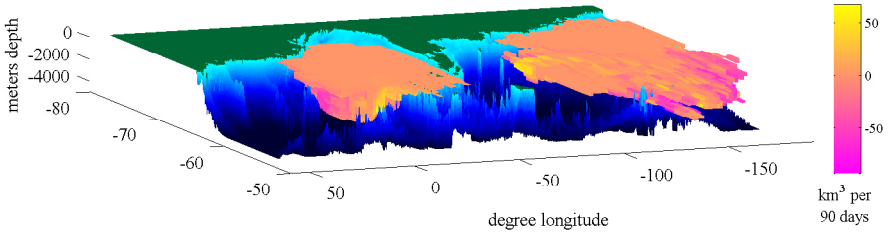

(d)

FIGURE 6.3: Coherent structures in the Weddell and Ross Sea in (a) summer, (b) autumn, (c) winter, and (d) spring. The coloring of the boxes shows the volume flux of water through boundary boxes over each season.

with this season we define a transition matrix

$$P = P^{August,2004;3} \cdot P^{May,2004;3} \cdot P^{February,2004;3} \cdot P^{November,2003;3},$$

which represents the dynamics over one year from the start of summer. To calculate the mean residence time of water originating from A^W with respect to P as described in Section 3.2.2 the technical assumption $\lim_{k\to\infty}(P|_{A^W})^k = 0$ for the restriction $P|_{A^W}$ of the transition matrix P to the set A^W has to be satisfied. This can be interpreted as follows: water mass originating from the coherent structure A^W will eventually leave the structure. Following Section 3.2.2, the average time t_i required for a particle originating in B_i, for an $i \in I$, to leave the set A^W is given by the solution of the linear equation

$$(\mathrm{Id} - P|_{A^W})t = (1, 1, \ldots, 1)^T,$$

where Id denotes the identity matrix.

This procedure is repeated for the other seasons. The mean residence time is plotted in Figure 6.4 which shows zonal sections along $-64°$S latitude. The coloring indicates the average time that a particle originating within the box will remain in the gyre for each season, respectively.

6.2.3 Pathway of Water

To investigate the pathway of water exiting or entering the gyre we define a vector $v \in \mathbb{R}^N$, which has uniform non-zero entries v_i if B_i is in the gyre or in a specified subregion and $v_i = 0$ otherwise, and multiply it sequentially by the transition matrix for each season (cf. Section 4.1). By repeating this procedure multiple times we can simulate the spreading out of water from any given region over multiple years. Of course, this repeated application neglects the year-to-year variations on the flow field. However, this approach has the advantage of being numerically efficient for the detection of such pathways,

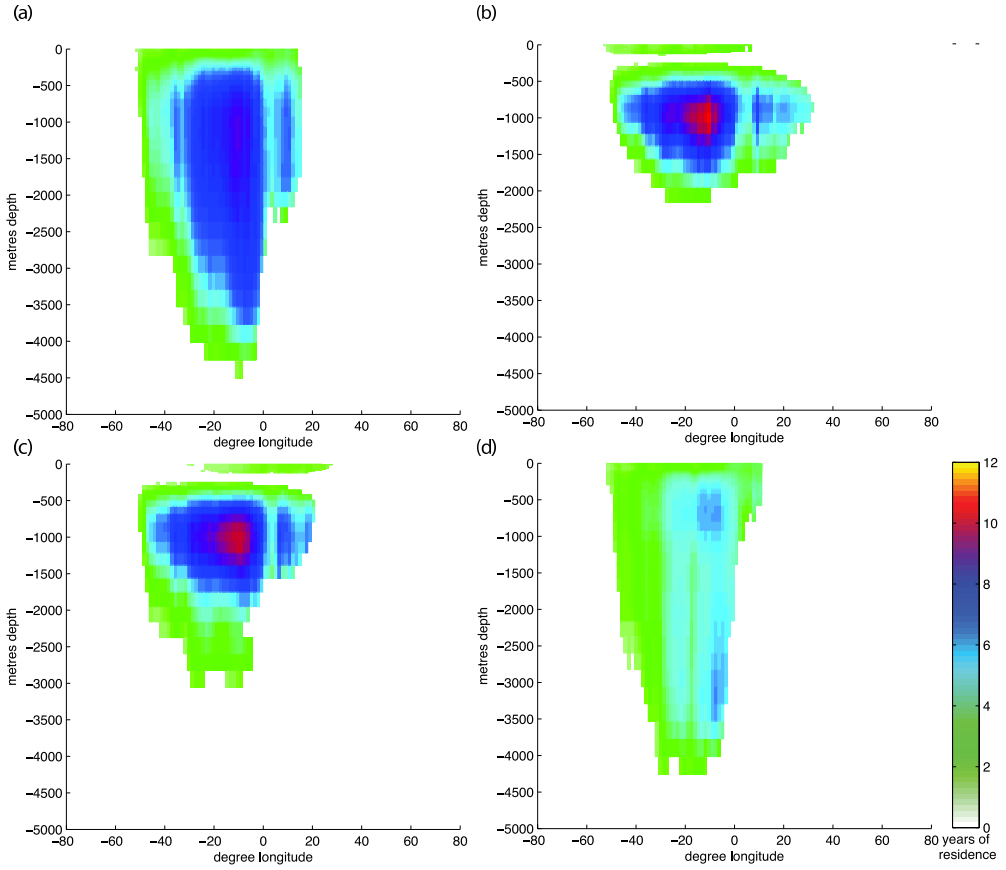

FIGURE 6.4: Zonal section of Weddell gyre during (a) summer, (b) autumn, (c) winter, and (d) spring along $-64°S$. Boxes are colored according to the mean residence time of water in the Weddell gyre in years.

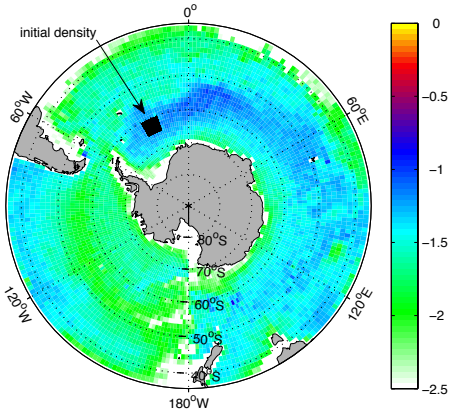

FIGURE 6.5: Horizontal surface section of the final state of an initial density after 50 years of evolution by 50 iterations of the one year transition matrix. Boxes are colored according to the logarithm of the normalized density.

since the transition matrices have been already calculated. Therefore, the time-stepping of a large number of Lagrangian particles can be efficiently achieved through a number of matrix-vector calculations. Figure 6.5 shows a horizontal surface section of the final state of such an initial density after 50 years of evolution by 50 iterations of the one year transition matrix.

This application shows the suitability of the transfer operator methods for the analysis of the oceanic fluid flow. It is shown that we are able to identify almost invariant sets in the fully three-dimensional domain of the Southern Ocean. In contrast, common oceanography techniques are restricted to the ocean's surface and cannot be used for a three-dimensional analysis. Additionally, we demonstrated that we can further analyze the almost invariant sets by calculating the flux and the mean residence times of water. In the next section we apply the transfer operator techniques to another region in the oceanic domain and we extend the two-dimensional oceanography techniques to the vertical direction for comparison.

6.3 Three-dimensional Characterization and Tracking of an Agulhas Ring

Transport induced by eddies is another important aspect of the analysis of mass transported by the global oceanic overturning as described in the beginning of this chapter. In this section we study an Agulhas ring using transfer operator techniques and compare the result with standard oceanographic approaches (cf. [FHR$^+$12]). Agulhas rings transport warm saline water form the Indian Ocean into the upper Atlantic Ocean (cf. Figure 6.1). The amount of heat and salt an Agulhas ring transports sensitively depends on the time the water remains within a ring as well as on its path (cf. [TBBM03]). Hence, the dynamical system approaches seeking maximally coherent structures are suitable for the study of single Agulhas rings. In comparison to the previous section, we search for coherent pairs rather than almost invariant sets, because the Agulhas rings are highly mobile within the oceanic domain.

6.3.1 Domain Preselection

Since the oceanic domain is large, a crucial part of the investigation is the preselection of a domain where we expect the occurrence of a single Agulhas ring. We developed a novel approach in Chapter 5 for the preselection of regions in the state space of a dynamical system containing a coherent pair. For the preselection of a domain containing a single Agulhas ring, we apply Corollary 5.3 and calculate eigenvalues and vectors of the transition matrix $P^{t,s}$ on a domain around the Agulhas retroflection zone, with s equal to one week and t equal to May, 1st, 2000. In Figure 6.6a an eigenvector of the transition matrix is shown indicating a region on the oceanic surface which contains a single Agulhas ring.

In ocean dynamics we can alternatively use satellite altimetry for a precise

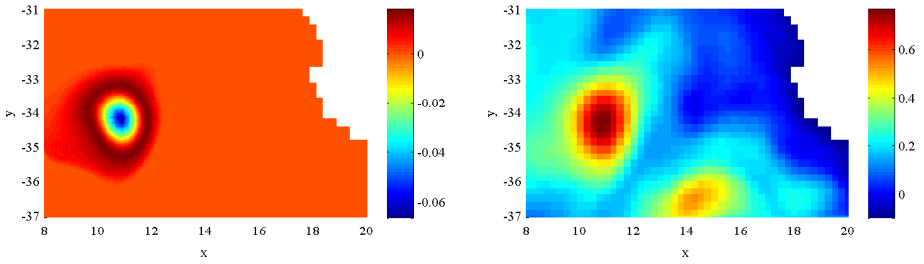

(a) (b)

FIGURE 6.6: Indication of the location of an Agulhas ring by (a) the peaks in the eigenvector of a transition matrix P and by (b) the peaks in the sea surface height (SSH) field.

localization of a domain containing a single ring-like structure. Namely, peaks in the sea surface height (SSH) indicate the existence of an ocean eddy. For a comparison to the dynamical system approach the SSH field around the Agulhas retroflection zone is shown in Figure 6.6b and we mention that the peak in the eigenvector in Figure 6.6a coincides with a peak in the SSH field.

From now on, we focus on a part of the ocean, specifically $X = \mathcal{X} \cap [8.5°E, 13°E] \times [36°S, 32.5°S] \times [0\,\text{m}, -5\,126\,\text{m}]$, which contains a single ring-like structure. The domain is subdivided into 13 359 boxes such that each box has a side-length of 0.1758° longitude and 0.2246° latitude. The ratio between the longitude and latitude side-length of the boxes is chosen in such a way that the boxes are approximately square on the surface of the ocean and the vertical extension is chosen in correspondence with the 46 non-uniform depth layers of the underlying ORCA025 model. We investigate the single Agulhas ring lying in the initial region over the time period from the beginning of May to the beginning of November. This time period has been chosen such that the computational effort is acceptable and that the Agulhas ring undergoes substantial decay, i. e. a substantial portion of water mass leaves the structure. In addition, the chosen period is very close to the average lifetime of mesoscale eddies in the global

ocean (cf. [CSS11]).

6.3.2 Application of the Product Approach

Due to the very turbulent Agulhas retroflection zone (cf. Figure 6.1), the calculation of a transition matrix over six months is a computationally difficult task. We must be careful about the integration step size and the number of test points for the approximation of Equation (6.2). If we choose too few test points over the integration time of 6 months, the final points do not represent the image of the initial boxes well. To avoid this problem, we apply Algorithm 3 which ensures that the box-covering of the image of the initial domain is still connected. Hence, the transition matrix $P^{May,2000;6}$ over the whole period is approximated by a product of transition matrices over one month each:

$$P^{May,2000;6} \approx P^{October,2000;1} \cdot P^{September,2000;1} \cdot \ldots \cdot P^{May,2000;1}.$$

A flow duration of one month is sufficiently short such that the initial test points in each box flow to a collection of boxes that represent the true one-month-image of the box very well. Finally, the singular values and vectors were calculated to obtain a coherent pair $(A_{May,2000}, A_{November,2000})$ as described in Algorithm 2.

The coherent pair $(A_{May,2000}, A_{November,2000})$ is illustrated in Figure 6.7. The coherence ratio is 0.7631, which means that over 6 months $76,31\%$ of the water mass from $A_{May,2000}$ flows into the set $A_{November,2000}$.

The sensitivity of the previous results with respect to changes of some parameters of the used technique is discussed in the following. Therefore, we calculate singular values and vectors of $P^{May,2000;3}$ and $P^{July,2000;1} \cdot P^{June,2000;1} \cdot P^{May,2000;1}$ to check the robustness of the choice of the parameter τ, for $\tau = 1$ and $\tau = 3$ in Algorithm 2. The result of the analysis of one month is displayed in Figure 6.8a and Figure 6.8b, where Figure 6.8a shows the surface slice of the normalized

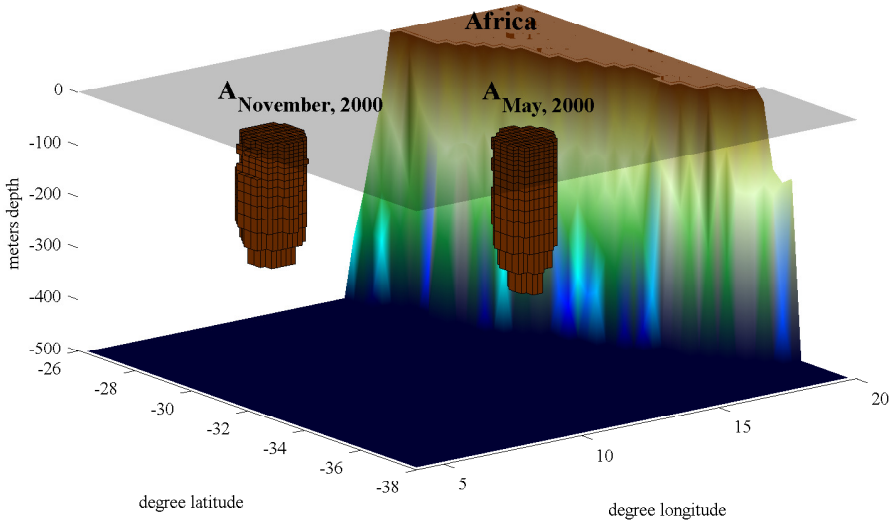

FIGURE 6.7: The initial $A_{May,2000}$ and final $A_{November,2000}$ set of the detected coherent pair. 76.31% of the water mass from $A_{May,2000}$ flows into the set $A_{November,2000}$ over 6 months.

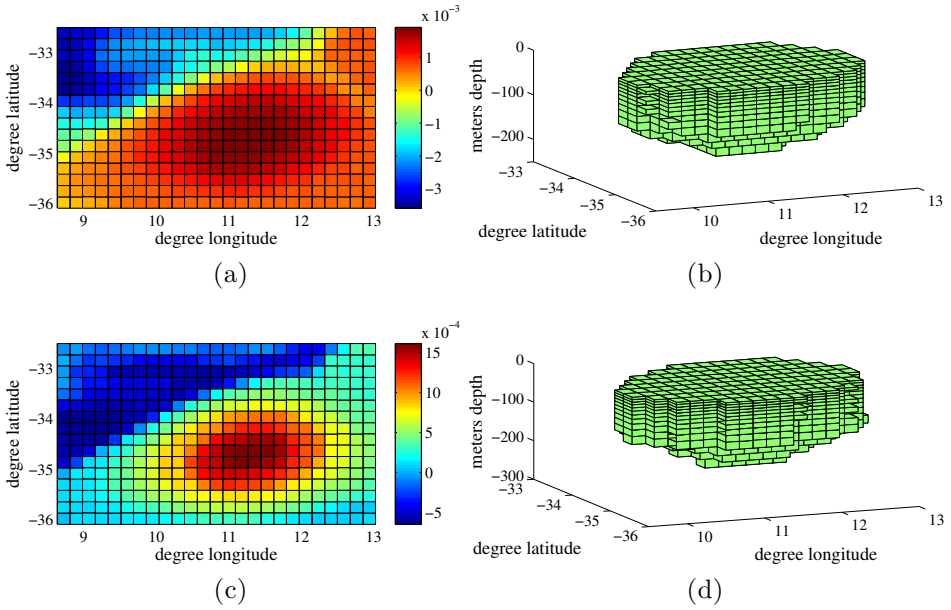

FIGURE 6.8: (a) Surface slice of the normalized left singular vector of the one month analysis indicating the Agulhas ring at May 2000. (b) The initial set of the detected coherent pair over one month. (c) Surface slice of the normalized left singular vector of the three month analysis indicating the Agulhas ring at May 2000. (d) The initial set of the detected coherent pair over three months.

left singular vector indicating the Agulhas ring at the surface and Figure 6.8b shows the corresponding Agulhas ring. Figure 6.8c and 6.8d indicate similar results for the investigation over three months. These two comparative studies identify initial coherent structures that are similar to the study over 6 months. Hence, the transfer operator approach is reasonably robust with respect to flow time.

Additionally, the sensitivity of the product approach (cf. Algorithm 3) has been investigated using different temporal subdivisions. For a comparative study we define 12 transition matrices each over a half month and two matrices

over three months each. The singular vectors indicate very similar structures attesting the robustness of the product approach developed in this thesis.

6.3.3 Comparison with Other Techniques

In the introduction of this chapter we mentioned that several methods exist for the investigation of eddies in the ocean surface. These techniques are based on sea surface height (SSH), the relative vorticity criterion (RV), and the Okubo-Weiss parameter (OW). In the investigation discussed in this section we analyze the three-dimensional shape of an Agulhas ring with transfer operator techniques. Therefore, we extend the surface techniques along the vertical direction for comparison.

Consider $u(x, y)$ and $v(x, y)$ as the velocity of a particle (x, y) on the surface in longitude and latitude direction, respectively. Then, the relative vorticity (RV) is given by

$$\mathrm{RV}(x, y) = \frac{\partial v}{\partial x} - \frac{\partial u}{\partial y}$$

and the Okubo-Weiss (OW) parameter by

$$\mathrm{OW}(x, y) = \left(\frac{\partial u}{\partial x} - \frac{\partial v}{\partial y}\right)^2 + \left(\frac{\partial v}{\partial x} + \frac{\partial u}{\partial y}\right)^2 + \mathrm{RV}(x, y)^2.$$

The interpolation of the RV and OW is performed based on the same grid on the surface as it is used for the approximation of the transfer operators, where the derivatives are calculated numerically. Coherent oceanic structures identified via the RV or the OW parameter are obtained by selecting regions where the RV or the OW parameter is above a certain threshold. We use a common threshold coefficient to define the edge of the Agulhas ring that we are investigating. For the RV we chose 0.2 times the maximum RV value at the surface and for the OW we select 0.2 times the standard deviation of OW

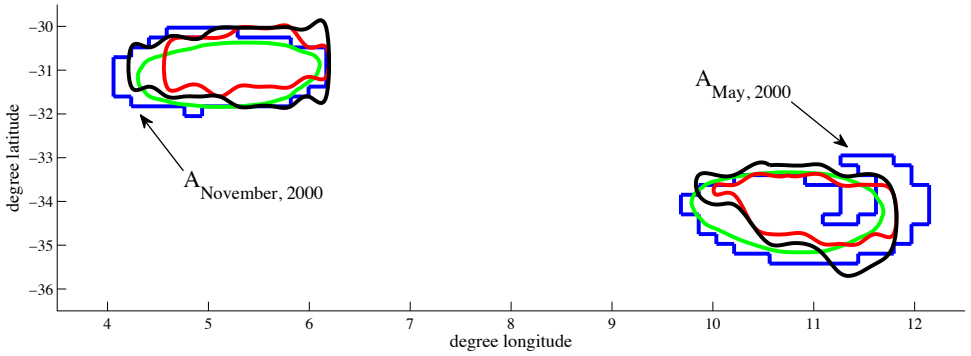

FIGURE 6.9: Surface extension of the sets $A_{May,2000}$ and $A_{November,2000}$ (blue) and the boundary of the corresponding structures given by the maximal SSH gradient (green), Okubo-Weiss parameter thresholded by 0.2 times the standard deviation (red) and relative vorticity thresholded by 0.2 times the maximum relative vorticity (black).

at the surface (cf. [CGG08]). Also, the maximum SSH gradient defines the edge of an Agulhas ring. Figure 6.9 demonstrates that the different techniques identify similar surface structures.

For a comparison of the coherence ratio of the three-dimensional structure defined by the transfer operator approach we extend the surface shape given by the techniques based on RV and OW up to the depth where the set $A_{May,2000}$ ends. In more detail, we calculate the OW and RV field for May and November 2000 at each depth level within the box discretization used for the approximation of the transfer operator. The threshold at the final time is chosen in such a way that the initial and final structures have equal volume. This is sufficient for the calculation of the coherence ratio. For the threshold of the initial structure we point out two options:

1. We firstly fix the threshold of the RV and OW at the surface and secondly use the same threshold on each depth level (layer by surface).

2. We threshold on each depth level separately (layer by layer).

These two options give almost identical coherence ratios. Therefore, we report only on the layer by surface results which are shown in row two and three of Table 6.2. Compared to the transfer operator results, we gain an improvement in the coherence ratio by $15\% - 24\%$ for the transfer operator method. However, the structures given by the OW and the RV approach are of quite different volumes (Table 6.2). The suggestion is that the transfer operator method identifies the core region of the Agulhas ring which is more coherent than the larger structures. Therefore, we adjust the threshold for the two approaches such that the volumes of the structures are almost identical to the ones identified by the transfer operator approach. Nevertheless, the transfer operator approach still represents an improvement of approximately 15% over the other methods (row four and five of Table 6.2). As a last step we thresholded both RV and OW by maximizing the coherence ratio which leads to almost the same coherence ratios (row six and seven of Table 6.2) as using the fitted volume approach. Finally, we can state that the transfer operator approach discussed in this thesis defines three-dimensional structures within the oceanic fluid flow that have higher coherence than the corresponding objects identified by RV and OW. The reason for this improvement in coherence is that the RV and the OW are essentially two-dimensional techniques extended to three-dimensions. Furthermore, the transfer operator method is designed to directly capture regions of maximal coherence.

It is shown that we capture the coherence of a single Agulhas ring more accurately than other common techniques based on two-dimensional velocity information. To substantiate the results, the application of the transfer operator techniques to other Agulhas rings and over longer time intervals has to be addressed in future research.

TABLE 6.2: Coherence ratios and volume of three-dimensional Agulhas ring characterization given by the transfer operator approach in comparison to the thresholding of the relative vorticity (RV) and the Okubo-Weiss criterium (OW).

	Method	**Volume**	**Coherence Ratio**
1	Transfer Operator Approach	5 481km^3	76.31%
2	OW (0.2 threshold)	7 752km^3	52.17%
3	RV (0.2 threshold)	9 547km^3	61.23%
4	OW (fitted volume)	5 495km^3	60.87%
5	RV (fitted volume)	5 492km^3	61.65%
6	OW (optimized threshold)	5 527km^3	60.98%
7	RV (optimized threshold)	5 693km^3	62.30%

CHAPTER 7

Conclusion

This work contains a wide range of aspects from dynamical systems theory to ocean dynamics. It is, therefore, necessary to take a look at the "big picture" of this thesis by summarizing the obtained results, discussing further directions of research as well as sketching ideas for possible future research. This is the task of this final chapter.

Autonomous Coherent Structures

In the autonomous case, *almost invariant sets* provide an established concept for the analysis of transport phenomena. We consider these autonomous structures in the more general context of time-dependent systems. Such structures are spatially fixed in state space and, therefore, can be used to determine fixed structures like large gyres in the oceanic domain. In this work, we use the notion of almost invariant sets to study the *seasonal variability* of the *subpolar gyres* in the fully three-dimensional domain of the *Southern Ocean*. Furthermore, there is a variety of dynamical system techniques which we present in the time-dependent setting and apply to the *oceanic fluid flow* in order to study the *water flux* and the *mean residence time* of water in the gyres as well as the *pathways of water* leaving the gyres.

For these investigations, we calculate a transition matrix for each season by considering time-t maps of the oceanic fluid flow over each season. By considering the product of these matrices, we approximate the one-year transition matrix of the oceanic fluid flow in the Southern Ocean and used this matrix e. g. to study the pathway of water or the mean residence time.

Non-Autonomous Coherent Structures

Coherent pairs are the time-dependent analog of almost invariant sets. For the efficient approximation of coherent pairs, we extend the current methods for the analysis of transport phenomena in non-autonomous dynamical systems by transfer operator techniques. In particular, we utilize a *product eigenvalue approach* to formulate a method for the efficient approximation of coherent pairs over *long time intervals*. In more detail, instead of calculating a transition matrix for a long time interval, we split up the time interval and approximate the transition matrix by a product of transition matrices over shorter time intervals. This procedure allows us to take into account certain physical properties of the underlying dynamical systems such as volume preservation. Furthermore, we prove a suitable error bound for this type of approximation and, in addition, we develop Algorithm 3 which automatically calculates the splitting based on a predefined error function. To demonstrate the capacity of this method, we apply it to an idealized example as well as to the oceanic fluid flow as a real world application, where an *Agulhas ring* in three dimensions over six months is investigated. This is the first fully three-dimensional investigation of an ocean eddy.

Furthermore, we design a method for the efficient approximation of coherent pairs. More precisely, for this task, it is necessary to run a high number of different simulations of the underlying process on the whole state space. We achieve the theoretical result that coherent pairs induce almost invariant sets over certain small time intervals (cf. Theorem 5.2). This fact is used to formulate Algorithm 4 for the *preselection of domains* as candidates containing one part of a coherent pair. Thereby, we can reduce the number of different simulations

considerably by only performing the ones on the existing almost invariant set. Thus, by this method, we can significantly reduce the computational effort for the approximation of coherent pairs. Additionally, we discuss the behavior of the algorithm under several parameter variations and make suggestions for the (automated) selection of the parameters of the algorithm. We show that this method can be used to identify regions in the oceanic domain containing a single Agulhas ring as opposed to the identification of such regions by the inspection of the sea surface height.

The methods developed here are utilized to analyze transport phenomena in the *oceanic fluid flow*. It is a fact that the climate system is substantially effected by the transport of warm and cold water in the ocean. However, the purpose of this thesis is not to obtain answers in the context of the complex climate system but to provide methods for the investigation of transport in the oceanic fluid flow by dynamical system techniques. Hence, this thesis provides a new perspective for the analysis of oceanic structures.

Future Research Directions

There still exist several challenging problems and directions for further research, as we discuss in the following.

For a given time span, Algorithm 3 is capable of calculating a series of transition matrices whose product approximates the transfer operator. We illustrate the effectiveness of the product approach by means of Example 4.11 and provide a heuristic based on an error function for the automated choice of a series of transition matrices (cf. Section 4.3). Also the study of a single Agulhas ring in Chapter 6 has only been possible by making use of this approach. Furthermore, we have proved that under certain conditions the error vanishes. However, to obtain suitable error functions, there is a need for further bounds on the approximation error with regard to spectral properties. In case, we approximate the transfer operator by a single transition matrix, there are bounds concerning the approximation quality of the fixed point or the corresponding Lyapunov

spectrum. Such bounds are discussed in the autonomous as well as in the non-autonomous case in the context of piecewise expanding maps (cf. [FLQ09, Li76]). To the author's best knowledge, there do not exist any practical results in the literature for the very general case as it is considered in this thesis. In order to obtain results in the context of products of transition matrices, one certainly has to restrict to certain classes of dynamical systems.

We show that coherent pairs can be captured by almost invariant sets on a small time scale under some weak restrictions, which is summarized in Algorithm 4 based on Theorem 5.2. In more detail, the theorem only gives a statement concerning the coherence ratio of a constructed set containing a part of the coherent pair. The length of the small time scale influences the runtime of Algorithm 4. Although we provide a heuristic in Section 5.2.3 for the automated choice of the small time scale during runtime, it would be even more suitable to choose it a priori. However, the results one can expect depend on the underlying application, and thus, one will have to restrict on certain subclasses of dynamical systems.

An important parameter of Algorithm 4 is the size of the almost invariant set. As for the choice of the small time scale, we provide a heuristic for the automated choice of size. The proposed method assumes monotony on the coherence ratio for a series of level-sets. However, we cannot be sure that the selected almost invariant set completely contains a part of the coherent pair. A possible heuristic would be to start with a single almost invariant set and calculate the singular values and singular vectors of the corresponding normalized transition matrix. The coherent pairs we seek are defined by level-sets of the singular vectors. If we select the maximal coherent level-set, it is either fully contained in the set we start with or the level-set intersects the boundary of the initial set. In the latter case, we cannot be sure that the set we started with is large enough, but we can extend the set successively and stop as soon as the maximal coherent level-set is completely contained.

Even though we show the applicability of the results to the oceanic fluid flow

by means of several examples, we cannot claim that the current research is capable of answering all the open questions in earth sciences. Nonetheless, we successfully provide methods for the investigation of specific oceanic structures and research should be continued by applying these methods to a wider range of applications. To reliably study the impact of the Agulhas rings, for instance, it is not enough to study single ones, but we have to investigate a series of them. For this task, an automated method has to be developed. The problem arising here is the selection of the time spans during which they exist. In order to obtain these time spans a possible approach might be to apply Algorithm 4 developed in Chapter 5 and to calculate a coherent pair for each almost invariant set. This successive exploration of a large oceanic domain is numerically very expensive, and consequently, there is a need for efficient data structures in which we can store already calculated trajectories to avoid redundant calculations. In this context, one will have to make use of massive parallel systems, since the trajectories involved for the approximation of the transition matrix can be calculated independently.

List of Figures

Bibliography

[Arn98] L. Arnold. *Random dynamical systems*. Springer, Berlin Heidelberg, 1998.

[ASY00] K. Alligood, T. Sauer, and J. Yorke. *Chaos; An introduction to dynamical systems*. Springer, New York, 2000.

[BDBZ11] L. M. Beal, W. P. M. De Ruijter, A. Biastoch, and R. Zahn. On the role of the Agulhas system in ocean circulation and climate. *Nature*, 472(7344):429–436, 2011.

[BMP+06] B. Barnier, G. Madec, T. Penduff, J.-M. Molines, A.-M. Treguier, J. Le Sommer, A. Beckmann, A. Biastoch, C. Böning, J. Dengg, C. Derval, E. Durand, S. Gulev, E. Remy, C. Talandier, S. Theeten, M. Maltrud, J. McClean, and B. De Cuevas. Impact of partial steps and momentum advection schemes in a global ocean circulation model at eddy-permitting resolution. *Ocean Dynamics*, 5-6:543–567, 2006.

[BP02] L. Barreira and Y. B. Pesin. *Lyapunov exponents and smooth ergodic theory*, volume 23 of *University Lecture Series*. American Mathematical Society, Providence, RI, 2002.

[Bré99] P. Brémaud. *Markov chains: Gibbs fields, Monte Carlo simulation, and queues*. Springer, New York, 1999.

[BS02] M. Brin and G. Stuck. *Introduction to dynamical systems*. Cambridge University Press, 2002.

[CGG08] A. Chaigneau, A. Gizolme, and C. Grados. Mesoscale eddies off Peru in altimeter records: Identification algorithms and eddy spatio-temporal patterns. *Progress In Oceanography*, 79(2-4):106–119, 2008.

[CSS11] D. B. Chelton, M. G. Schlax, and R. M. Samelson. Global observations of nonlinear mesoscale eddies. *Progress in Oceanography*, 91(2):167–216, 2011.

[Den05] M. Denker. *Einführung in die Analysis dynamischer systeme*. Springer, Berlin, 2005.

[DFH+09] M. Dellnitz, G. Froyland, C. Horenkamp, K. Padberg-Gehle, and A. Sen Gupta. Seasonal variability of the subpolar gyres in the Southern Ocean: a numerical investigation based on transfer operators. *Nonlinear Processes in Geophysics*, 16:655–664, 2009.

[DFHP09] M. Dellnitz, G. Froyland, C. Horenkamp, and K. Padberg. On the approximation of transport phenomena - a dynamical systems approach. *GAMM-Mitteilungen, Themenheft: "Mathematical Analysis of Nonlinear Phenomena"*, 32(1):47–60, 2009.

[DFJ01] M. Dellnitz, G. Froyland, and O. Junge. The algorithms behind GAIO – set oriented numerical methods for dynamical systems. In B. Fiedler, editor, *Ergodic Theory, Analysis, and Efficient Simulation of Dynamical Systems*, chapter 7, pages 145–174. Springer, 2001.

[DFS00] M. Dellnitz, G. Froyland, and S. Sertl. On the isolated spectrum of the Perron-Frobenius operator. *Nonlinearity*, 13(4):1171–1188, 2000.

[DH12] M. Dellnitz and C. Horenkamp. The efficient approximation of

coherent pairs in non-autonomous dynamical systems. *Discrete and Continuous Dynamical Systems - Series A*, 32(9):3029–3042, 2012.

[DHFS00] P. Deuflhard, W. Huisinga, A. Fischer, and C. Schütte. Identification of almost invariant aggregates in reversible nearly uncoupled Markov chains. *Linear Algebra and its Applications*, 315(1-3):39–59, 2000.

[DHJR97] M. Dellnitz, A. Hohmann, O. Junge, and M. Rumpf. Exploring invariant sets and invariant measures. *Chaos: An Interdisciplinary Journal of Nonlinear Science*, 7(2):221–228, 1997.

[DJ97] M. Dellnitz and O. Junge. Almost invariant sets in Chua's circuit. *International Journal of Bifurcation and Chaos in Applied Sciences and Engineering*, 7(11):2475–2485, 1997.

[DJ99] M. Dellnitz and O. Junge. On the approximation of complicated dynamical behavior. *SIAM Journal for Numerical Analysis*, 36(2):491–515, 1999.

[DJK+05] M. Dellnitz, O. Junge, W. S. Koon, F. Lekien, M. W. Lo, J. E. Marsden, K. Padberg, R. Preis, S. D. Ross, and B. Thiere. Transport in dynamical astronomy and multibody problems. *International Journal of Bifurcation and Chaos in Applied Sciences and Engineering*, 15(3):699–727, 2005.

[DJL+05] M. Dellnitz, O. Junge, M. W. Lo, J. E. Marsden, K. Padberg, R. Preis, S. D. Ross, and B. Thiere. Transport of Mars-crossing asteroids from the quasi-Hilda region. *Physical Review Letters*, 94(23), 2005.

[dM10] P. C. du Toit and J. E. Marsden. Horseshoes in hurricanes. *Journal of Fixed Point Theory and Applications*, 7(2):351–384, 2010.

[Doo94] J. L. Doob. *Measure theory*. Springer, New York, 1994.

[dvD04] L. de Steur, P. J. van Leeuwen, and S. S. Drijfhout. Tracer leakage from modeled Agulhas rings. *Journal of Physical Oceanography*, 34(6):1387–1399, 2004.

[FA01] G. Froyland and K. Aihara. Estimating statistics of neuronal dynamics via Markov chains. *Biological Cybernetics*, 84(1):31–40, 2001.

[FD03] G. Froyland and M. Dellnitz. Detecting and locating near-optimal almost-invariant sets and cycles. *SIAM Journal on Scientific Computing*, 24(6):1839–1863, 2003.

[FHR+12] G. Froyland, C. Horenkamp, V. Rossi, N. Santitissadeekorn, and A. Sen Gupta. Three-dimensional characterization and tracking of an Agulhas ring. *Ocean Modelling*, 52-53:69–75, 2012.

[FJK13] G. Froyland, O. Junge, and P. Koltai. Estimating long-term behavior of flows without trajectory integration: the infinitesimal generator approach. *SIAM Journal on Numerical Analysis*, 51(1):223–247, 2013.

[Fli81] G. R. Flierl. Particle motions in large-amplitude wave fields. *Geophysical & Astrophysical Fluid Dynamics*, 18(1-2):39–74, 1981.

[FLQ09] G. Froyland, S. Lloyd, and A. Quas. Coherent structures and isolated spectrum for Perron-Frobenius cocycles. *Ergodic Theory and Dynamical Systems*, 30:729–756, 2009.

[FLS10] G. Froyland, S. Lloyd, and N. Santitissadeekorn. Coherent sets for nonautonomous dynamical systems. *Physica D*, 239:1527–1541, 2010.

[FP09] G. Froyland and K. Padberg. Almost-invariant sets and invariant manifolds – connecting probabilistic and geometric descriptions of coherent structures in flows. *Physica D*, 238:1507–1523, 2009.

[FPET07] G. Froyland, K. Padberg, M. England, and A. M. Treguier. Detection of coherent oceanic structures via transfer operators. *Physical Review Letters*, 98(224503), 2007.

[Fro95] G. Froyland. Finite approximation of sinai-bowen-ruelle measures of anosov systems in two dimensions. *Random Comput. Dynam.*, 3(4):251–264, 1995.

[Fro01] G. Froyland. Extracting dynamical behavior via Markov models. In *Nonlinear dynamics and statistics (Cambridge, 1998)*, pages 281–321. Birkhäuser Boston, Boston, MA, 2001.

[Fro05] G. Froyland. Statisctically optimal almost-invariant sets. *Physica D*, 200:205–219, 2005.

[Fro13] G. Froyland. An analytic framework for identifying finite-time coherent sets in time-dependent dynamical systems. *Physica D*, 250:1–19, 2013.

[FSM10] G. Froyland, N. Santitissadeekorn, and A. Monahan. Transport in time-dependent dynamical systems: Finite-time coherent sets. *Chaos*, 20(4):043116, 2010.

[FSPD08] G. Froyland, M. Schwalb, K. Padberg, and M. Dellnitz. A transfer operator based numerical investigation of coherent structures in three-dimensional Southern Ocean circulation. *Proceedings of the 2008 International Symposium on Nonlinear Theory and its Applications*, pages 313–316, 2008.

[Hal00] G. Haller. Finding finite-time invariant manifolds in two-dimensional velocity fields. *Chaos*, 10(1):99–108, 2000.

[Hal01] G. Haller. Distinguished material surfaces and coherent structures in three-dimensional fluid flows. *Physica D: Nonlinear Phenomena*, 149(4):248–277, 2001.

[HB12] G. Haller and F. J. Beron-Vera. Geodesic theory of transport barriers in two-dimensional flows. *Physica D: Nonlinear Phenomena*, 241(20):1680–1702, 2012.

[HS05] W. Huisinga and B. Schmidt. Metastability and dominant eigenvalues of transfer operators. In *Advances in Algorithms for Macromolecular Simulation*. Springer, 2005.

[Hun94] F. Y. Hunt. A Monte Carlo approach to the approximation of invariant measures. *Random & Computational Dynamics*, 2(1):111–133, 1994.

[HY00] G. Haller and G. Yuan. Lagrangian coherent structures and mixing in two-dimensional turbulence. *Physica D: Nonlinear Phenomena*, 147:352–370, 2000.

[JK09] O. Junge and P. Koltai. Discretization of the Frobenius-Perron operator using a sparse haar tensor basis: the sparse Ulam method. *SIAM Journal on Numerical Analysis*, 47(5):3464–3485, 2009.

[KH97] A. Katok and B. Hasselblatt. *Introduction to the Modern Theory of Dynamical Systems*. Cambridge University Press, 1997.

[KKS99] P. E. Kloeden, H. Keller, and B. Schmalfuß. Towards a theory of random numerical dynamics. In H. Crauel and M. Gundlach, editors, *Stochastic Dynamics*, pages 259–282. Springer, New York, 1999.

[KS97] P. E. Kloeden and B. Schmalfuß. Nonautonomous systems, cocycle attractors and variable time-step discretization. *Numerical Algorithms*, 14(1-3):141–152, 1997.

[Li76] T.-Y. Li. Finite approximation for the Frobenius-Perron operator. a solution to Ulam's conjecture. *Journal of Approximation Theory*, 17(2):177–186, 1976.

[LY73] A. Lasota and J. A. Yorke. On the existence of invariant measures for piecewise monotonic transformations. *Transactions of the American Mathematical Society*, 186:481–488 (1974), 1973.

[MS12] J. Marshall and K. Speer. Closure of the meridional overturning circulation through Southern Ocean upwelling. *Nature Geoscience*, 5(1391):171–180, 2012.

[MW98] N. Malhotra and S. Wiggins. Geometric structures, lobe dynamics, lagrangian transport in flows with aperiodic time-dependence, with applications to Rossby wave flow. *Journal of Nonlinear Science*, 8:401–456, 1998.

[Nad98] M. G. Nadkarni. *Basic Ergodic Theory*. Birkhäuser, 1998.

[Pad05] K. Padberg. *Numerical Analysis of Transport in Dynamical Systems*. PhD thesis, University of Paderborn, 2005.

[Rud87] W. Rudin. *Real and Complex Analysis*. Tata McGraw-Hill Publishing Company Limited, 1987.

[SFM10] N. Santitissadeekorn, G. Froyland, and A. Monahan. Optimally coherent sets in geophysical flows: A transfer-operator approach to delimiting the stratospheric polar vortex. *Physical Review E*, 82(5):056311, 2010.

[SHD01] C. Schütte, W. Huisinga, and P. Deuflhard. Transfer operator approach to conformational dynamics in biomolecular systems. In *Ergodic Theory, Analysis, and Efficient Simulation of Dynamical Systems*, chapter 9, pages 191–223. Springer, 2001.

[SLM05] S. C. Shadden, F. Lekien, and J. E. Marsden. Definition and properties of Lagrangian coherent structures from finite-time Lyapunov exponents in two-dimensional aperiodic flows. *Physica D*, 212, 2005.

[ST08] S. C. Shadden and C. Taylor. Characterization of coherent struc-

tures in the cardiovascular system. *Annals of Biomedical Engineering*, 36:1152–1162, 2008.

[TBBM03] A. M. Treguier, O. Boebel, B. Barnier, and G. Madec. Agulhas eddy fluxes in a 1/6 ° Atlantic model. *Deep Sea Research Part II: Topical Studies in Oceanography*, 50(1):251–280, 2003.

[Ula60] S. M. Ulam. *A Collection of Mathematical Problems*. Interscience Publishers, New York, 1960.

[Var62] R. S. Varga. *Matrix iterative analysis*. Prentice-Hall Inc., Englewood Cliffs, N.J., 1962.

[Wat07] D. S. Watkins. *The matrix eigenvalue problem*. Society for Industrial and Applied Mathematics (SIAM), Philadelphia, PA, 2007.

[WRSD02] W. Weijer, W. P. M. D. Ruijter, A. Sterl, and S. S. Drijfhout. Response of the Atlantic overturning circulation to South Atlantic sources of buoyancy. *Global and Planetary Change*, 34(3-4):293–311, 2002.